PURPOSE AND MAIN OBJECTIVES OF THE THESIS

The term photocatalysis is often used to refer to processes carried out in the presence of photoactive materials and aimed toward wastewater decontamination or water splitting for the generation of hydrogen as a fuel. However, the idea that photocatalysis can provide an alternative to more conventional synthetic pathways has been gradually emerging [1-13].

In its broadest sense, photocatalysis for synthetic purposes concerns the use of light to induce chemical transformations of organic or inorganic substrates that are transparent in the wavelength range employed. The radiation is absorbed by a photocatalyst, whose electronically excited states are able to trigger the chemical reactions of interest. The overall process can be considered photocatalytic when i) the photoactive species is regenerated in its initial state at the end of a reaction cycle, just as happens in thermal catalysis; ii) the photocatalyst is consumed less than in stoichiometric amounts, while light is a stoichiometric reagent.

Selectivity is a key issue in photocatalytic processes aimed at the production of functionalized intermediates of interest in fine chemistry. In order to pursue this objective, all steps of the catalytic process must be optimized. The high selectivity of the mild photochemical routes are especially attractive for the manufacture of fine chemicals.

Heterogeneous systems represent a suitable means to tailor efficiency and selectivity of photocatalytic processes through the control of the microscopic environment surrounding the photoactive centre, which is located on the catalyst surface or inside pores or in a thin liquid film at the surface. In particular, type and textural characteristics of the employed material may affect important physical and chemical properties of the photocatalytic system that act as rate determining steps: absorption of light, adsorption equilibria of reaction intermediates, control of the diffusion of reactants and products in or out of catalytic sites located inside of a porous network. It is in this context that recent developments in the discovery of

new synthetic routes for the preparation of materials with well-defined structures at the nanometric scale may afford better design of active sites for selective catalytic processes, including photocatalytic processes [14]. Of course, another main role of a solid support is to render the photocatalyst more easily handled and recyclable.

In this doctoral thesis, the photochemical technique (near UV light) is used for the activation of inorganic heterogeneous catalytic systems. These have been investigated in the partial oxidation of alcohols by using molecular oxygen, as largely available and clean reagent, and working at room temperature and atmospheric pressure with a minimal environmental impact. Particular attention has been devoted to the relationship between morphology and photocatalytic behaviour in order to prepare materials with predictable properties able to provide the desired selectivity.

In more detail, the following photocatalytic systems have been prepared, characterized and investigated:

- $(n\text{-}Bu_4N)_4W_{10}O_{32}$ incorporated in a silica matrix by a sol-gel procedure. Two photocatalysts, with two different loadings, were prepared and their photocatalytic properties have been studied in the oxidation of primary and secondary aliphatic alcohols. Selectivity in the partial oxidation of primary alcohols to aldehydes is an important issue, since it is usually difficult in oxidative catalysis to stop the oxidation at the carbonylic product without the formation of carboxylic acid.
- $Na_4W_{10}O_{32}$ entrapped in a silica matrix by a sol-gel procedure. The primary photoprocess and the photocatalytic properties of this heterogeneous system have been investigated in the oxidation of glycerol. The large functionalization of this alcohol renders its selective oxidation particularly difficult. As a consequence, any improvement in selectivity is noticeable if one considers that all oxygenated derivatives of glycerol are of practical value. Moreover, since glycerol is an important by-product in biodiesel production, the

development of processes able to convert it into higher value products is an urgent need and a challenging opportunity.

- a derivative of iron(III) *meso*-tetrakis(2,6-dichlorophenyl) porphyrin covalently linked on the surface of MCM-41 and of amorphous silica. This photocatalytic system has been studied in the oxidation of 1,4-pentanediol and effects of the two supports, very different in morphology, on the selectivity of the photoprocess have been considered.

The classes of compounds under investigation (polyoxotungstates and iron-porphyrin complexes) are characterized by common primary photoprocesses, as schematized in Figure 1: photochemical excitation leads to simultaneous reduction of the metal centre (tungsten or iron) and to the oxidation of an organic substrate. Then, the photocatalytic cycle is closed by oxygen that regenerates the metal centre in its starting oxidation state undergoing a reductive activation.

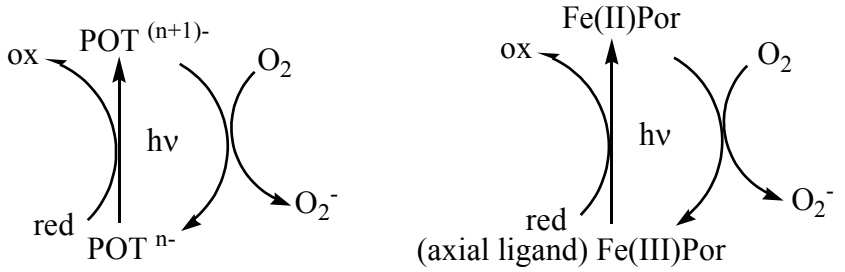

Figure 1. Photocatalytic cycle of polyoxotungstates and iron porphyrins.

During the PhD period the following papers have been published:

1. "Matrix effects on the photocatalytic oxidation of alcohols by $[nBu_4N]_4W_{10}O_{32}$ incorporated into sol-gel silica", A. Molinari, A. Bratovcic, G. Magnacca, A. Maldotti, *Dalton Transactions*, 2010, 39, 7826-7833 [15] .

2. “Fe(III)-porphyrin heterogenized on MCM-41: matrix effects on the oxidation of 1,4-pentandiol”, A. Molinari, A. Maldotti, A. Bratovcic, G. Magnacca, *Catalysis Today*, 161, 2011, 64 [16] .
3. “Photocatalytic properties of sodium decatungstate supported on sol-gel silica in the oxidation of glycerol”, A. Molinari, A. Maldotti, A. Bratovcic, G. Magnacca, *Catalysis Today,* http://dx.doi.org/10.1016/j.cattod.2011.11.033 [17]

INTRODUCTION

1. POLYOXOTUNGSTATES

1. 1 GENERAL FEATURES, SYNTHESIS AND STRUCTURES

The term polyoxometalate (POMs) is used to indicate an extremely large group of anionic clusters with frameworks built from transition metal and oxo anions linked together by shared oxide ions. Generally, two types of polyoxometalates are distinguished on the basis of their chemical composition: isopolyanions and heteropolyanions. The formers can be represented by the general formula: $[M_mO_y]^{p-}$ and the latters by $[X_xM_mO_y]^{q-}$, ($x \leq m$). The heteroatom X can be one of the 65 elements belonging to all groups of the Periodic Table except the rare gases. The most common transition metal atoms present in the clusters are molybdenum and tungsten in their highest oxidation states (d^0, d^1 configuration), while vanadium and niobium are less frequent. Polyoxomolybdates and polyoxotungstates are widespread among POMs since they are the result both of a favourable combination of ionic radius and charge and of ability to form dπ-pπ M-O bonds. There are also mixed polyoxometalates with general formula $[M_mM'_nO_y]^{p-}$ and $[X_xM_mM'_nO_y]^{q-}$, where M and M' are two different metals. The weights of POMs are in the range of 1000-10000 a.m.u., with sizes between 6 and 25 Å [18-21]. Considering the possible values of the ratio m/x, and the variety of M, M', X atoms that may be employed, the number of polyoxometalates that can be obtained is considerably large [22].

Polyoxometalates are a class of inorganic compounds studied in detail over the past decades because they offer interesting applications in catalysis. In particular, some groups of researchers are investigating POMs as catalysts in the oxidation of organic compounds [23-31]. It is noteworthy, that the enormous versatility of polyoxometalates offers significant opportunities for clean synthesis of fine and specialty chemicals.

The history of polyoxometalates dates back to 1826 when Berzelius [32] described the yellow precipitate of ammonium 12-molybdophosphate

that is produced when ammonium molybdate is added to phosphoric acid. Later, in 1848, Svanberg and Struve [33] introduced this compound into analytical chemistry for the determination of phosphorus. The structure of polyoxometalates remained a mystery for more than a century since their discovery. Werner [34], Miolati [35], Rosenheim [36] and Pauling [37] proposed structures based on an arrangement of metal-oxygen octahedra surrounding a central XO_4 tetrahedron. In 1933 Keggin solved the structure of the most important 12:1 type heteropolyanion $H_3[PW_{12}O_{40}] \times 5H_2O$ by X-ray diffraction study [38]. He showed that this structure contained 12 WO_6 octahedra linked by shared edges and corners, with the heteroatom occupying a tetrahedral hole in centre. In 1948, Evans [39] determined the structure of $[TeMo_6O_{24}]^{6-}$, that belongs to the 6:1 heteropolyanions series – previously only suggested by Anderson. In 1953, Dawson [40] reported the new new structure of a 18:2 heteropolyanion, $[P_2W_{18}O_{62}]^{6-}$. This structure was shown to be closely related to the Keggin one. By the early 1970, the chemistry of polyoxometalates greatly expanded. By 1995, the X-ray structures of approximately 180 polyoxometalates had been reported. The application of modern characterisation techniques had led to much better understanding of the structural principles of polyoxometalates and their properties.

The polyoxomolybdates and polyoxotungstates (POT) can be isolated both in aqueous solution or in organic solvent and are generally prepared by a condensation reaction of MoO_4^{2-} and WO_4^{2-} in acidic solutions. If condensation occurs in the presence of a heteroatom X (such as P^V, As^V, Si^{IV}, Fe^{III}, etc.), it can be embedded in the structure of the polyoxometalate to give the heteropoly anion, as shown in reaction (1) for the case of POTs:

$$12WO_4^{2-} + HPO_4^{2-} + 23H^+ \rightarrow PW_{12}O_{40}^{3-} + 12H_2O \qquad (1)$$

In many cases, equilibrium constants and rates of formation are largely enough to allow crystallization of POTs as salts from stoichiometrically acidified mixtures of the components even at room temperature. Sometimes,

it is necessary to use an excess of the heteroatom and to control temperature and pH of the solution. It may be also relevant the sequence of addition of reagents [41].

The structure of polyoxoanions can be described as an aggregation of metal-centred polyhedra MO_n, linked through vertices, edges or, more rarely, faces (sharing the oxygen atoms).

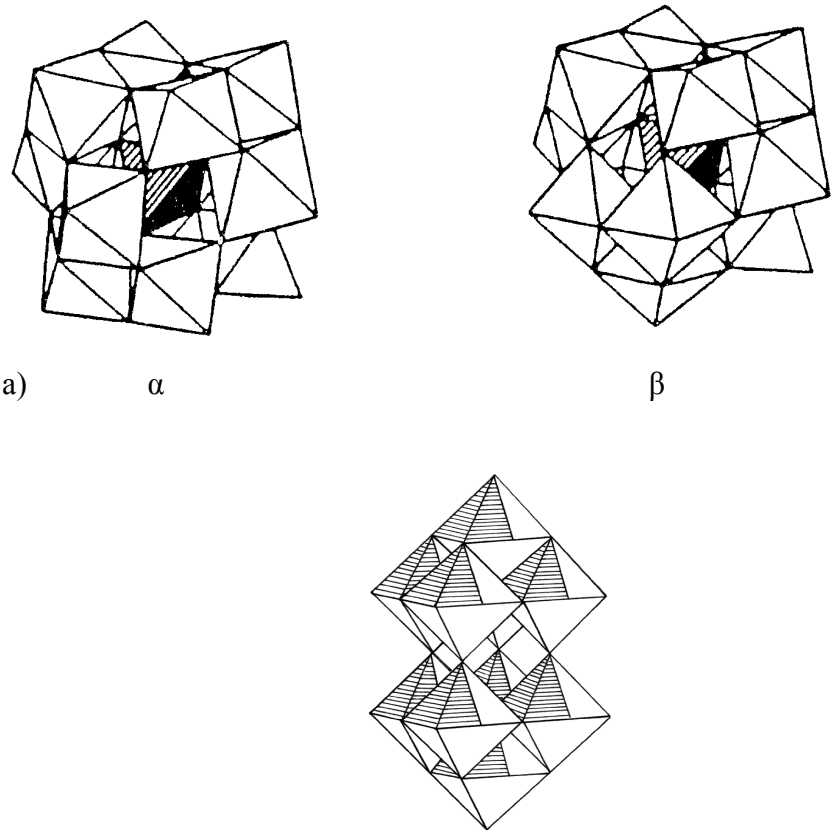

a) α β

b)

Figure 2. a) α and β isomers of $PW_{12}O_{40}^{3-}$; b) $W_{10}O_{32}^{4-}$.

The ionic radii of polyoxoanions [42] are in agreement with the hexacoordination, commonly observed for these elements. In many cases, however, the metal ion does not lie at the centre of the polyhedron of oxide ions, but it is shifted toward the outside of the structure, i.e. to a vertex or an edge of its polyhedron.

Lipscomb noted that MO_6 octahedra were not present in structures with more than two oxygen atoms in common [43], while, at the same time, two types of dispositions of the metal centre M have been identified in polyoxoanions: type I that has always a terminal oxygen atom with the metal occupying a site of symmetry approximate C_{4v} and type II that has two terminal oxygen atoms. The MO_6 octahedra of type I may contain metals with electronic configuration d^0, d^1, d^2, while the octahedra of type II are limited to metals d^0 [44].

Among a wide variety of heteropoly compounds, the Keggin's (Figure 2a) are the most stable and more easily available. These, together with some of their derivatives, are the most important in catalysis. The Keggin anion has a diameter of ca. 12Å and is composed of a central tetrahedron XO_4 surrounded by 12 edge- and corner-sharing metal-oxygen octahedra MO_6. The octahedra are arranged in four M_3O_{13} groups. Each group is formed by three octahedra sharing edges and having an oxygen atom in common which is also shared by the central tetrahedron XO_4.

The structure of the isopolytungstate $W_{10}O_{32}^{4-}$ also known as "y tungstate" [45] has D_{4h} symmetry [46, 47] and is shown in Figure 2b. The anion is constituted of two units W_5O_{18} linked together by four oxygen atoms, each shared by two octahedra, forming an internal octahedral space that is empty.

1. 2 REDOX PROPERTIES

The redox chemistry of polyoxometalates is characterized by their ability to accept and subsequently release a certain number of electrons in distinct stages. The reduction of POMs proceeds without substantial changes of their structure. In the reduced form they are coloured in blue, giving the so-called heteropolyblue, whose UV-vis absorption spectrum is characterized by a broad absorption band around 700 nm. The formation of heteropolyblue species was observed for the Keggin structure $[XM_{12}O_{40}]^{3-}$ and other

compounds of type I, such as: $[X_2M_{18}O_{62}]^{6-}$ X = P, As and M = Mo, W; $[M_6O_{19}]^{2-}$, M = Mo, W, $[W_{10}O_{32}]^{4-}$ [48, 49].

The reduction is often followed by protonation, which makes the corresponding potential dependent on pH. An increase in pH and in charge shifts the redox potential towards more negative values [50]. The molybdates are reduced more easily than the corresponding tungstates [51]. Anions with structures 2:18 are reduced to slightly more positive potentials and maintain the structure even after the addition of a number of electrons higher than the corresponding compounds 1:12.

The reduced compounds are more stable in basic solutions than non-reduced ones [50, 52]. The addition of electrons over a certain number results in a distortion of the structure, and an increase of metal-metal character [53]. In mixed polyoxoanions, added electrons are localized on the more electronegative metal [54].

The POMs in their oxidized form are characterized by oxygen-metal charge transfer bands in the visible and near ultraviolet region (200-350 nm). Generally, molybdates absorb at longer wavelengths than tungstates. The reduced forms contain metal ions in different oxidation states and are included in the category of mixed-valence compounds. The reduction of POM leads to a decrease of OMCT band and to the formation of the IVCT band in the visible and near IR region (W^{V} – O - W^{VI}/W^{VI} – O - W^{V}) [55,56].

1. 3 PHOTOCATALYTIC ACTIVITY OF POLYOXOTUNGSTATES

Polyoxotungstates, can be considered soluble models of semiconductor metal oxide surfaces. They have been intensively studied over the past 20 years because they exhibit interesting properties as photocatalysts [7, 8, 28, 57, 58]. Among them, the decatungstate anion $W_{10}O_{32}^{4-}$ is the most investigated, since its absorption spectrum partially overlaps the UV solar emission spectrum (with a λ_{max} at 325 nm), opening the possibility to carry out benign solar-photoassisted applications [7-9, 59]. Some of the

photocatalyst investigated in this doctorate thesis are based on the use of this polyoxotungstate. The cascade of events that follows light absorption by $W_{10}O_{32}^{4-}$ has been deeply studied and is summarized in the following (Figure 3) [29, 60-62].

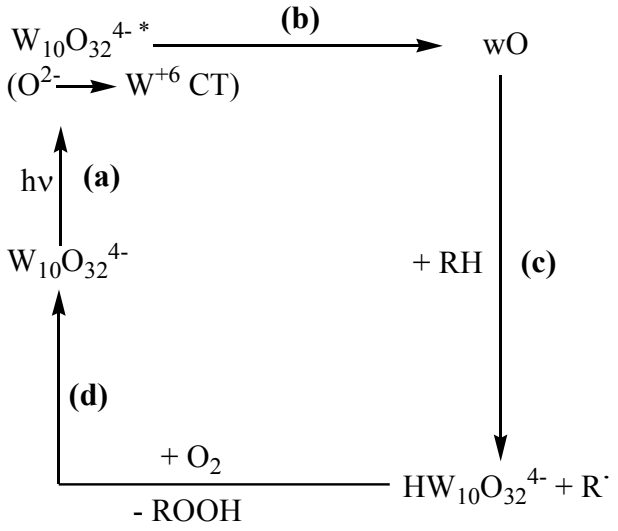

Figure 3. Photocatalytic behaviour of $W_{10}O_{32}^{4-}$.

Excitation of $W_{10}O_{32}^{4-}$ ($\lambda > 300$ nm) leads to an oxygen to metal [O^{2-}-W^{6+}] charge transfer excited state ($W_{10}O_{32}^{4-*}$, Figure 3 **(a)**), [8, 30, 63]. Then, $W_{10}O_{32}^{4-*}$ decays in less than 30 ps to a very reactive non-emissive transient, indicated as wO (step **(b)**). This species has an oxyradical-like character due to the presence of an electron deficient oxygen centre and has a lifetime of 65 ± 5 ns and a quantum yield of formation of 0.57 [29]. The wO species possesses a very high reactivity towards any organic substrate RH: quenching of wO may occur either by hydrogen-atom abstraction or electron transfer mechanism, depending on the chemical nature of RH. In any case, both mechanisms lead to the one electron reduced form of decatungstate ($HW_{10}O_{32}^{4-}$) and to the substrate derived radical (R•) (step **(c)**). At this stage, O_2 can regenerate the starting $W_{10}O_{32}^{4-}$ with parallel formation of peroxy compounds (step **(d)**).

1. 4 HETEROGENIZATION OF POLYOXOTUNGSTATES

1. 4. 1 *HETEROGENIZATION BY IMPREGNATION*

The first attempts to prepare heterogeneous photocatalysts through impregnation of $(n\text{-}Bu_4N)_4W_{10}O_{32}$ and $H_3PW_{12}O_{40}$ on amorphous silica go back to about ten years ago [59, 64-68]. Main features of these photoactive materials are that they are easily handled and recyclable photocatalysts and they can be employed in reaction media where they are insoluble. It has been reported that photoexcitation of heterogenized $(n\text{-}Bu_4N)_4W_{10}O_{32}$ and $H_3PW_{12}O_{40}$ dispersed in neat cyclohexane leads to the oxidation of cycloalkane to cyclohexanol and cyclohexanone [64]. The heterogeneous photocatalysts can be recycled without leaching and any loss in photoactivity. Moreover, they do not cause any mineralization of cyclohexane to CO_2, indicating that they are very promising photocatalysts for applied synthetic purposes.

Further research developments have been devoted to improve the selective conversion yield of cyclohexane to cyclohexanone, the intermediate of interest in the production of nylon 6 and nylon 66. It has been found that, depending on the nature of the cation, the heterogeneous photocatalysts show different and tunable photoreactivities (Table 1) [65]: $n\text{-}Bu_4N^+$ cations enhance the efficiency of cyclohexane photooxidation, likely because they create a hydrophobic environment around the photoactive species, favouring the approach and the subsequent oxidation of the cycloalkane. NH_4^+ and Na^+ cations improve the chemoselectivity, since the concentration ratios cyclohexanone/cyclohexanol are 1.8 and 2.3 respectively. Likely, cyclohexanol, remaining close to the polar surface of these materials, is easily oxidized to cyclohexanone.

Table 1. Surface areas, polarity measurements[a] and photocatalytic properties of $(n\text{-}Bu_4N)_4W_{10}O_{32}/SiO_2$, $(NH_4)_4W_{10}O_{32}$ and of $Na_4W_{10}O_{32}$.

Material	Surface area (m^2/g)	E_T^N [a]	Cyclohexanol + cyclohexanone (M)	Cyclohexanone/ cyclohexanol
SiO_2	95 ± 2	0.93	---------	-------
$Na_4W_{10}O_{32}/SiO_2$	83 ± 2	0.83	0.3×10^{-3}	2.3
$(NH_4)_4W_{10}O_{32}/SiO_2$	83 ± 2	0.80	0.6×10^{-3}	1.8
$(n\text{-}Bu_4N)_4W_{10}O_{32}/SiO_2$	54 ± 2	0.51	1.7×10^{-3}	1.0

[a] polarity measurements were carried out following a reported procedure using Reichardt's dye. E_T^N values ranges from 0 to 1 with surface polarity increase.

In 2002, Maldotti and co-workers reported on the immobilization of $(n\text{-}Bu_4N)_4W_{10}O_{32}$ on the mesoporous silica MCM-41 (mesopores ranging from 20 to 100 Å and surface area of ~ 1000 m^2/g) [66]. Thanks to the large surface area of MCM-41, decatungstate is well dispersed, providing a great number of photocatalytic sites that leads to an enhancement of photochemical efficiency. Concerning the chemoselectivity in the photocatalytic oxidation of cyclohexane, the maximum value of ketone/alcohol ratio is 2.6. Authors report that the polar surface of MCM-41 favours the accumulation of formed cyclohexanol at the interfaces and, consequently, its subsequent oxidation to ketone by the photoexcited decatungstate.

The photocatalytic properties of $(n\text{-}Bu_4N)_4W_{10}O_{32}$ impregnated on amorphous silica have been also investigated in the oxidation of cycloalkenes, (cyclohexene and cyclooctene). This study has been carried out in the presence of Fe^{III}[*meso*-tetrakis(2,6-dichlorophenyl)porphyrin] chloride (Fe(TDCPP)Cl) as a co-catalyst [67]. Cycloalkenes are mainly oxidized to the corresponding hydroperoxides by the photoexcited

decatungstate. The iron porphyrin reacts with the allylic hydroperoxides to give the corresponding alcohols as main products.

Photooxidation of benzyl alcohols by $W_{10}O_{32}^{4-}$ impregnated on silica and γ-alumina has been investigated by Orfanopoulos and co-workers [69]. These photocatalysts have been studied in the oxidation of a series of p-alkyl-substituted benzyl alcohols, 1-7 (Figure 4). These substrates bear two distinguishable benzylic hydrogen atoms, one on the alcohol carbon and one on the p-alkyl substituent, both of which potentially can be cleaved under photooxidation conditions to give aryl ketones 1a-7a or deoxygenated products 1b-7b respectively. A strong preference for the hydrogen atom abstraction from the alcohol carbon is observed: selectivity for 1a-7a compounds is, in most cases, higher than 80%. This can be ascribed to the surface polarity of the supports that probably favours accumulation of the polar alcohol moiety.

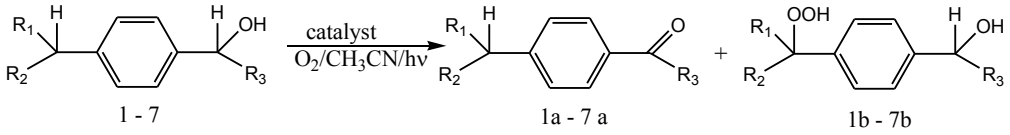

1 - 7 1a - 7 a 1b - 7b

R_1	R_2	R_3	
H	H	CH_3	1
CH_3	H	CH_3	2
CH_3	CH_3	CH_3	3
Ph	H	CH_3	4
Ph	Ph	CH_3	5
CH_3	H	Ph	6
CH_3	CH_3	Ph	7

Figure 4. Oxidation of p-alkyl-substituted benzyl alcohols by $W_{10}O_{32}^{4-}$ impregnated on silica and γ-alumina.

Shen and co-workers report that $H_3PW_{12}O_{40}$ impregnated on MCM-41 is able to photooxidize several alcohols to the corresponding carbonylic derivatives in the presence of O_2 [70]. In particular, an enhancement in

activity is observed if an ionic liquid is used as dispersing medium instead of CH_3CN.

Zeolite Y (in the Na^+ form) has been used as a solid support for $H_2NaPW_{12}O_{40}$, $H_4SiW_{12}O_{40}$ and $H_3PMo_{12}O_{40}$ [71]. The photocatalytic activities of these systems have been investigated choosing 1,2-dichlorobenzene as oxidizable probe. The constrained environment is responsible of a rate enhancement of the reaction, since it increases the encounter probability between photoexcited polyoxometalate and 1,2-dichlorobenzene, suppressing back electron transfer reaction.

1. 4. 2 *HETEROGENIZATION BY SOL-GEL PROCEDURE*

Some years ago Hu et al. set a new heterogenization procedure, where a POT, such as $H_3PW_{12}O_{40}$, $H_4SiW_{12}O_{40}$, $(n\text{-}Bu_4N)_4W_{10}O_{32}$ or $Na_4W_{10}O_{32}$, is encapsulated inside a silica network via a sol-gel technique [72, 73]: CH_3CN/H_2O solution of the chosen POT, adjusted at pH 2, is added dropwise to a solution of tetraethyl orthosilicate (TEOS) and 1-butanol. After some hours of stirring and kind warming, the hydrogel is dried and calcined to fasten the formation of silica network. Structural integrity of $W_{10}O_{32}^{4-}$ is preserved and protonated silanol groups act as counter-ions for the polyoxoanion. Following this procedure, Farhadi and Afshari entrapped $(n\text{-}Bu_4N)_4W_{10}O_{32}$ and $H_3PW_{12}O_{40}$ in a silica matrix and used these photocatalysts in the oxidation of benzylic alcohols in the presence of O_2 [74, 75]. They performed a screening study choosing a variety of ring-substituted primary and secondary benzylic alcohols. These substrates are efficiently oxidized to the corresponding carbonylic compounds, without overoxidation of benzaldehydes to carboxylic acids. This result is in contrast to what reported by Orfanopoulos with decatungstate immobilized on silica by impregnation [69], so indicating that different preparation methods lead to a completely dissimilar morphology of the photocatalyst and, consequently, to a different photoreactivity.

Zirconia-supported $Na_4W_{10}O_{32}$ and $H_3PW_{12}O_{40}$ have been prepared via sol-gel procedure by the Farhadi's group [76, 77]. $Na_4W_{10}O_{32}/ZrO_2$ is more active than the homogeneous $Na_4W_{10}O_{32}$ in the photooxidation of primary and secondary benzylic alcohols. This fact is tentatively attributed to a synergistic effect between the polyoxoanion and the support that is a semiconductor. Interestingly, in the $H_3PW_{12}O_{40}/ZrO_2$ system, the absorption band typical of $H_3PW_{12}O_{40}$ at 270 nm is not present and a new broad band, shifted to the visible region, is observable. Authors attribute the photocatalytic activity of the nanocomposite system to the existence of this broad band. $Na_4W_{10}O_{32}/ZrO_2$ has been also employed for the reductive cleavage of a series of substituted azobenzenes into their corresponding amines using 2-propanol as hydrogen source under a N_2 atmosphere [78]. Amines are obtained in high to excellent yields (76-94%) and with short reaction times. Efficiency of the photocatalytic process is influenced by steric factor: substituents in ortho- or meta - positions to the N=N functional group decrease the reaction rate. Interestingly, no other reducible substituents, such as $–NO_2$, are affected by the photocatalyst.

Colloidal $Cs_3PW_{12}O_{40}$, synthesized by metathesis of $H_3PW_{12}O_{40}$ and CsCl in water, has been supported on silica via sol-gel procedure using tetraethyl ortosilicate (TEOS) [79]. The obtained material is extremely porous (pore size centred at 23 Å) and with a very large surface area. It is effective in the photooxidation of aqueous solutions of propan-2-ol to acetone and it does not undergo to any leaching of polyoxometalate. A deep investigation on the factors influencing the efficiency of this heterogeneous photocatalyst, such as events that follow the absorption of light and substrate adsorption, has been published by the same authors in 2000 [80].

1. 4. 3 *HETEROGENIZATION BY ION EXCHANGE*

As an alternative to the conventional impregnation or sol-gel entrapment procedures, it has been reported that $W_{10}O_{32}^{4-}$ can be supported on a silica matrix previously functionalized with different ammonium cations, covalently bound on the solid support [81]. The polyoxoanion is firmly held on the support by ionic bond with tetraalkylammonium cations in Si-(alkyl)$_4$NW, with trialkylammonium cations in Si-(alkyl)$_3$NHW and with monoalkylammonium cations in Si-alkylNH$_3$W (Figure 5).

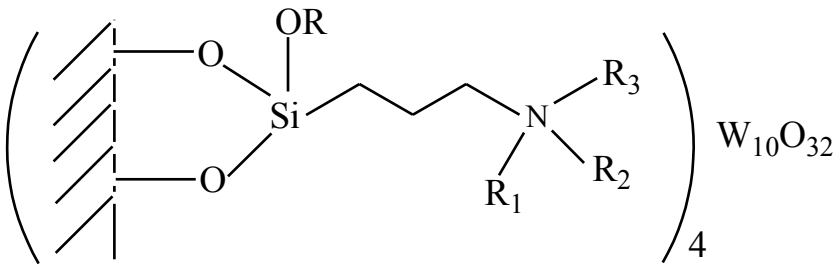

R_1, R_2, R_3 = H, H, H Si-alkylNH$_3$W

R_1, R_2, R_3 = Et, Et, H Si-(alkyl)$_3$NHW

R_1, R_2, R_3 = Et, Et, Et Si-(alkyl)$_4$NW

Figure 5. The polyoxoanion is held on the support by ionic bond with alkylammonium cations.

These materials have been employed as photocatalysts for the O_2-assisted oxidation of 1,3-butanediol and 1,4-pentanediol. For both the investigated diols, the only obtained products are the hydroxy-aldehyde and the hydroxy-ketone. The ratio between aldehyde and ketone depends on the nature of the alkyl-ammonium cations; in particular, it increases markedly (from 0.06 to 0.63 for 1,3-butanediol and from 3.0 to 7.5 for 1,4-pentanediol) as the alkyl chains are substituted by hydrogen atoms. This substitution enhances the polarity of the environment surrounding $W_{10}O_{32}^{4-}$, favouring the preferential adsorption of primary OH group of the more hydrophilic head of diol

molecule with respect to the secondary OH group placed in the more hydrophobic tail. Concerning the stability, these photocatalysts are robust and reusable at least five times without leaching of polyoxotungstate anion.

The decatungstate $W_{10}O_{32}^{4-}$ has been immobilized on a hydrophobically organomodified mesoporous silica SBA-15 by the Cao's group [82]. Introduction of an hydrophobic organic fragment onto the silica surface, which is intrinsically hydrophilic, produces a photocatalyst where the active sites are more easily accessible to hydrocarbon molecules. The organo-modified SBA-15 is prepared by initial insertion of alkyl groups of chosen length using C_n-Si(OEt)$_3$ (n = 2, 4, 8, 16), followed by grafting of 3-aminopropyl groups. The resultant material is acidified and then ion exchange by decatungstate is carried out. The 3-ammoniumpropyl groups (-$(CH_2)_3NH_3^+$) immobilize $W_{10}O_{32}^{4-}$ on the pore walls, while the alkyl chains form hydrophobic regions around decatungstate. These novel photocatalysts have been investigated in the oxidation of some aryl alkanes to the corresponding phenones by O_2. Length of alkyl chains affects the photocatalytic efficiency, with the octyl-grafted (n = 8) showing the best performance. Interestingly, this photocatalyst is also able to convert cyclohexane to cyclohexanone with very high yield, complete selectivity and high stability.

A simple ion-exchange procedure allowed Fornal and Giannotti to immobilize $W_{10}O_{32}^{4-}$ on poly(4-vinylpyridine), cross-linked methyl chloride quaternary salt [83]. The ionic interaction is strong enough to prevent the release of the polyoxoanion into the solution. This material has been investigated in the photooxidation of cyclohexane in the presence of O_2. Cyclohexyl hydroperoxide is the main product but cyclohexanol and cyclohexanone are also formed. The selectivity depends on the decatungstate loading: cyclohexanone production is promoted by lower loadings, whereas cyclohexyl hydroperoxide formation is favoured by higher loadings.

Amberlite IRA-900 in the chloride form has been employed as support for $(n\text{-}Bu_4N)_4W_{10}O_{32}$ by Maldotti's research group [84]. The ion exchange of Cl^- with $W_{10}O_{32}^{4-}$ is favoured by the soft character of $-N(CH_3)_3^+$ cations. This photocatalytic system promotes the conversion of olefins to the corresponding bromohydrins and dibromoalkanes in the presence of NaBr (Table 2). By simply adjusting the pH value, bromohydrins can be quantitatively transformed into epoxides, which are important intermediates in organic synthesis. Photoexcited $(n\text{-}Bu_4N)_4W_{10}O_{32}$ causes the reductive activation of O_2 to alkyl hydroperoxides. These, in turn, reacting with bromide ions, give a brominating species that attacks C=C double bond of olefins. A nucleophile such as H_2O or Br^- leads to bromohydrin and dibromo-derivative respectively. Under analogous experimental conditions, phenol and anisole are converted to their monobrominated derivatives, a transformation of particular interest if one considers the otherwise difficult monobromination of activated arenes. From Table 2, it is seen that polymeric matrix increases the yields to epoxides and bromohydrins and inhibits undesirable autooxidation processes leading to monooxygenated products. It is evident the crucial role of the resin in fostering the enrichment of Br^- ions close to the surface, promoting their reaction with photogenerated alkyl hydroperoxides, before their diffusion in the solution bulk.

Table 2. Photocatalytic properties of Amb/$W_{10}O_{32}^{4-}$ and of $W_{10}O_{32}^{4-}$ in the bromide-assisted functionalization of alkenes.

Alkene	System	Alkene products distribution (%)		
		EP + BrOH[a]	BrBr[a]	OMP[a]
cyclohexene	Amb/$W_{10}O_{32}^{4-}$	36	42	22
	$W_{10}O_{32}^{4-}$	24	7	69
1-methyl-1-cyclohexene	Amb/$W_{10}O_{32}^{4-}$	69	5	26
	$W_{10}O_{32}^{4-}$	38	4	58
styrene	Amb/$W_{10}O_{32}^{4-}$	44	2	50
	$W_{10}O_{32}^{4-}$	22	0	70

[a]EP = epoxide, BrOH = bromohydrin, BrBr = dibromoalkane, OMP = other monooxygenated products, such as allylic alcohols and ketones.

1. 4. 4 *HETEROGENIZATION WITH MEMBRANES*

Among the different techniques for the immobilization of decatungstate, the occlusion in polymeric membranes offers new developments in aqueous photocatalysis. In fact, in water, the choice of an appropriate hydrophobic support may be the key to discriminate among reactants. In this context, Bonchio and co-workers have embedded $W_{10}O_{32}^{4-}$ in several polymeric membranes, using a phase inversion technique or a hydrosilylation reaction [85, 86]. Polyvinylidene fluoride (PVDF) and polydimethylsiloxane (PDMS) are the most resistant membranes, in terms of self-induced degradation upon irradiation in water. These systems have been studied in the photooxidation of several water soluble alcohols (*n*-pentanol, cyclohexanol, cyclopentanol). Carbonyl products accumulate in solution up

to a substrate conversion in the range 10 - 30% and then they undergo consecutive oxidation. In comparison with homogeneous $Na_4W_{10}O_{32}$, the heterogeneous photooxidation is slower but proceeds to completion in a few hours. Interestingly, heterogeneous matrix exerts specific substrate recognition, a key factor to achieve selective processes: the preferential interaction with the polymeric membrane promotes the oxidation, favouring adsorption equilibrium and leading to substrate enrichment on the surface close to the photoactive sites. Concerning the stability, the PDMS - $W_{10}O_{32}^{4-}$ photocatalyst is the most stable and effective in multiple runs, probably thanks to an optimal surface dispersion of decatungstate and to a better substrate supply. The same group of researchers has prepared a new hybrid photocatalyst by embedding the fluorous-tagged decatungstate $(R_fN)_4W_{10}O_{32}$ (R_fN = $[CF_3(CF_2)_7(CH_2)_3]_3CH_3N^+$) within fluoropolymeric films, like Hyflon® [86, 87]. The perfluoropolymer has thermal and oxidative resistance and high permeability of O_2. The resulting hybrid materials exhibit remarkable activity in the solvent-free oxygenation of benzylic hydrocarbons. As an example, with tetraline and indane high turnover numbers (> 6000) are obtained.

A very new generation of catalytically active membranes has been developed by using low-temperature-plasma surface modification technique, which allows to modify or functionalize by grafting, in a controlled way, only the topmost few layers of membranes while retaining their mechanical, physical and bulk properties. Poly(vinylidene fluoride) (PVDF) membrane is modified by plasma treatment to graft amino groups at its surface, which, in turn, are used as anchor groups for the immobilization of decatungstate and of phosphotungstic acid ($H_3PW_{12}O_{40}$) in a highly precise way [88, 89]. These novel heterogeneous systems, used for the complete aerobic degradation of phenol, exhibit improved photocatalytic performances with respect to the corresponding homogeneous systems. Although no applications for synthetic purposes are present in literature up today, we consider these results as a first successful example of plasma treatments

applied for the heterogenization of polyoxotungstates on polymeric membranes.

2. IRON PORPHYRINS

2.1 GENERAL FEATURES

Porphyrins are macrocycles composed of four pyrrole subunits interconnected at their α carbon atoms via methine bridges (=CH-). Porphyrins obey Hüchel's rule for aromaticity, possessing (4 n + 2) π electrons delocalized over the macrocycle leading to a highly-conjugated system. As a consequence, they typically present very intense absorption bands in the visible region and are deeply coloured.

Metalloporphyrins have demonstrated a significant catalytic ability in a wide variety of reactions over the last 30 years. In particular, Fe (III) porphyrins are well known for their ability to catalyze the oxidation of various substrates including inert molecules such as alkanes under mild conditions in the presence of an oxygen atom donor. For this reason, they are considered to be able to mimic the catalytic cycle of cytochrome P450-dependent monooxygenases [90-95]. The main problem in catalysis by iron porphyrins is the stability of the ring that easily undergoes radical attacks that open the macrocycle. One approach to solve this problem has been the introduction of *meso*-aryl substituents on the porphyrin periphery (Figure 6). These protect methinic groups and produce more robust and resistant catalysts [96-99].

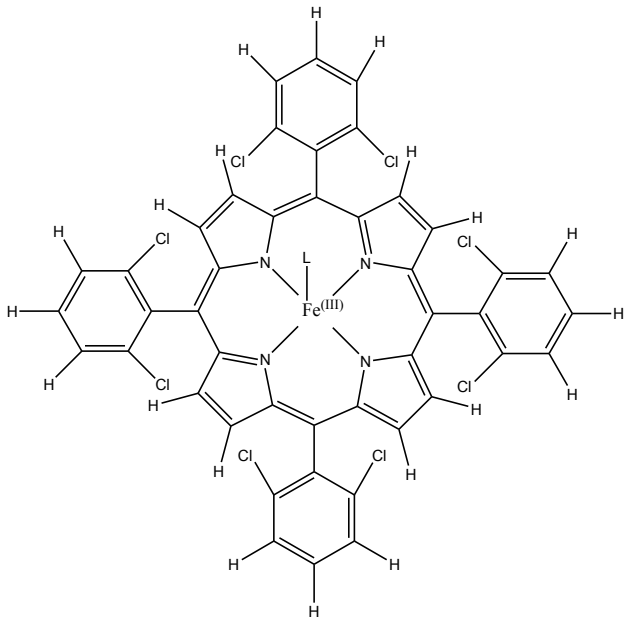

Figure 6. Structure of iron(III) *meso*-tetrakis(2,6-dichlorophenyl)porphyrin – Fe(III)(TDCPP).

In this doctoral thesis a derivative of the iron (III) *meso*-tetrakis(2,6-dichlorophenyl)porphyrin - Fe(III)(TDCPP) reported in Figure 6 has been considered. In this complex eight chlorine atoms are in the *ortho* positions of the *meso*-aryl groups and provide a steric protection of the porphyrin ring against its radical induced oxidative degradation [100].

2. 2 PHOTOCATALYTIC ACTIVITY OF IRON PORPHYRINS

On the basis of their photochemical activities, metalloporphyrins can be divided in two main groups: 1) emitting and 2) no emitting complexes. Iron porphyrins belong to the group of no emitting porphyrins, since the metal is open shell and the excited states have very short lifetimes. For this reason bimolecular reactions are not allowed for them [101]. However, iron porphyrins can undergo photoinduced intramolecular charge transfer processes. In particular, irradiation in the near ultraviolet region can induce

an electron transfer from the axial ligand to the metal centre [102, 103]. As a consequence of this process, Fe^{III} is reduced to Fe^{II} and the axial ligand is oxidized to a radical species (Figure 7).

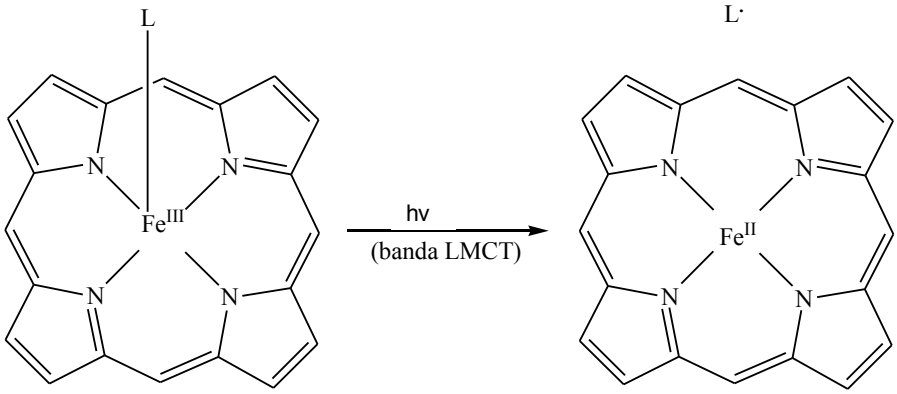

Figure 7. Primary photochemical process of iron (III) porphyrin complexes

The validity of this mechanism has been demonstrated following both the photo reduction of iron(III) through pulsed laser flash photolysis or spectrophotometric measurements under continuous irradiation and the formation of radicals through EPR spectroscopy. Several axial ligands that can undergo this photo-oxidation process are: alcohols, azide, imidazole, pyridine, halides. The rate of recombination of the photogenerated radical with the reduced iron depends on various factors such as the nature of the ring and of the axial ligand.

It has been demonstrated that Fe(II) formation is the key step for reductive oxygen activation. In fact, O_2 coordination on Fe(II) leads to an iron (III)-superoxide complex (equations 1-4 in Scheme 1).

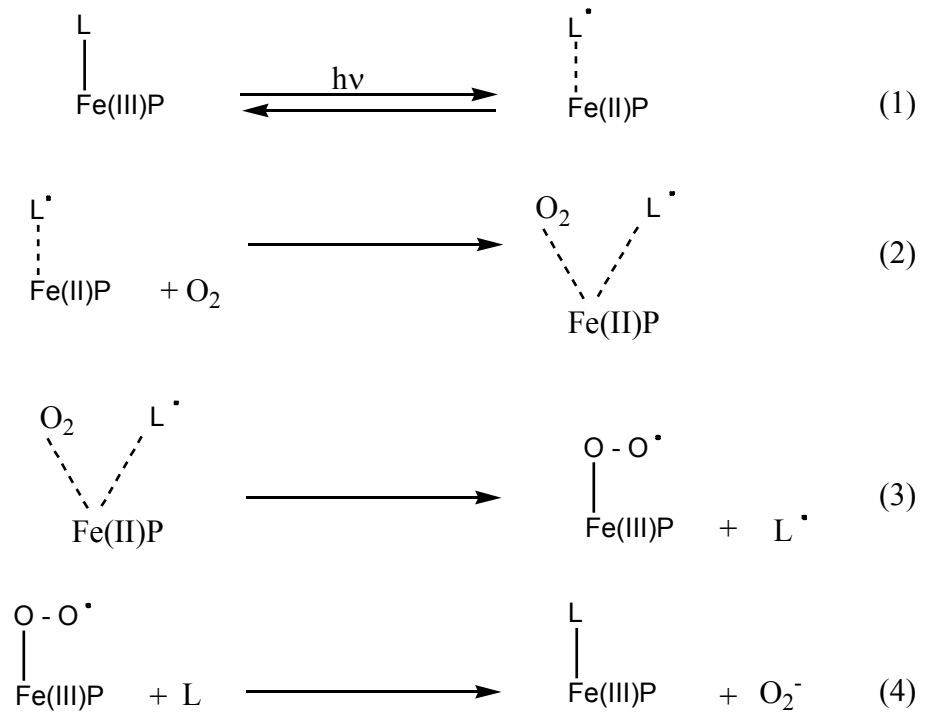

Scheme 1. Primary photochemical processes of iron (III) porphrins in aerated conditions.

Moreover, the formation of a radical species from the axial ligand can initiate the oxidation of inert substrates such as alkanes [104-109].

2. 3 HETEROGENIZATION OF PORPHYRINS

Heterogenization of metalloporphyrins has a number of advantages compared to homogeneous catalysis:

a) the support can stabilize the porphyrin preventing the formation of μ-oxo dimers that are photochemically inactive,

b) recovery and recycling of the catalyst are easy,

c) any problems of solubility of the catalyst are avoided.

It is also to outline that the matrix structure can provide a better selectivity, by controlling the approach of the substrate to the active sites of

the immobilized metallocomplex, where the catalytic oxidation takes place. In general, immobilization methods include physical entrapment, covalent or ionic bonding or surface adsorption.

2. 3. 1. *TYPES OF SUPPORTS*

The employed supports must satisfy a number of requirements:

a) their interaction with the metal porphyrin must be strong enough to prevent the release of the complex in solution;

b) they must be very resistant to oxidation for not competing with the substrate, decreasing the efficiency of the desired process;

c) the reaction rate should remain appreciable; a good distribution of the substrate around the catalytic site must be accomplished.

Many different inorganic and organic solids have been investigated as supports for metalloporphyrin immobilization (Figure 8): inorganic solids, such as silica, alumina, zeolites and clays, cross-linked organic polymers, such as polystyrenes/divinylbenzene resins and Nafion membranes, micelles.

The techniques for anchoring metal porphyrins on supports are quite different and can be summarized as follows:

- a covalent bond between porphyrin and support [110] provides a good stability;
- ionic interactions between anionic or cationic porphyrins and supports containing groups of opposite charge [111-113];
- copolymerization of the catalyst with the support [114] to give a polymer matrix in which the porphyrin is attached as a monomer.

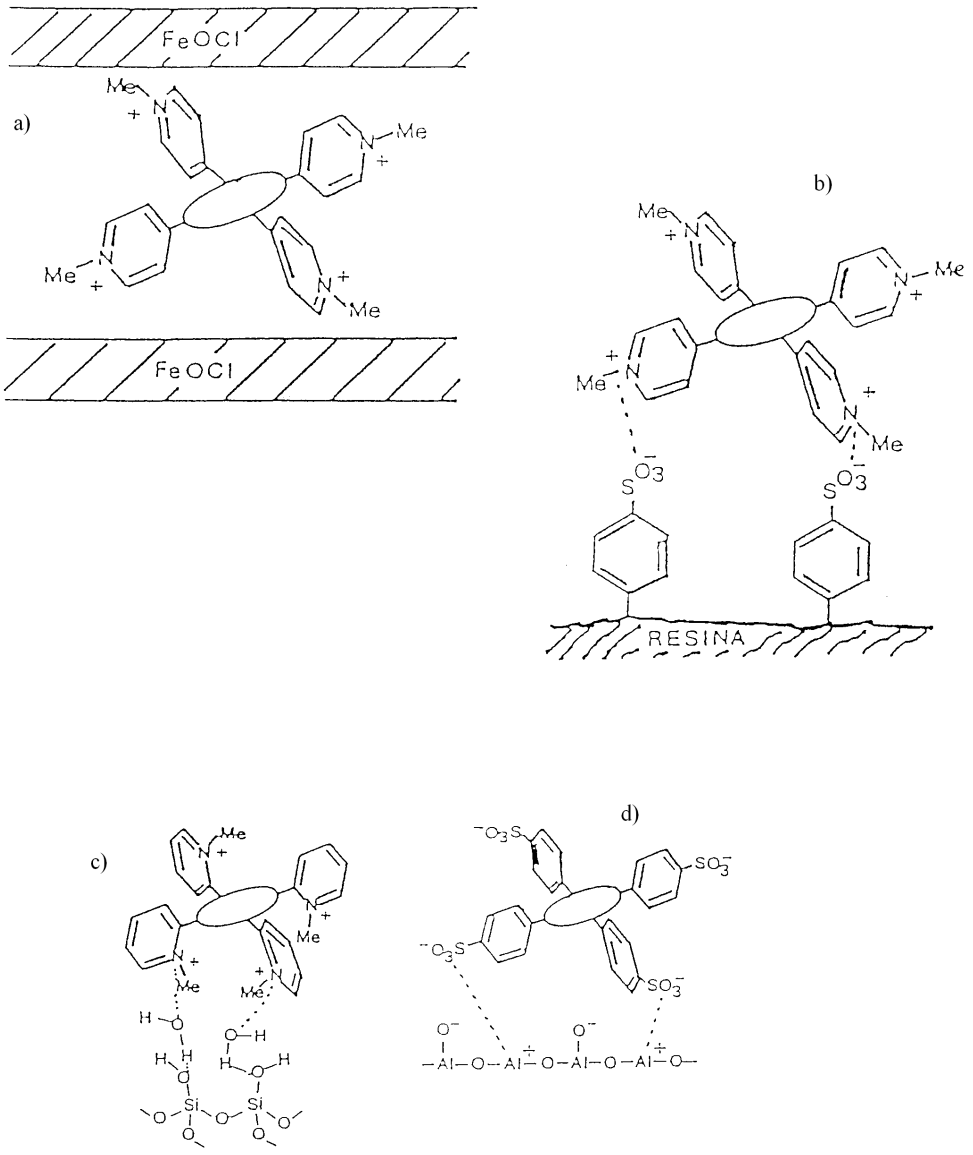

Figure 8. Several types of materials used to support metal porphyrin complexes: a) lamellar inorganic matrices, b) polymeric resin, c) silica, d) alumina

Porous networks containing metalloporphyrins have proven to be potentially applicable as efficient heterogeneous catalysts [115] after immobilization of the complex in organic polymers, or inorganic matrices, such as silica [116-117], zeolites [118, 119], clays [120-122], layered double hydroxides [123, 124], tubular and fibrous matrices, [125] silica matrix

obtained by the sol-gel process [126-133]. Catalyst immobilization enables site-isolation of the metal center and it is one of the approaches aimed to reduce metalloporphyrin degradation since it prevents molecular aggregation or bimolecular self-destruction reactions, [130] which all lead to deactivation of the catalytically active metalloporphyrin species [129, 131]. It has been reported that metalloporphyrins containing electron-withdrawing substituents [134] immobilized on inorganic supports leads to efficient and selective catalysts for hydrocarbon oxidation. The inorganic support can provide a peculiar environment around the active species, which would not occur in homogeneous medium. In the sol-gel methodology, control of the preparation conditions can easily alter the structure and properties of the obtained materials. As already reported [126], the presence of porphyrins can contribute to the polymerization of the silica network. In 2010 Castro et al. reported [135] about preparation of catalysts based on iron (III) porphyrins heterogenized on silica obtained by sol-gel route, using the Stöber methodology, to obtain spherical particles [136].

The photocatalytic activity of iron (III) porphyrin complexes is maintained after heterogenization. In fact, the primary photochemical act of Fe(III)TDCPP hosted inside different heterogeneous and microheterogeneous systems is the reduction of the metal center and the oxidation of the axial ligand to a radical species, as shown in equations of Scheme 1. Fe(III)TDCPP(Cl) has been physically entrapped inside cross-linked polystyrene using solvent-dependent swelling. Its photoexcitation in the presence of cyclohexene leads to the formation of allylic oxidation products with a quantum yield of 2.2×10^{-2} at 365 nm [137].

Some researches investigated the photocatalytic behaviour of Fe(III)TDCPP in micellar aggregates. The use of micelles has some positive implications such as i) optically transparent solutions readily amenable to photochemical investigation, ii) water as a medium for carrying out organic transformations and iii) reagents and reaction intermediates confined in small hydrophobic cavities [138]. For example, N,N-dimethyltetradecylamine N-oxide (DTAO)

is able to dissolve Fe(III)TDCPP and considerable amounts of cycloalkenes. The photocatalytic process occurs mainly in the non-polar region of the micelles and the reactivity of reaction intermediates and therefore the chemoselectivity of the oxidation process is controlled by the microenvironment [139].

Nafion is an optically transparent polymer consisting of a perfluorinated backbone connected to sulphonic groups through short chains of perfluoropropylene ether. The monocationic iron porphyrin Fe(III)TDCPP(iPrOH) can be caged inside the anionic cavities of Nafion simply by swelling the membrane in an alcoholic medium [112, 113]. The system favours reactions in proximity of the metal center inhibiting autooxidation processes in the solution bulk. Thanks to the great affinity of Nafion for O_2, heterogenization inside these membranes significantly improves both efficiency and stability of the iron porphyrin photocatalyst. Concerning the selectivity, the presence of cyclohexene epoxide, that is not formed in homogeneous conditions, is an indication of the involvement of biomimetic high-valent intermediates of the iron porphyrin.

RESULTS AND DISCUSSION

1. Photocatalytic properties of tetrabutyl-ammonium decatungstate incorporated into sol-gel silica in the oxidation of aliphatic alcohols.

Photocatalysis with polyoxotungstates (POTs) for oxidation reactions continues to be the object of intense research [8, 24, 29, 30]. In particular, photocatalysis with decatungstate anion $W_{10}O_{32}^{4-}$ is interesting because it may be carried out with i) molecular oxygen, a wide available and cheap oxidant; ii) under mild temperature and pressure conditions; iii) by illumination with sunlight, a completely renewable source of energy that allows the conception of short and efficient reaction sequences, minimizing side processes [8, 9, 24, 29, 30, 62, 140-143].

As reported in the introduction of this thesis, considerable attention has been recently focused on heterogenization of $W_{10}O_{32}^{4-}$ [59, 64-66, 71, 81, 84-87, 144, 145]. Much attention is devoted to the design of these heterogeneous photocatalysts to tailor efficiency and selectivity of oxidation processes through control of the microscopic environment surrounding the catalytic centre.

For this, I prepared two photoactive materials by entrapment of $W_{10}O_{32}^{4-}$ in a silica matrix with different decatungstate loadings, following a previously reported sol-gel procedure [146]. Chemical-physical characterization of these materials has been studied in detail. The effect of the hydrophobic/hydrophilic surface character, the porosity and surface area were related to the reactivity of primary and secondary aliphatic alcohols. The results of this study have been the object of an article published in Dalton Transactions [15].

1. 1 EXPERIMENTAL SECTION

1. 1. 1 SYNTHESIS OF $(n\text{-}Bu_4N)_4W_{10}O_{32}$

Tetrabutylammonium decatungstate $[(n\text{-}Bu_4N)_4W_{10}O_{32}]$ was obtained following a literature procedure [147, 148] . The salt was prepared by mixing boiling solutions of $Na_2WO_4{\cdot}2H_2O$ (4 g in 25 mL of water) and of HCl (3 M, 8.4 mL) upon vigorous stirring. The gelatinous precipitate locally formed disappears. After boiling for a few minutes, the clear yellow solution was precipitated by addition of an aqueous solution of $(n\text{Bu}_4N)Br$ (1.6 g in 2.5 mL). The pale yellow precipitate was filtered, washed with boiling water, ethanol, and finally diethyl ether, dried with air and then recrystallized from CH_3CN at 80 °C by cooling the solution at room temperature. The yellowish prismatic crystals thus obtained are washed with diethyl ether and air-dried [UV-vis in CH_3CN: 323 nm; IR (pellets of KBr): 958 (vs), 942 (s), 801 (vs), 405 (vs), 331 (m) cm^{-1})].

1. 1. 2. SYNTHESIS OF $(n\text{-}Bu_4N)_4W_{10}O_{32}/SiO_2$

The composite photocatalysts $(n\text{-}Bu_4N)_4W_{10}O_{32}/SiO_2$ was synthesized following a literature procedure, with some modifications, concerning the preparation of microporous POMs by a sol-gel technique [144, 149] . The reaction pathway is illustrated in Scheme 2. Tetraethyl-orthosilicate (TEOS) was selected as silica source. The process consists in the hydrolysis of TEOS in the presence of $(n\text{-}Bu_4N)_4W_{10}O_{32}$ at pH 2.0. During TEOS hydrolysis, subsequent slow dehydration and final calcination, the POM cluster was entrapped into the porous silica network.

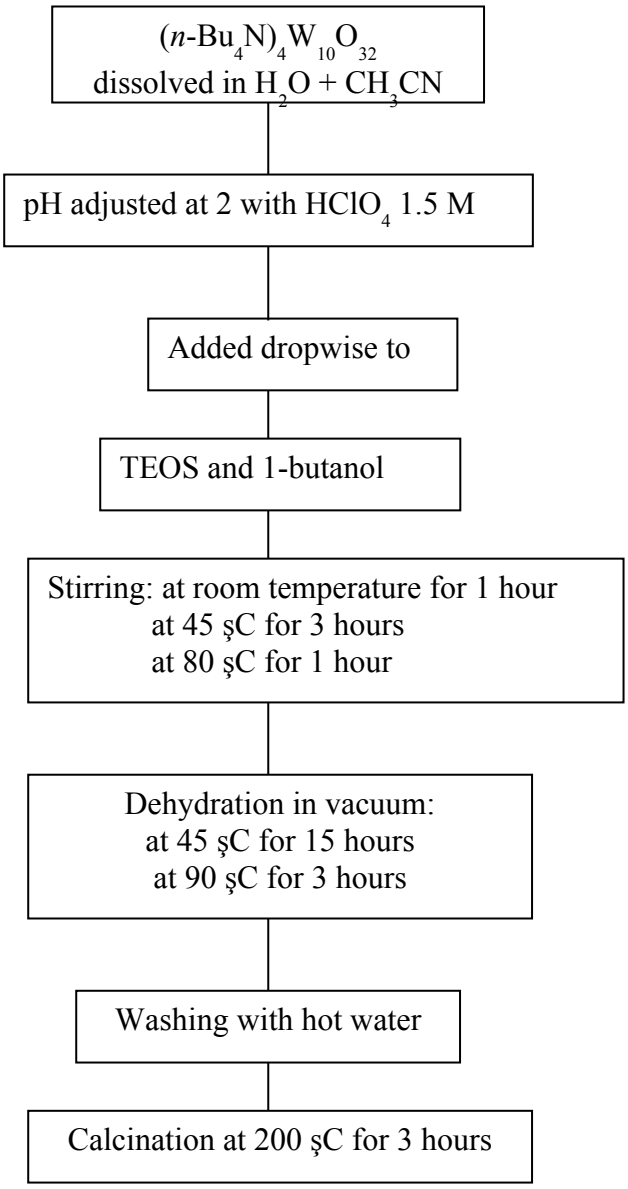

Scheme 2. Reaction pathway for the preparation of silica supported microporous $W_{10}O_{32}^{4-}$

In particular, $(n\text{-}Bu_4N)_4W_{10}O_{32}$ was dissolved in a mixture of CH_3CN and H_2O (0.5 g in 10 mL of CH_3CN and 5 mL of H_2O). Then, the acidity of the solution was adjusted to pH 2 with $HClO_4$ (1.5 M). After acidification, the solution was added dropwise to a mixture of TEOS and 1-butanol (5 mL and 4.5 mL respectively). The obtained mixture was stirred at room temperature

for 1 h, at 45 ºC for 3 h and finally at 80 ºC for 1 h. The pH was maintained at 2 by adding $HClO_4$ during the course of the reaction. The hydrogel obtained was slowly dehydrated at 45 ºC for 15 h and then at 90 ºC for 3 h in a rotary evaporator. The particulate gel was extracted with water at 90 ºC several times until the filtrate was neutral and then the product was calcined at 200 ºC for 3 h. On the basis of the solid mass obtained at the end of the preparation and the initial amount of $(n\text{-}Bu_4N)_4W_{10}O_{32}$ used, it has been possible to estimate that the prepared material $(n\text{-}Bu_4N)_4W_{10}O_{32}/SiO_2$ contained 30% (w/w) of decatungstate (SiO_2/W30%). A second photocatalyst was obtained simply by washing the first sample SiO_2/W30% several times with aliquots of CH_3CN until tetrabutylammonium decatungstate was no longer released in detectable amounts into the solvent. CH_3CN was chosen because it is the only solvent with a good affinity for $(n\text{-}Bu_4N)_4W_{10}O_{32}$. On the basis of the UV-vis spectra of the CH_3CN aliquots employed in the washing, we could estimate that the new sample (SiO_2/W10%) contained 10% w/w of $(n\text{-}Bu_4N)_4W_{10}O_{32}$. Moreover, a sample not including decatungstate (SiO_2) was also prepared, following the procedure described above but without adding $(n\text{-}Bu_4N)_4W_{10}O_{32}$.

1. 1. 3 TEXTURAL CHARACTERIZATION

Diffuse reflectance UV/vis spectra were recorded with a Jasco V-570 using an integrating sphere and $BaSO_4$ as reference. The plotted spectra were obtained by the Kubelka-Munk transformation ($F(R) = 1 - R^2/2R$) versus the wavelength.

IR spectra were recorded with a Bruker Vertex 70 instrument, fitted with a Spectra-Tech collector diffuse reflectance attachment. KBr pellet technique was used. A solid sample was ground into a very fine powder and, then, the spectrum was recorded. The results were analyzed by Bruker Opus 6.5 software.

The morphology of the solid samples was investigated with a Hitachi H-800 transmission electron microscope (TEM). The sample for TEM analysis was prepared by dropping a water dispersion of the photocatalyst on a copper grid.

N_2 adsorption-desorption experiments were carried out at 77 K by means of ASAP2020 instrument (Micromeritics). Before each measurement, the sample was outgassed overnight at 150 ºC with a rotative pump (residual pressure about 10^{-2} mbar).

1. 1. 4 ADSORPTION EXPERIMENTS

Adsorption experiments were carried out by suspending each photocatalyst (33 g L^{-1}) in 300 µl of CH_3CN or CH_2Cl_2 solutions containing increasing concentrations of alcohol and keeping in the dark for 20 minutes under magnetic stirring. The amount of adsorbed alcohol was obtained evaluating its concentration decrease in the solution by gas chromatographic analysis. For sensitivity reasons, these experiments have been carried out reducing the volume of alcohol employed and increasing the amount of solid sample in respect to the photocatalytic experiments (see next paragraph).

1. 1. 5 PHOTOCATALYTIC EXPERIMENTS

Solvents were UV grade, alcohols used as substrates and corresponding aldehydes and ketones used as standards were purchased in the highest purities available from Sigma-Aldrich and employed without further purification.

Photocatalytic experiments were carried out inside a Pyrex tube of 15 mL capacity at 298 ± 1 K. The desired amount of photocatalyst (8 g/L) was suspended in 3 mL of suitable solvent containing the alcohol under investigation (5 x 10^{-3} M), ultrasonicated for 20 min and then magnetically stirred for other 20 min before irradiation. SiO_2/W10% was dispersed both

in CH_3CN and CH_2Cl_2, while suspensions of SiO_2/W30% were feasible only in CH_2Cl_2 in order to prevent the unavoidable leaching of $(n\text{-}Bu_4N)_4W_{10}O_{32}$ in CH_3CN. The pyrex photoreactor was filled with O_2 and then joined through an inlet tube to a balloon filled with O_2. Photochemical excitation was performed by irradiating the Pyrex tube with an external Helios Q400 Italquartz medium-pressure Hg lamp, selecting wavelengths higher than 290 nm with a cut off filter for 60 min. The photon flux, measured with a MACAMUV203X ultraviolet radiometer, was 15 $mWcm^{-2}$.

At the end of the photocatalytic experiment, the sample was centrifuged, the products adsorbed on the irradiated powders were extracted with CH_2Cl_2 (2 x 3 mL), and the organic phases were analyzed by gas-chromatography. Product analyses were carried out using a HP 6890 gas chromatograph equipped with a flame ionisation detector. HPWAX capillary column (cross-linked polyethylene glycol, 30 m, internal diameter 0.32 mm, film thickness 0.50 μm) was used for pentanols and heptanols, when CH_2Cl_2 was the dispersing medium, while DB 624 capillary column (30 m, internal diameter 0.32 mm, film thickness 0.18 μm) was employed for pentanols and heptanols, when CH_3CN was used as solvent. The programme temperature was 333 K (5 min), 10 K/min, 433 K (20 min) when HPWAX capillary column was used and 343 K (5 min), 10 K/min, 443 K (3 min) when DB-624 capillary column was employed. Quantitative analyses were performed with calibration curves obtained with authentic samples. Each experiment was repeated three times in order to evaluate the error, which remained in the ± 5% interval around mean values. Homogeneous photocatalytic experiments were carried out dissolving $(n\text{-}Bu_4N)_4W_{10}O_{32}$ in CH_3CN solutions containing the alcohol (5 x 10^{-3} M). The decatungstate concentration in these solutions (2 x 10^{-4} M) warranted the complete absorption of the incident photons. After irradiation, the samples were analyzed as described above.

Control experiments were run irradiating SiO_2 (8 g/L) suspended in CH_3CN or CH_2Cl_2 solutions containing an alcohol (5 x 10^{-3} M) or keeping

SiO_2/W10% (or SiO_2/W30%, 8 g/L) dispersed in the solution containing the alcohol in the dark.

Other experiments were carried out in order to test the stability of SiO_2/W10%: after a photocatalytic run, the used photocatalyst was separated from the reaction mixture, washed with CH_2Cl_2 and CH_3CN, dried at 50 ºC for one hour and then recycled for a subsequent photocatalytic experiment. This procedure has been repeated 3 times. The possible release of polyoxoanion in the solution phase was evaluated by UV-vis analysis of the solution before and after irradiation.

1. 1. 6 DETERMINATION OF CO_2

In order to establish the amount of carbon dioxide eventually formed, samples prepared as described in the previous paragraph were irradiated maintaining the reactor firmly closed. Experiments were carried out using CH_2Cl_2 as dispersing medium. At the end of irradiation, 3 mL of a NaOH solution (0.1M) were put inside the reactor with a syringe and mixed with the irradiated solution. Then, 2.5 mL of the aqueous solution were taken and kept into a vial. After the addition of 1 mL of a saturated citric acid solution, carbon dioxide released was measured by pH meter BasiC 20 CRISON equipped with the gas sensing probe (Crison 9666). Quantitative analysis was made through a calibration curve built from standard solutions of $NaHCO_3$. Results obtained from the irradiated samples were compared with those coming from analogous samples kept in the dark for the same period.

1. 2 TEXTURAL CHARACTERIZATION

Textural characterization has been carried out at the University of Torino in collaboration with Dr. Giuliana Magnacca.

Figure 9 reports the UV-vis spectra of SiO_2/BuW10% and of SiO_2. It is seen that the material containing decatungstate still presents an intense absorption at wavelengths in the range 300-400 nm, typical of $W_{10}O_{32}^{4-}$. This absorption

is not present in SiO_2 indicating that the polyanion has been supported without modifications.

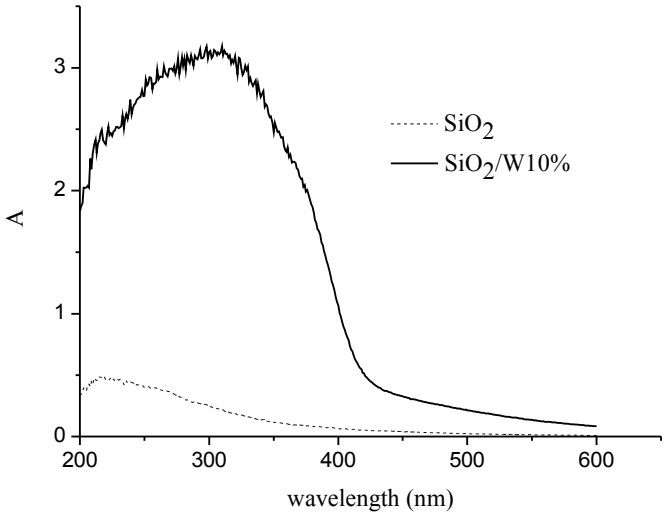

Figure 9. UV-vis spectra of SiO_2/W10% and of SiO_2.

Figure 10 shows the IR spectrum of SiO_2/W30% and that of (n-$Bu_4N)_4W_{10}O_{32}$ for comparison. It is seen that the infrared pattern of decatungstate from 2000 to 500 cm^{-1} is maintained in the heterogeneous system. Moreover, Fig. 10 gives also evidence that n-Bu_4N^+ cations do not undergo any significant modification during the heterogenization procedure, since the C-H bond stretching at about 2870 cm^{-1} is retained.

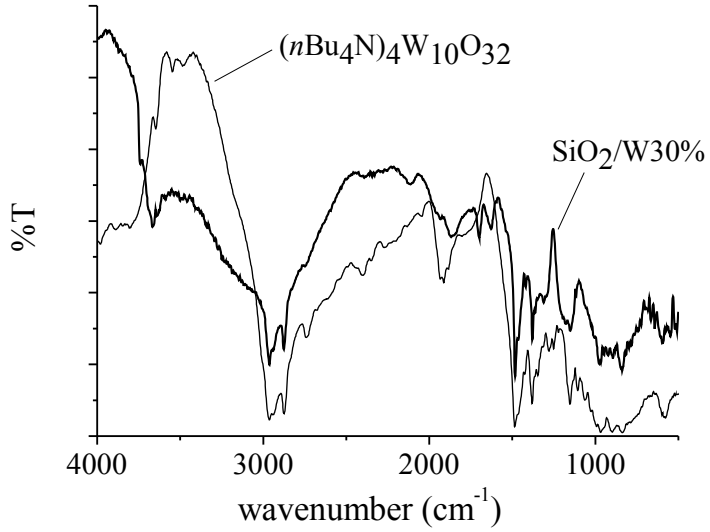

Figure 10. IR spectra (n-$Bu_4N)_4W_{10}O_{32}$ and of SiO_2/W30%.

Therefore, UV-vis and infrared spectroscopic measurements indicate that the structure of (n-$Bu_4N)_4W_{10}O_{32}$ is retained after its heterogenization to give SiO_2/W30% and SiO_2/W10%. TEM images reported in Figure 11 reveal that both SiO_2/W30% and SiO_2/W10% powders are composed of aggregates of fine particles that posses spherical morphology and a size distribution in the range 20-50 nm.

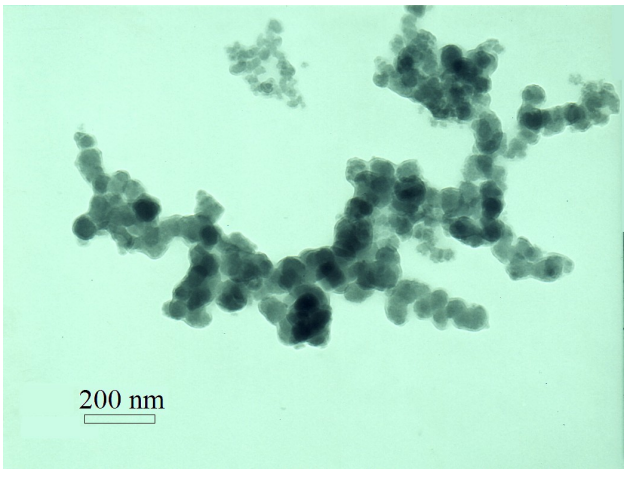

Figure 11. TEM images of SiO_2/W10%.

Gas-volumetric adsorption of N_2 at 77 K gives important information about the morphological features of SiO_2/W10%, SiO_2/W30% and SiO_2. As far as the surface specific area is concerned, we characterized the SiO_2/W10% and SiO_2/W30% samples by means of the BET [150] method and SiO_2 using the Langmuir [151] model because of the extensively microporous nature of this sample. This choice is due to the fact that the BET method, which is based on the formation of adsorbed multilayers on the material, is not appropriate for a microporous system: in cases like the present one, it is much better to apply the Langmuir model, which considers a single layer of N_2 molecules to be formed in the very small microporous cavities of the solid. Table 3 reports the specific surface areas of SiO_2, SiO_2/W10% and SiO_2/W30%.

Table 3. Morphological features of decatungstate-containing SiO_2–based materials.

Sample	SSA/m^2g^{-1}	V_{tot}/cm^3g^{-1}	V_{micro} (<15 Å width, cm^3 g^{-1})	V_{meso} (>15 Å width, cm^3 g^{-1})
SiO_2	772	0.176	0.131	0.045
SiO_2/W30%	394	0.185	0.098	0.087
SiO_2/W10%	544	0.250	0.148	0.102

Mesoporosity and microporosity of analogous composite materials were previously evaluated [72, 144, 145, 149] with good results by means of Barret-Joyner and Halenda (BJH) [152] and Horvath-Kowazoe (HK) [153] models. In the systems investigated here, the presence of a class of pores (vide infra) on the boundary between the two kinds of porosities, that can be typically investigated with BJH and HK methods, makes the separate determination of the meso and micro porosities with these two models quite not exhaustive. In fact, it is known that the BJH model is not able to determine quantitatively mesopores with diameters smaller than 20 Å. Moreover, the HK model underestimates micropores with widths of about 10-15 Å. In order to overcome this problem, we employ here isotherm deconvolutions in accordance with Density Functional Theory (DFT), which considers both micro- and mesoporosity at the same time [154]. This DFT

method is based on a software developed by Micromeritics for carbons [155], subsequently extended to other kind of materials. The pore volumes reported in Table 3 and Figure 12 are classified on the basis of the pore size distribution determined via the DFT method and quantified considering the DFT cumulative pore volume curves. The porosity examined through this method gives good results in the isotherm simulation considering slit-shaped pores.

Figure 12 shows the incremental pore volume as a function of the pore width obtained via the DFT method and allows us to recognize the fraction of pores with widths between 10 and 20 Å. It is seen that SiO_2/W30% is characterized by the presence of micropores with width of about 7 Å, in agreement with previous literature data on the entrapment of polyoxometalates in silica matrices via sol-gel techniques [72-74, 77, 85, 144, 146]. In addition to these micropores, SiO_2/W30% also contains micropores around 15 Å and mesopores around 25 Å.

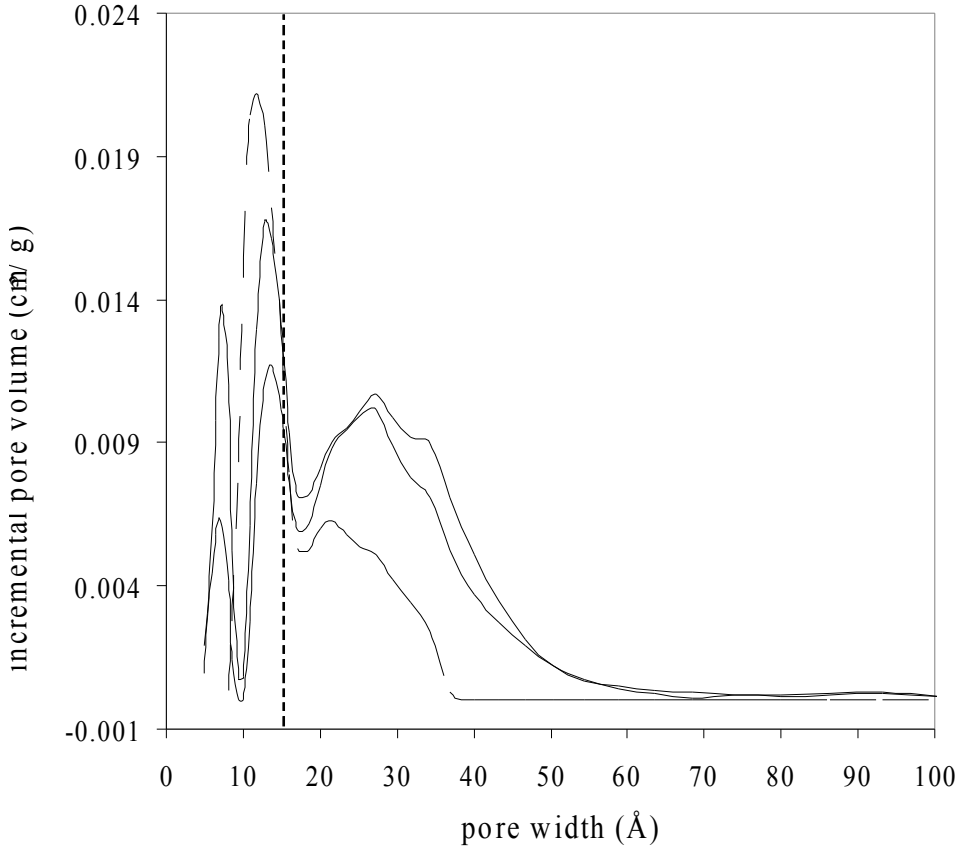

Figure 12. DFT pore analysis (slit pores) for SiO_2/W30% (broken line), SiO_2/W10% (solid line) and SiO_2 (dotted line). The vertical broken line represents the threshold value (15 Å) between micro- and mesopores.

Table 3 and Figure 12 show that morphological features of SiO_2/W30% differ markedly from those of its parent material SiO_2. In particular, SiO_2 does not contain 7 Å micropores, but is characterized by a high degree of microporosity at about 12 Å in width (about 75% of the total volume from Table 3). Moreover, SiO_2 presents a degree of mesoporosity lower than that of SiO_2/W30%. These results indicate that the incorporation of the decatungstate precursor during the synthesis of the silica-based photocatalyst induces a significant modification of the porous texture of the siliceous material, suggesting that the tetrabutylammonium decatungstate can act as a templating agent during the formation of the porous material.

The data in Table 3 and Figure 12 give also evidence that there are significant differences between the morphologies of SiO_2/W30% and SiO_2/W10%. In particular, the total pore volume and specific surface area of SiO_2/W10% are markedly higher than those of SiO_2/W30%. These differences may be due to the removal of the decatungstate not firmly incorporated inside the silica network and weakly adsorbed on the external surface. In fact, the SiO_2/W10% sample is obtained by washing SiO_2/W30% with CH_3CN until the decatungstate is no longer leached in detectable amounts. The strength of the interaction of $(n\text{-}Bu_4N)_4W_{10}O_{32}$ with silica in composite systems prepared via sol-gel technique has been discussed in literature: porous nature of the silica network and adsorption phenomena due to electrostatic interactions between ≡Si-OH groups and $(n\text{-}Bu_4N)_4W_{10}O_{32}$ are proposed to prevent the removal of the polyoxoanion from this kind of material [66, 72, 149]. Moreover, hydrogen bonding between the oxygen atoms of the polyoxoanion and the ≡Si-OH groups of silica should also contribute to the adsorption of $(n\text{-}Bu_4N)_4W_{10}O_{32}$ on the silica matrix as suggested by previous investigations on the modes of the decatungstate adsorption on zirconia [77]. The possibility of stronger interactions, which exist in the composite $H_3PW_{12}O_{40}/SiO_2$ and $Na_4W_{10}O_{32}/SiO_2$ systems, between the protonated silanol groups $\equiv Si\text{-}OH_2^+$ and the polyoxoanion, is somewhat remote in $(n\text{-}Bu_4N)_4W_{10}O_{32}$ photocatalyst, because of the relatively strong electrostatic interaction between the large cation $(n\text{-}Bu_4N)^+$ and $W_{10}O_{32}^{4-}$ [72].

Considering the relatively high size of the decatungstate (about 25 Å long and 8 Å wide), the removal of "external" $(n\text{-}Bu_4N)_4W_{10}O_{32}$ is expected to uncover some mesopores of SiO_2/W30%, and above all, to render available a large number of micropores, probably blocked by the presence of the large anionic species: this yields a material with a more remarkable porous network. In fact, from the data in Table 3 and Figure 12 we can determine that, while the volume of mesopores increases by 17% upon converting SiO_2/W30% to SiO_2/W10%, the corresponding increase in the

micropore volume is about 51%. This accounts for the 40% increase in specific surface area passing from SiO_2/W30% to SiO_2/W10%.

1. 3 PHOTOCATALYTIC ACTIVITY

The photocatalytic activity of SiO_2/W10% has been assessed studying the oxidation of 1-pentanol, 2-pentanol and 3-pentanol dissolved in CH_3CN or CH_2Cl_2. The well known ability of photoexcited $(nBu_4N)_4W_{10}O_{32}$ to induce oxidation of alcohols is retained inside the silica network [9, 13, 24, 29, 62, 140-142]. In fact, photoexcitation with light of wavelengths higher than 290 nm, at room temperature and under 760 torr of O_2, leads to the conversion of 1-pentanol, 2-pentanol and 3-pentanol to pentanal, 2-pentanone and 3-pentanone, respectively. In all cases, we were able to estimate that the mass balance between detected products and reacted alcohol was about 90%. Moreover, carbonylic products accounted for about 95% of the overall gas chromatographic areas of the detected photoproducts. Control experiments carried out by irradiating a powder dispersion of the raw silica material SiO_2 did not lead to the formation of detectable amounts of oxidation products, allowing us to rule out the possibility that some kind of photoactivation of the silica support occurs. Additional control experiments indicate that no oxidation products are formed after the contact between the heterogenized decatungstate and the alcohol in the absence of light.

The cascade of events that follow the absorption of light by $W_{10}O_{32}^{4-}$ has been already discussed in the Introduction of this thesis (see Introduction paragraph 1.3). When the substrate is an alcohol, the very reactive transient wO reacts with it through hydrogen atom abstraction from the C-H bond in the α position to the OH group, leading to the reduced decatungstate and to an organic radical, which, finally, is oxidized to a carbonylic compound (Scheme 3). Molecular oxygen provides for the reoxidation of the photoreduced decatungstate with parallel formation of peroxy compounds.

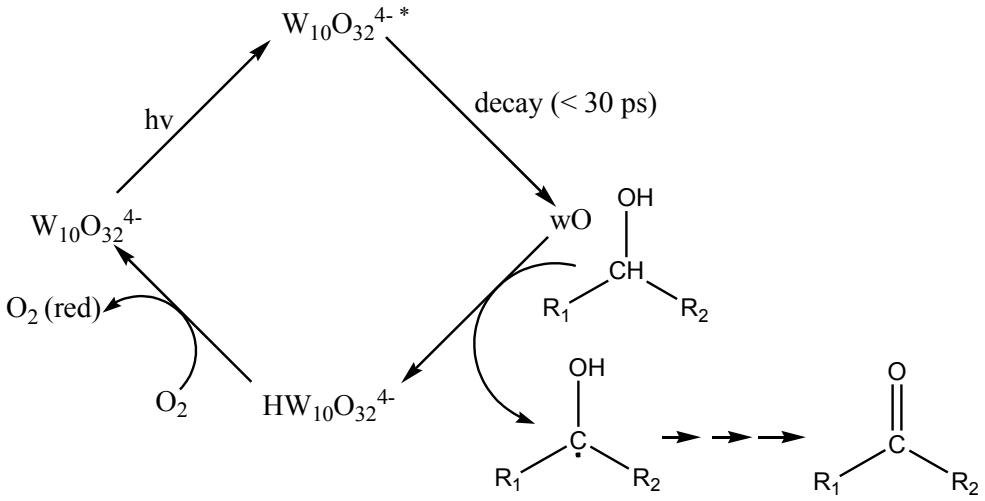

Scheme 3. Photocatalytic behaviour of $W_{10}O_{32}^{4-}$ in the presence of alcohols.

In order to optimise the slurry amount of photocatalyst with respect to absorption of incident light, some photocatalytic experiments were carried out varying the amount of suspended material. Figure 13 reports the concentrations of pentanal and 3-pentanone after one hour irradiation of increasing amounts of SiO_2/W10% dispersed in CH_3CN. This plot shows that, in the concentration range examined, the optimum amount of photocatalyst is 8 g/L for both alcohols. Measurements with an ultraviolet radiometer indicate that 8 g/L of photocatalyst are able to absorb 90% of the impinging radiation at 313 nm, which is the emission line of the employed light source closest to the absorption maximum of $W_{10}O_{32}^{4-}$ at 325 nm. For this reason, this quantity of photocatalyst was used throughout this work to compare the reactivity of all the alcohols investigated.

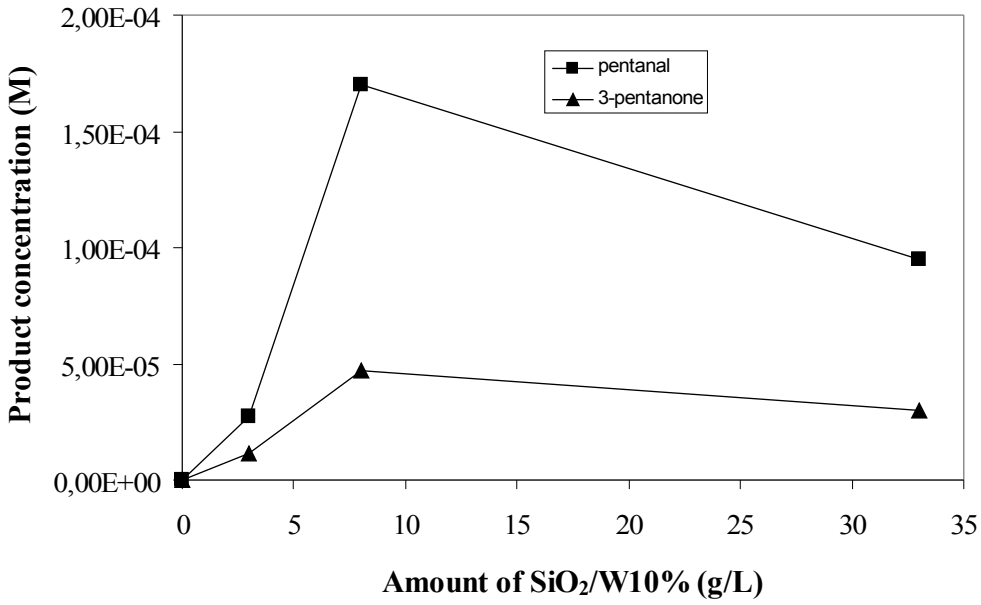

Figure 13. Pentanal and 3-pentanone concentrations obtained after 60 min irradiation ($\lambda > 290$ nm) of increasing amounts of SiO_2/W10% dispersed in 3 mL of CH_3CN, containing 1-pentanol or 3-pentanol 5 x 10^{-3} M. The point corresponding to 0 gL^{-1} of photocatalyst was obtained by irradiating 8 g/L of the raw silica material SiO_2.

Table 4 reports the results of the photocatalytic experiments carried out with SiO_2/W10% dispersed in CH_3CN solutions containing 1-, 2- or 3-pentanol. Results obtained irradiating $(n\text{Bu}_4\text{N})_4\text{W}_{10}\text{O}_{32}$ dissolved in CH_3CN in the presence of pentanols are also reported for comparison. As explained in the experimental section, the photocatalyst SiO_2/W30% could not be used with acetonitrile as dispersing medium. Reported values are μmol of carbonylic products obtained after 60 min irradiation. The relative reactivity of primary and secondary alcohols is reported in the last column of Table 4 in terms of the ratio between the aldehyde and ketone obtained.

Table 4. Photocatalytic oxidation of pentanols in CH_3CN [a]

Exp	Photocatalytic system	Alcohol	Products (μmoles) [b]			
			Pentanal	2-pentanone	3-pentanone	Aldehyde/ ketone
1	$(n\text{-}Bu_4N)_4W_{10}O_{32}$ in CH_3CN	1-pentanol	0.92	/	/	
2		2-pentanol	/	0.97	/	1.0
3		3-pentanol	/	/	0.96	1.0
4	SiO_2/W10% dispersed in CH_3CN	1-pentanol	0.51	/	/	
5		2-pentanol	/	0.28	/	1.8
6		3-pentanol	/	/	0.13	3.9

[a] In a typical experiment SiO_2/W10% (8 g/L) or $(n\text{-}Bu_4N)_4W_{10}O_{32}$ ($2x10^{-4}$ M) were suspended or dissolved in CH_3CN solutions containing the desired alcohol (5×10^{-3} M) and irradiated (60 min, $\lambda > 290$ nm) at 298 ± 1 K and 760 Torr of O_2. Reported values are the mean of three repeated experiments with ± 5% of precision.

[b] Amount of carbonyl compounds as μmoles produced in 3 mL of solution.

Experiments 1, 2 and 3 show the photocatalytic activity of the decatungstate dissolved in CH_3CN solutions of the three alcohols. Under these conditions, efficiency in photooxidation is similar since the molar concentration ratio between aldehyde and both ketones is 1.0. Interestingly, with SiO_2/W10% these values increase to 1.8 for 2-pentanol and to 3.9 for 3-pentanol (Experiments 4-6), indicating that the silica matrix favours the reaction of 1-pentanol with respect to secondary pentanols. We draw attention to the fact that this higher reactivity of 1-pentanol is unexpected if one considers the photooxidation mechanism summarized in Scheme 3, in which hydrogen-atom abstraction by wO should occur preferentially from the secondary carbon atom of alcohol.

The high specific surface area and the porosity of SiO_2/W10% suggest that the hydrophilic character of the silica surface can play an important role in differentiating the reactivity between primary and secondary pentanols during the photocatalytic experiments. For this reason, we decided to carry out some adsorption measurements with 1-pentanol and 3-pentanol, which show the highest aldehyde/ketone ratio, suspending

SiO_2/W10% in CH_3CN containing variable concentrations of alcohols. As mentioned in the experimental part, the volume of alcohol solutions had to be reduced and the amount of solid sample increased in order to minimize the experimental error. More specifically, evaluation of the adsorption degree of 1-pentanol and 3-pentanol was performed suspending the photocatalyst SiO_2/W10% (33 g/L) in 300 μL of CH_3CN containing alcohol at different concentrations. The amount of alcohol adsorbed was then evaluated *via* GC measurements after 20 min of stirring.

Figure 14 indicates that 1-pentanol is adsorbed to a much greater extent than 3-pentanol. This result may be ascribed to the fact that the hydrophilic character of the silica surface favours its interaction with the OH group of the hydrophilic head of 1-pentanol with respect to the OH group of 3-pentanol, placed in the centre of a hydrophobic chain of five carbon atoms. An intermediate situation is probably occurring in the case of 2-pentanol.

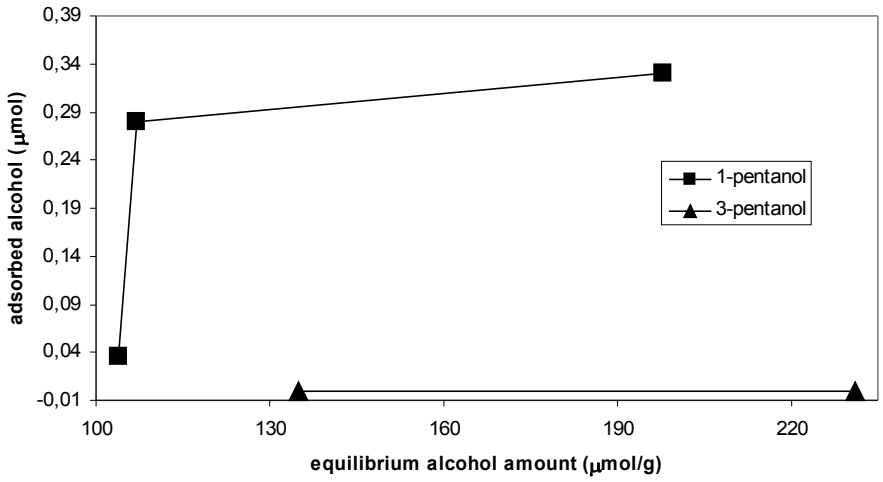

Figure 14. Adsorption of increasing amounts of 1-pentanol and 3-pentanol on SiO_2/W10% (33 g L^{-1}) suspended in 0.3 mL of CH_3CN.

Figure 14 gives also evidence that adsorption of 1-pentanol is greater than that of 3-pentanol from an amount of about 100 μmoles of alcohol per gram of photocatalyst onwards. Therefore, we can infer that the interaction of 1-

pentanol with the silica surface is stronger than that of 3-pentanol also during the photocatalytic experiments, which were carried out in the presence of 500 μmoles of alcohol per gram of SiO_2/W10%. On this basis, we conclude that the alcohol that more readily interacts with the hydrophilic surface of catalyst also interacts better with the photoactive decatungstate groups and undergoes a more rapid oxidation. This statement is in line with obtained yields for the three alcohols (see Table 4) and also with previous investigations on the photooxidation of alcoholic substrates with TiO_2 [156, 157] and with $(nBu_4N)_4W_{10}O_{32}$ covalently bound on the surface of SiO_2 [66].

The importance of surface effects on the photocatalytic activity of SiO_2/W10% is further supported by the finding that the undesired conversion of 1-pentanol to over-oxidized products occurs in homogeneous solutions to a much greater extent than in heterogeneous systems. In fact, pentanal obtained in CH_3CN solutions of $(nBu_4N)_4W_{10}O_{32}$ and quantified by GC measurements constitutes only 75% of all the photoproducts formed (compared with the 95% value obtained with SiO_2/W10%, as reported above). This is easily explainable considering that the photoactive surface of SiO_2/W10% favours the approach of the alcoholic substrate but inhibits, at the same time, the interaction with the photoproduced aldehyde, avoiding its further oxidation.

A second series of photocatalytic experiments has been carried out with 1-, 2- and 3-pentanol in CH_2Cl_2 as dispersing medium and allowed us to compare the properties of the two prepared heterogeneous photocatalysts SiO_2/W10% and SiO_2/W30%. The obtained results are reported in Table 5.

Table 5. Photocatalytic oxidation of pentanols in CH_2Cl_2 [a]

			Products (μmoles) [b]	

Exp	Photocatalytic system	Alcohol	Pentanal	2-pentanone	3-pentanone	Aldehyde/ ketone
1	SiO_2/W10%	1-pentanol	0.72	/	/	
2		2-pentanol	/	0.51	/	1.4
3		3-pentanol	/	/	0.27	2.7
4	SiO_2/W30%	1-pentanol	1.0	/	/	
5		2-pentanol	/	1.1	/	0.9
6		3-pentanol	/	/	0.72	1.4

[a] In a typical experiment the photocatalyst employed (8 g/L) was suspended in CH_2Cl_2 solutions containing the desired alcohol (5×10^{-3} M) and irradiated (60 min, $\lambda > 290$ nm) at 298 $\pm$ 1 K and 760 Torr of O_2. Reported values are the mean of three repeated experiments with $\pm$ 5% of precision.

[b] Amount of carbonyl compounds as μmoles produced in 3 mL of solution.

Experiments 1-3 of Table 5 show that the oxidation of 1-pentanol on SiO_2/W10% is faster than that of 2- and 3-pentanol also when the photocatalytic experiments were carried out in CH_2Cl_2. In fact, aldehyde/ketone ratio is 1.4 in the case of 2-pentanol and raises to 2.7 with 3-pentanol. On the contrary, SiO_2/W30% is less selective than SiO_2/W10%. It is likely that the presence of a higher amount of the organic cations *n*-Bu_4N^+ confers to the surface of SiO_2/W30% a less hydrophilic character with respect to SiO_2/W10% and thus the adsorption of the hydrophilic head of 1-pentanol on SiO_2/W30% is not so favoured. This is confirmed in Fig. 15, which shows that 3-pentanol is preferentially adsorbed on SiO_2/W30% over 1-pentanol. A similar situation is expected for 2-pentanol.

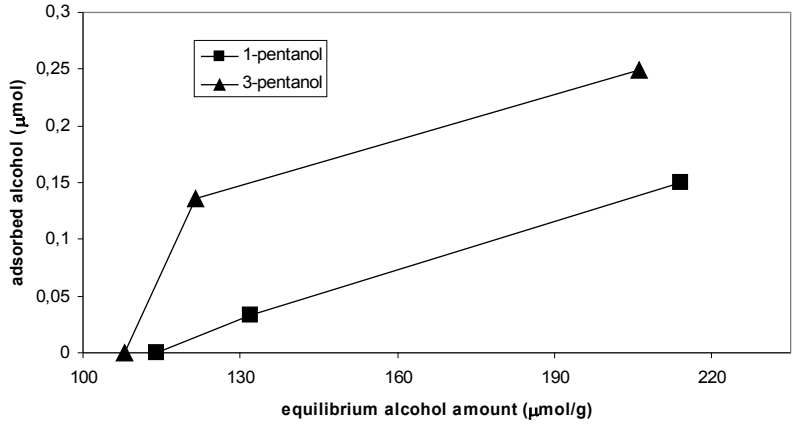

Figure 15. Adsorption of increasing amounts of 1-pentanol and 3-pentanol on SiO_2/W30% (33 g/L) suspended in 0.3 mL of CH_2Cl_2.

A comparison between the photocatalytic results of Experiments 4-6 of Table 5 and the adsorption data of Fig. 15 indicate that, besides adsorption phenomena, the microporous structure of the heterogeneous photocatalysts favours the contact between the photoexcited decatungstate and the less hindered primary OH group of 1-pentanol. In fact, the reactivity of 1-pentanol in the presence of SiO_2/W30% continues to be higher than that observed for 3–pentanol, even when 3-pentanol is preferentially adsorbed.

Adsorption measurements have been also performed suspending SiO_2/W10% in CH_2Cl_2 containing variable concentrations of 1-pentanol and 3-pentanol and the results are reported in Fig. 16. It is seen that with 170 μmoles of alcohol per gram of photocatalyst, 1-pentanol is already adsorbed in this solvent in a greater extent than 3-pentanol.

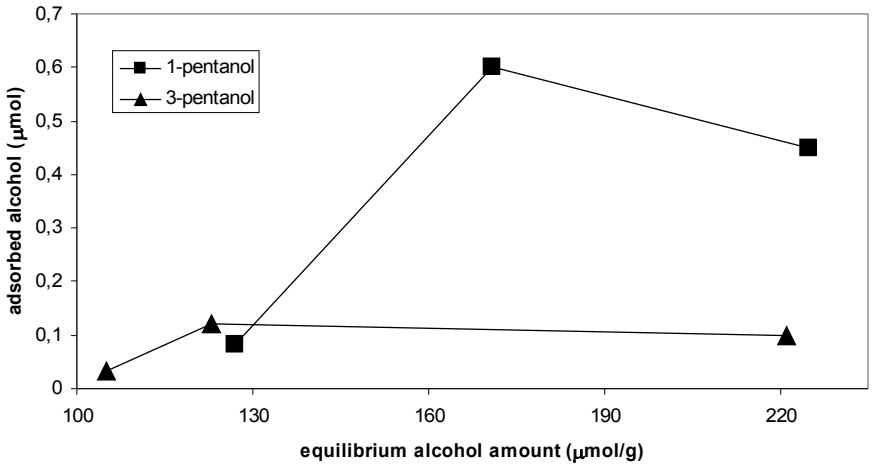

Figure 16. Adsorption of increasing amounts of 1-pentanol and 3-pentanol on SiO_2/W10% (33 gL^{-1}) suspended in 0.3 mL of CH_2Cl_2.

It is also seen in Fig. 16 that experimental conditions (120 μmoles of alcohol per gram of photocatalyst) can be found under which the relative reactivity of 1-pentanol and 3-pentanol can be compared when their adsorption is about the same. Some experiments indicate that 60 min photoexcitation of SiO_2/W10% in the presence of 120 μmoles of 1-pentanol or 3-pentanol leads to a molar concentration ratio between pentanal and 3-pentanone formed of 1.5. This ratio is significantly lower than that obtained with an amount of alcohol large enough to lead to prevalent adsorption of 1-pentanol (concentration ratio of 2.7, from experiments 1 and 3 of Table 5), so providing an additional evidence that adsorption phenomena strongly control the photoreactivity towards 1-pentanol and 3-pentanol. Nevertheless, the ratio of 1.5 is still higher than that observed in homogeneous solution (1.0, from experiments 1 and 3 of Table 4), suggesting that, besides adsorption phenomena, other textural parameters of the catalytic materials must affect the reactivity of the alcoholic substrates. We propose that the predominance of aldehyde as oxidation product even under conditions of comparable adsorption between 1- and 3-pentanol may be ascribed to some kind of shape selectivity towards the two reactants. In particular, the

microporous structure of the heterogeneous photocatalyst likely favours the contact between the photoexcited decatungstate and the less hindered primary OH group of 1-pentanol.

In order to gain insight into the effective role of microporosity in controlling regioselectivity, we have extended our study to the pair of heptanols 1-heptanol and 4-heptanol. Moreover, 2,6-dimethyl-4-heptanol, which presents an important steric hindrance around the OH group, has been also considered. Table 6 reports the results obtained upon irradiation of SiO_2/W10% dispersed in CH_3CN in the presence of 1-heptanol or 4-heptanol. This couple consists of a primary alcohol and of a secondary alcohol with the OH group placed in the middle of the aliphatic chain. For this reason, we can compare these results with those previously obtained with 1- and 3-pentanol, whose data are reported here again for an easy comparison. Moreover, results with bulky 2,6-dimethyl-4-heptanol have been also reported.

Table 6. Photocatalytic properties of SiO_2/W10% in the oxidation of pentanols and heptanols in CH_3CN [a]

		Products (μmoles) [b]			
Exp	Alcohol	Pentanal 3-pentanone	Heptanal 4-heptanone	2,6-dimethyl 4-heptanone	Aldehyde/ ketone
1	1-pentanol	0.51	/	/	
2	3-pentanol	0.13	/	/	3.9
3	1-heptanol	/	0.26	/	
4	4-heptanol	/	0.04	/	6.5
5	2,6-dimethyl 4-heptanol	/	/	0.014	18.6

[a] In a typical experiment SiO_2/W10% (8 g/L) was suspended in CH_3CN solutions containing the desired alcohol (5×10^{-3} M) and irradiated (60 min, $\lambda > 290$ nm) at 298 $\pm$ 1 K and 760 Torr of O_2. Reported values are the mean of three repeated experiments with $\pm$ 5% of precision. [b] Amount of carbonyl compounds as μmoles produced in 3 mL of solution.

As the carbon chain increases in length, the alcohols become more hydrophobic and their approach to the hydrophilic surface is less favoured. This can explain the general decrease of efficiency in the photooxidation of

heptanols with respect to the shorter analogues. However, 1-heptanol continues to be oxidized with quite good efficiency, while the same cannot be claimed for 4-heptanol. In this case a decrease in yield of about 70% is observed with respect to what obtained with 3-pentanol. As a consequence, an important enhancement in the aldehyde/ketone ratio up to 6.5 is seen for the pair of heptanols. We believe that the microporous structure of SiO_2/W10% has an important role in affecting the ability of 4-heptanol to enter the pores and to reach the photoactive species. This hypothesis is confirmed considering that 2,6-dimethyl-4-heptanol, which has two methyl groups that protect the central OH group by each side of the molecule, is scarcely oxidized with respect to 4-heptanol, giving an aldehyde/ketone ratio of 18.6.

I reported above (Table 5) some data for comparing photocatalytic activity of SiO_2/W10% and SiO_2/W30% dispersed in CH_2Cl_2 in the oxidation of 1-pentanol and 3-pentanol. In those experiments it was not possible to irradiate the photocatalyst in a mixture of the two alcohols because 3-pentanol and pentanal were not sufficiently separated in the GC column. However, the simultaneous presence in the dispersing medium of both alcohols should give direct information about the relative affinity of each substrate for the surface. For this reason, when chromatographic separation between substrates and oxidation products was feasible, pairs of primary and secondary alcohols with the same number of carbon atoms have been put in direct competition for the two photocatalysts. Results are collected in Table 7.

Table 7. Photocatalytic properties of SiO_2/W10% and of SiO_2/W30% in the oxidation of pairs of aliphatic alcohols in CH_2Cl_2 [a]

		Alcohol	Products (μmoles)[b]

Exp	Photocatalytic system		Heptanal 4-heptanone	Heptanal 2,6-dimethyl-4-heptanone	Aldehyde/ ketone
1	SiO_2/BuW10%	1-heptanol & 4-heptanol	0.3 0.07		4.3
2		1-heptanol & 2,6-dimethyl 4-heptanol		0.23 < 0.01	> 23
3	SiO_2/BuW30%	1-heptanol & 4-heptanol	0.35 0.11		3.2
4		1-heptanol & 2,6-dimethyl 4-heptanol		0.15 0.04	3.8

[a] In a typical experiment the photocatalyst employed (8 g/L) was suspended in CH_2Cl_2 solutions containing the desired pair of alcohols (4×10^{-3} M each) and irradiated (60 min, $\lambda > 290$ nm) at 298 $\pm$ 1 K and 760 Torr of O_2. Reported values are the mean of three repeated experiments with $\pm$ 5% of precision.

[b] Amount of carbonyl compounds as μmoles produced in 3 mL of solution.

As far as the couple 1-heptanol and 4-heptanol is concerned, the photocatalyst SiO_2/BuW10% leads to the highest aldehyde/ketone ratio. This result is in agreement to what has been obtained for pentanols. However, the use of 2,6-dimethyl-4-heptanol enhances the morphologic differences between the two photocatalysts. SiO_2/BuW10%, that has the photoactive species inside pores, is able only to slightly oxidize the bulky alcohol because the substrate can not enter the pores and reach the decatungstate. For this the aldehyde/ketone ratio is higher than 23. On the contrary, SiO_2/BuW30%, that arranges the polyanion on the surface rendering it easily available, is able to oxidize 2,6-dimethyl 4-heptanol, giving an aldehyde/ketone ratio that is a little higher than that obtained with 4-heptanol.

In order to evaluate the effect of the length of the carbon chain we have carried out some experiments using the following pairs of primary alcohols: 1-pentanol/1-heptanol and 1-pentanol/1-nonanol. These experiments have been carried out in CH_2Cl_2 as dispersing medium in order to compare both photocatalytic materials with different decatungstate loadings. In a typical experiment, the photocatalyst employed (8 g/L) was suspended in a CH_2Cl_2 solution containing the two alcohols (4×10^{-3} M each) and irradiated (60 min, $\lambda > 290$ nm) at 298 $\pm$ 1 K and 760 Torr of O_2. Results are shown in Table 8.

Table 8. Photocatalytic properties of SiO_2/W30% and of SiO_2/W10% in the oxidation of the following pairs of alcohols: 1-pentanol/1-heptanol and 1-pentanol/1-nonanol.[a]

Exp	Photocatalytic system	Alcohols pair	Aldehydes [b] (μmoles)	Aldehydes ratio
1	SiO_2/BuW10%	1-pentanol &	0.42	1.3

		1-heptanol	0.32	
2		1-pentanol & 1-nonanol	0.41 0.07	5.9
3	SiO_2/BuW30%	1-pentanol & 1-heptanol	0.15 0.18	0.8
4		1-pentanol & 1-nonanol	0.33 0.16	2.1

[a] In a typical experiment the photocatalyst employed (8 g/L) was suspended in CH_2Cl_2 solutions containing the desired pair of alcohols (4×10^{-3} M each) and irradiated (60 min, $\lambda > 290$ nm) at 298 $\pm$ 1 K and 760 Torr of O_2. Reported values are the mean of three repeated experiments with $\pm$ 5% of precision.

[b] Amount of aldehydes as μmoles produced in 3 mL of solution.

Concerning the couple 1-pentanol/1-heptanol, it is seen that the two photocatalysts show different preferences for them. The more hydrophilic SiO_2/BuW10% slightly favours the oxidation of the shorter alcohol 1-pentanol (ratio between pentanal and heptanal is 1.3) while the more hydrophobic surface of SiO_2/BuW30% allows a good approach by 1-heptanol (ratio between pentanal and heptanal is 0.8). When 1-nonanol is used together with 1-pentanol, the differences are enhanced: in fact, photooxidation of 1-nonanol on SiO_2/BuW10% is very difficult (ratio between pentanal and nonanal is 5.9) while it occurs efficiently on SiO_2/BuW30% (ratio between the two aldehydes is 2.1). The nature and the morphology of the surfaces are able to control the photooxidation of the investigated primary alcohols that differ each other only in the length of the aliphatic chain. In particular, it is observed that photocatalytic material SiO_2/BuW10% is more selective than SiO_2/BuW30% and this behaviour is in agreement with previous experiments where reactivities of primary and secondary alcohols have been compared. Hydrophilic/hydrophobic character and porosity of these materials, as well as the shape of substrate can affect the selectivity. Lengthening of aliphatic carbon chain increases the

hydrofobicity of the molecule and, even if it has a primary OH group, its approach to the surface of hydrophilic SiO_2/BuW10% and its entering inside pores where the photoactive species is located is made difficult. On the contrary, hydrophobicity of SiO_2/BuW30% and availability of decatungstate on the surface of the material allows the oxidation also of long chain alcohols.

1. 4 STABILITY AND PROLONGED IRRADIATION

Some additional experiments were carried out in order to evaluate the stability of SiO_2/W10%. 1-pentanol was used as substrate. Figure 17 shows that the amount of pentanal increases quite linearly during the first 2 hours of photoexcitation in the presence of 1-pentanol, which indicates that the photocatalyst is rather robust. It is noteworthy that after 200 min of irradiation, pentanoic acid is not formed in detectable amounts. This is particularly relevant because aldehydes are known to be important building blocks in applied organic synthesis [158, 159] but it is quite difficult to limit the oxidation of an alcohol at the aldehyde stage. Moreover, some experiments have been carried out as described in the experimental section (1.1.6) in order to verify if carbon dioxide was an undesired product of the reaction. Results obtained enable us to conclude that carbon dioxide was not formed in detectable amounts during the photocatalytic oxidation of the investigated alcohols. This result is expected since the formation of CO_2 was never detected when the decatungstate is used as a photocatalyst in organic solvents. We also have experimental evidence that when the reaction filtrate is further irradiated under O_2, no additional formation of carbonylic product is observed, confirming that the photoreaction is heterogeneous in nature. Moreover, UV-vis spectra demonstrate that the decatungstate anion is not released in detectable amounts during the photocatalytic experiments.

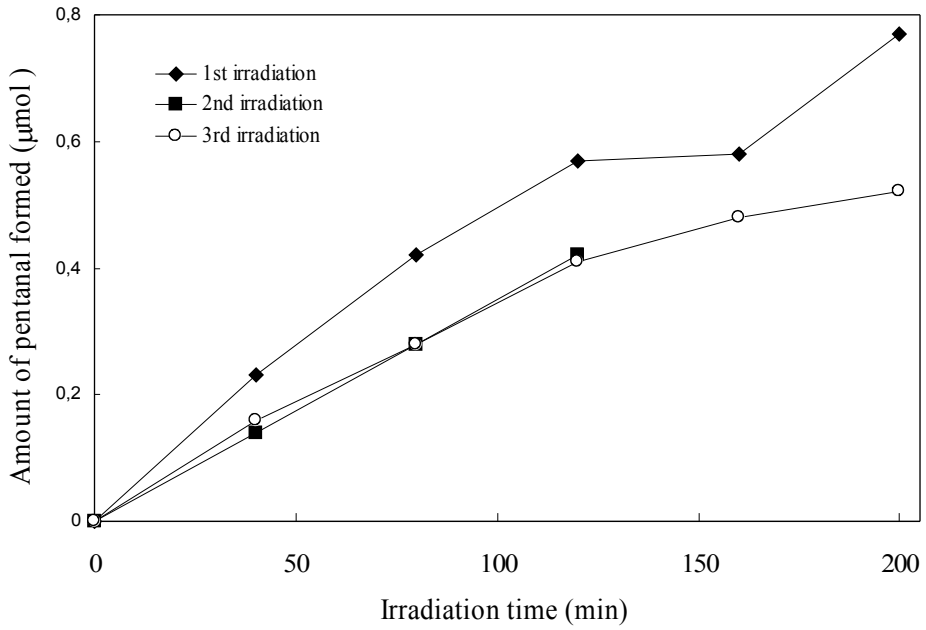

Figure 17. Micromoles of pentanal formed vs. irradiation time. The irradiation was carried out with $\lambda > 295$ nm, 298 K, 760 Torr of O_2 on 8 gL^{-1} of SiO_2/W10% suspended in a CH_3CN solution of 1-pentanol 5 x 10^{-3} M.

The stability of SiO_2/W10% was also assessed in repeated photocatalytic experiments after washing and drying the material. Figure 17 shows that the loss of activity is less than 15 % after the first cycle. Interestingly, the photocatalytic system mantains the same level of activity after the first recycle. In fact, in the third photocatalytic experiment, the photooxidation rate of 1-pentanol does not change.

1.5 CONCLUSIONS

Entrapment of tetrabutyl-ammonium decatungstate in a silica matrix through a sol-gel procedure gives a heterogeneous photocatalyst (SiO_2/W30%) that presents micro- and mesopores. The removal of the decatungstate weakly adsorbed on the more exposed surface of SiO_2/W30% leads to a significant increase of micropores in SiO_2/W10%. Both photocatalysts are robust and able to induce the O_2-assisted oxidation of

primary and secondary aliphatic alcohols to the corresponding carbonylic products. The solid support has a very strong effect on the relative reactivity of primary and secondary alcohols and, due to preferential adsorption effects, it controls nature of the products and yields of the photocatalytic process. Hyrophilicity/hydrophobicity of the catalyst surface also affects the approach of primary alcohols with aliphatic chains of increasing lengths. Furthermore, other textural parameters, related to the microporous structure of the heterogeneous photocatalysts favour the approach to the surface of the less hindered primary OH group and at the same time render difficult that of secondary alcohols with the OH group placed in the middle of an aliphatic chain of the same length.

2. Photocatalytic properties of sodium decatungstate supported on sol-gel silica in the oxidation of glycerol.

Sodium decatungstate is a very attractive photocatalyst since it is highly soluble in water and exhibits an absorption spectrum (λ_{max} = 323 nm) that partially overlaps the UV solar emission spectrum and that of TiO_2, the most used semiconductor in aqueous photocatalysis for abatement of pollutants. Continuing my study on the photocatalytic properties of heterogeneous decatungstate, I used the sol-gel procedure described in the previous chapter for entrapping $Na_4W_{10}O_{32}$ inside a silica matrix. Moreover, in order to explore the possible effects of the heterogenization on its photoreactivity, I decided to use glycerol as oxidizable molecule in aqueous medium. In fact, the large functionalization of this alcohol with similarly reactive hydroxyl groups renders its selective oxidation particularly difficult. As a consequence, any improvement in selectivity is noticeable if one considers that all oxygenated derivatives of glycerol are of practical value. Since glycerol is an important by-product in biodiesel production, the development of processes able to convert it into higher value products is an urgent need and a challenging opportunity.

Up to now, only TiO_2 has been used for the photocatalytic oxidation of glycerol [160, 161]. A common issue in this case is the need to control the high oxidation power of this photoexcited semiconductor, which may induce over-oxidation of the primary products up to carbon dioxide. Good selectivity to dihydroxyacetone and glyceraldehyde was obtained with surface fluorinated TiO_2 [160], while the use of rutile or anatase-rutile polymorphic phases did not prevent degradation of glycerol to CO_2 [161]. In this respect, I believe that heterogenized $Na_4W_{10}O_{32}$ can represent a valid alternative to titania systems.

2.1 EXPERIMENTAL SECTION

2. 1. 1 SYNTHESIS OF $Na_4W_{10}O_{32}$

$Na_4W_{10}O_{32}$ was prepared following a literature procedure [162], by addition of a boiling aqueous HCl solution (1M, 65 mL) to a boiling aqueous solution of $Na_2WO_4 \cdot 2H_2O$ (11 g in 62 mL of water). The resulting solution was allowed to boil for 40 s, after which it was transferred to a 2-L beaker and rapidly cooled to 0 ºC in an ice bath of ammonium carbonate solution under stirring. Solid NaCl was added to saturation while the temperature was maintained at 0 ºC. The formed precipitate was collected on a fritted funnel, washed with a small amount of cold water, ethanol, and diethyl ether and transferred to a 250-mL beaker. This precipitate was suspended in hot acetonitrile (32.5 mL); then the suspension was filtered and the filtrate was placed in a freezer overnight. Large pale-lime crystals of sodium decatungstate were collected on a fritted funnel and dried (2.35 g). From the mother liquor, it was possible to obtain more crystals upon concentration. The absorbance spectrum in acetonitrile or in water comprised a well-defined maximum at 324 or 323 nm, respectively.

2. 1. 2 SYNTHESIS OF $Na_4W_{10}O_{32}/SiO_2$

The composite photocatalyst $Na_4W_{10}O_{32}/SiO_2$ has been prepared following a procedure analogous to that already described for the preparation of $(n\text{-}Bu_4N)_4W_{10}O_{32}/SiO_2$ (see paragraph 1.1.2).

An amount of 0.5 g of $Na_4W_{10}O_{32}$ was dissolved in 5 mL of H_2O. Then, the acidity of the solution was adjusted to pH 2 with $HClO_4$ 1.5 M. After acidification, the solution was added dropwise to a mixture of 5 mL of TEOS and 4.5 mL of 1-butanol. Then, the obtained mixture was treated as described in paragraph 1.1.2. On the basis of the solid mass obtained at the end of the preparation and the initial amount of $Na_4W_{10}O_{32}$ it has been

possible to estimate that the prepared material $Na_4W_{10}O_{32}/SiO_2$ contained 30% (w/w) of decatungstate. The photocatalyst was washed several times with aliquots of water. UV-vis spectra of these aliquots showed that the release of $Na_4W_{10}O_{32}$ into the solution was negligible. Moreover, a sample not including decatungstate (SiO_2) was also prepared, following the same procedure but without adding $Na_4W_{10}O_{32}$.

2. 1. 3 TEXTURAL CHARACTERIZATION

Diffuse reflectance UV/vis spectra and N_2 adsorption-desorption experiments were carried out as described above in paragraph 1.1.3.

2. 1. 4 EPR SPIN-TRAPPING EXPERIMENTS

EPR spin-trapping experiments were carried out with a Bruker 220 SE spectrometer equipped with a TE 201 resonator, at a microwave frequency of 9.4 GHz. The samples for epr spin-trapping experiments were H_2O/CH_3CN (85/15) solutions containing 5,5-dimethylpyrroline *N*-oxide (DMPO, 3 x 10^{-2} M) as spin trap, $Na_4W_{10}O_{32}$ (2.4 x 10^{-3} M) and, when requested, glycerol (1 x 10^{-2} M). CH_3CN was necessary in order to dissolve the spin trap. In heterogeneous experiments, the solid $Na_4W_{10}O_{32}/SiO_2$ was suspended in the solution containing DMPO and, when necessary, glycerol as described above. Then, samples were put into a flat quartz cell and directly irradiated into the EPR cavity at $\lambda > 290$ nm with a Hg medium pressure mercury lamp. No EPR signals were obtained in the dark and during irradiation of the solution in the absence of photocatalyst.

2. 1. 5 PHOTOCATALYTIC EXPERIMENTS

Photocatalytic experiments were carried out inside a closed Pyrex tube of 15 mL capacity at 298 ± 1 K. The desired amount of photocatalyst (4 x 10^{-4} M

in the case of $Na_4W_{10}O_{32}$ solution or 8 g/L in the case of $Na_4W_{10}O_{32}/SiO_2$ suspension) was placed in 3 mL of an aqueous solution containing glycerol (1×10^{-2}M) and magnetically stirred for 20 min. The pyrex photoreactor was filled with O_2 and then joined through an inlet tube to a balloon filled with O_2. Photochemical excitation was performed for 120 min by an external Helios Q400 Italquartz medium pressure Hg lamp, selecting wavelengths higher than 290 nm with a cut-off filter. The photon flux, measured with a MACAM UV230X ultraviolet radiometer, was 15 $mWcm^{-2}$.

At the end of the photocatalytic experiment, the sample was centrifuged (when requested) and analyzed by HPLC system equipped with a photodiode array detector. The column used was an Alltech IOA-1000 Organic Acids, 300 x 7,8 cm by GRACE. Double distilled water was the eluent, filtered before use by a vacuum filtration system equipped with Whatman Nylon Membrane Filters 0.2 μm. The detected products were glyceraldehyde, dihydroxyacetone, glyceric acid. Quantitative analyses were carried out by calibration curves with commercial products. Each photocatalytic experiment was repeated three times in order to evaluate the errors, which never exceeded ± 5%. Control experiments were run irradiating SiO_2 suspended in the solution containing glycerol (1×10^{-2} M) or keeping (120 min) the photocatalyst dispersed in the solution in the dark. When $Na_4W_{10}O_{32}/SiO_2$ was employed as a photocatalyst, the possible release of polyoxoanion in the solution phase was evaluated by UV-vis analysis of the solution at the end of irradiation.

2. 1. 6 DETERMINATION OF CO_2

In order to establish the amount of carbon dioxide eventually formed, aqueous samples (3 mL) were irradiated maintaining the reactor firmly closed. At the end of irradiation 1.5 mL of a NaOH solution (0.1M) were put inside the reactor with a syringe and mixed with the irradiated solution. Then, 3.5 mL of the aqueous solution were taken and kept into a vial. Then

the determination of CO_2 was performed as described in paragraph 1.1.6. Results obtained from the irradiated samples were compared with those coming from analogous samples kept in the dark for the same period. The yield of CO_2 was referred to the number of carbon atoms present in glycerol.

2. 2 TEXTURAL CHARACTERIZATION

Textural characterization has been carried out at the University of Torino in collaboration with Dr. Giuliana Magnacca.

Fig. 18 (a) shows the UV-visible spectrum of heterogeneous $Na_4W_{10}O_{32}/SiO_2$ (curve A). Spectra of homogeneous $Na_4W_{10}O_{32}$ and of silica, obtained with the sol-gel procedure, are also reported for a comparison (curves B and C respectively). It is seen that $Na_4W_{10}O_{32}/SiO_2$ presents an intense absorption at wavelengths lower than 400 nm, that is typical of $W_{10}O_{32}^{4-}$ and that is not present in the silica matrix. Fig 18 (b) reports the visible spectrum of $Na_4W_{10}O_{32}/SiO_2$ irradiated in the presence of glycerol under anaerobic conditions (curve A). It is observed an important increase of absorption above 600 nm, in the region where the blue $W_{10}O_{32}^{5-}$ typically absorbs (see for comparison curve C relative to homogeneous reduced decatungstate). Exposure to air of the irradiated powder leads to the reoxidation of decatungstate in its oxidized state, that not absorbs in the visible region (curve B). These results are in line with the known primary photochemical process of decatungstate anion [29] and represent a further evidence that the polyoxoanion is unchanged in nature after its heterogenization.

(a)

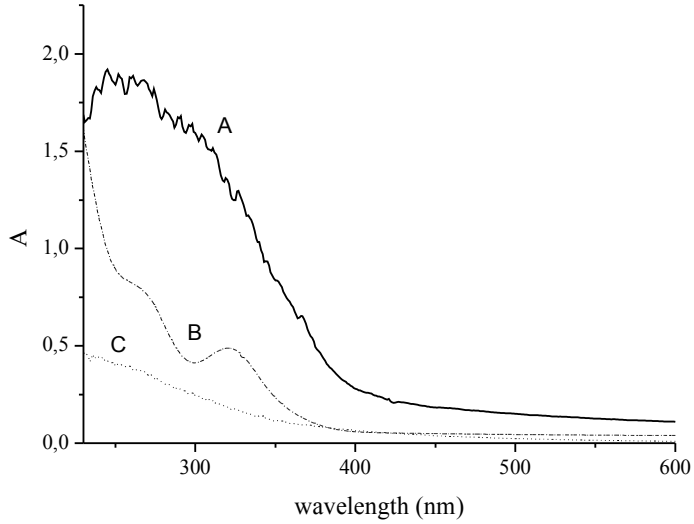

(b)

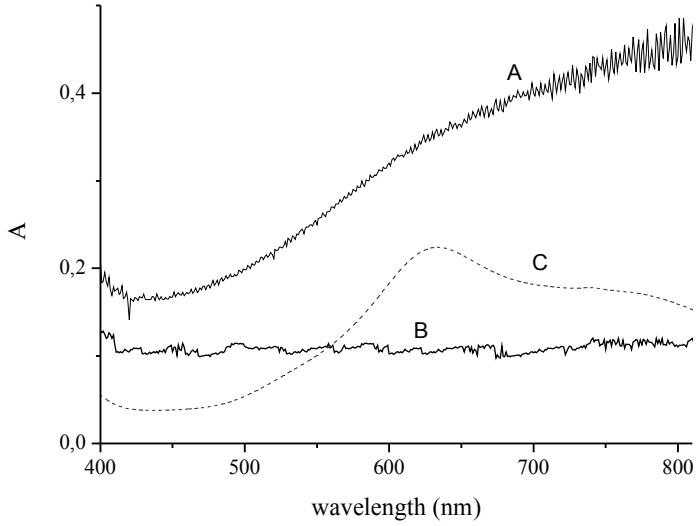

Figure 18: (a) UV-vis spectra of $Na_4W_{10}O_{32}/SiO_2$ (curve A), of homogeneous $Na_4W_{10}O_{32}$ (curve B) and of SiO_2 (curve C); (b) visible spectra of reduced $Na_4W_{10}O_{32}/SiO_2$ (curve A), of oxidized $Na_4W_{10}O_{32}/SiO_2$ (curve B) and of reduced homogeneous $Na_4W_{10}O_{32}$ (curve C).

Gas-volumetric adsorption of N_2 at 77 K gives useful information about the morphological features of $Na_4W_{10}O_{32}/SiO_2$ to comparison with SiO_2. Table 9 shows that the introduction of $Na_4W_{10}O_{32}$ into the silica matrix causes a decrease in surface specific area value. At the same time it is observed a 35% increase in the total pore volume.

$Na_4W_{10}O_{32}/SiO_2$ material presents both mesoporosity and microporosity (Table 9). To evaluate both and, in particular, to reveal the porosity eventually present at the boundary between micro and mesoporosity regions, we employ here the same method which we used for the investigation of $(n\text{-}Bu_4N)_4W_{10}O_{32}$ encapsulated inside a silica matrix [see paragraph 1.2 and Ref. 15], that consists in the isotherm deconvolutions in accordance to Density Functional Theory (DFT) [154]. The pore volumes reported in Table 9 and Figure 19 are classified on the basis of the pore size distribution determined via the DFT method and quantified considering the DFT cumulative pore volume curves.

Table 9. Morphological features of $Na_4W_{10}O_{32}/SiO_2$

Sample	SSA/m^2g^{-1}	V_{tot}/cm^3g^{-1}	V_{micro} (< 18 Å width, cm^3g^{-1})	V_{meso} (> 18 Å width, cm^3g^{-1})
SiO_2	772	0.176	0.131	0.045
$Na_4W_{10}O_{32}/SiO_2$	521	0.240	0.162	0.078

Figure 19, which shows the incremental pore volume as a function of the pore width obtained via the DFT method, allows us to recognize the fraction of pores with widths between 10 and 20 Å. $Na_4W_{10}O_{32}/SiO_2$ is characterized by micropores with width of about 7 Å, in agreement with previous literature data on the entrapment of polyoxometalates in silica matrices via sol-gel techniques [72]. In addition to these micropores, $Na_4W_{10}O_{32}/SiO_2$ also contains micropores around 13 Å and mesopores around 30 Å.

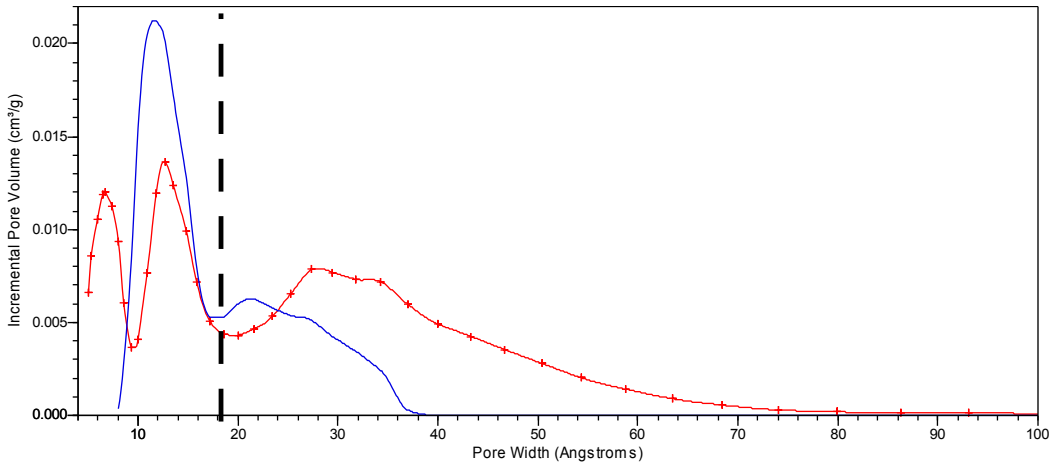

Figure 19. DFT pore analysis for $Na_4W_{10}O_{32}/SiO_2$ (cross symbols) and for SiO_2 (solid line). The vertical broken line represents the threshold value considered (18 Å) between micro and mesopores.

Table 9 and Figure 19 show that the morphological features of $Na_4W_{10}O_{32}/SiO_2$ differ markedly from those of its parent material SiO_2. In fact, SiO_2 does not present 7 Å micropores, but 75% of its porosity is characterized by micropores with width of 11-12 Å. Moreover, the degree of mesoporosity is lower than in $Na_4W_{10}O_{32}/SiO_2$. These results indicate that the incorporation of sodium decatungstate during the synthesis of the silica-based photocatalyst induces an important modification of the porous texture of the siliceous material, suggesting that sodium decatungstate can act as a templating agent.

It has been reported in literature that the formation of microporous decatungstate is due to the chemical interaction between sodium decatungstate and the silica network [72]. Since during the preparation the hydrolysis of TEOS in the presence of $Na_4W_{10}O_{32}$ is carried out at pH 2, the silanol group (≡Si-OH) is protonated in the acidic medium to form ≡Si-OH_2^+. This can, in turn, act as a counterion for $W_{10}O_{32}^{4-}$ yielding the couple (≡Si-OH_2^+)($Na_3W_{10}O_{32}^-$) by acid-base reaction. This strong interaction could explain why the salt is no longer released although $Na_4W_{10}O_{32}/SiO_2$ is

dispersed in aqueous media. It is noteworthy to evidence that the substitution of Na^+ ions with organic and less polar groups such as tetrabutylammonium ions [15] decreases the strength of the interaction between $W_{10}O_{32}^{4-}$ and SiO_2 matrix, as observed in the effect induced by CH_3CN washing of the material (loss of 20% of the starting decatungstate amount).

2. 3 EPR SPIN-TRAPPING INVESTIGATION

2. 3. 1 IN HOMOGENEOUS PHASE

EPR spin-trapping investigation is a powerful technique for detecting the formation of short-lived radicals [163] and has been fruitfully employed in photochemical studies on polyoxometalates in order to better understand photochemical primary processes [67, 157, 164-167]. This technique is based on the ability of some molecules such as nitrones to trap radicals to give nitroxides stable enough to be successfully detected and studied. In particular, 5,5-dimethylpyrroline *N*-oxide (DMPO) is able to trap radicals (R•) to give more stable nitroxides according to Scheme 4. In some instances, the nature of the trapped radical can be identified by the parameters obtainable from the EPR spectrum.

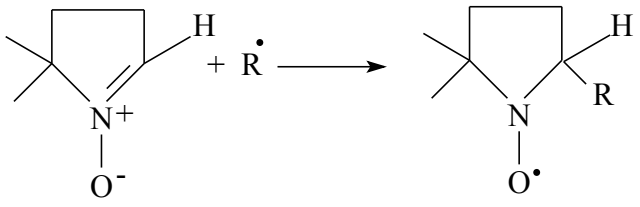

Scheme 4. Reaction between DMPO and radical species to form a more stable paramagnetic nitroxide.

Evidences of radical formation as a consequence of photoexcitation of $Na_4W_{10}O_{32}$ in homogeneous solution have been obtained irradiating ($\lambda > 290$ nm) H_2O/CH_3CN (85/15 v/v) solutions containing $Na_4W_{10}O_{32}$ (2.4×10^{-3} M), glycerol (1×10^{-2} M) and DMPO (3×10^{-2} M) as a spin trap, directly inside the EPR cavity. Illumination causes the prompt formation of a quartet (1:2:2:1, $a_N = a_H = 14.5$ gauss), which is shown in Fig. 20. Signal pattern and coupling constant values are in agreement with the trapping of $OH^{\bullet}$ radicals by DMPO to form the paramagnetic adduct $[DMPO\text{-}OH]^{\bullet}$ according to step 2 of Scheme 5 [163]. No signals relative to the trapping of radicals coming from glycerol are detected even after some minutes irradiation. The same quartet is also obtained during irradiation of $Na_4W_{10}O_{32}$ dissolved in an aqueous solution containing the spin trap but in the absence of glycerol, suggesting that the alcohol does not take part directly to the primary photoprocess. Control experiments show that no signal is observed neither in the dark or during irradiation but in the absence of decatungstate.

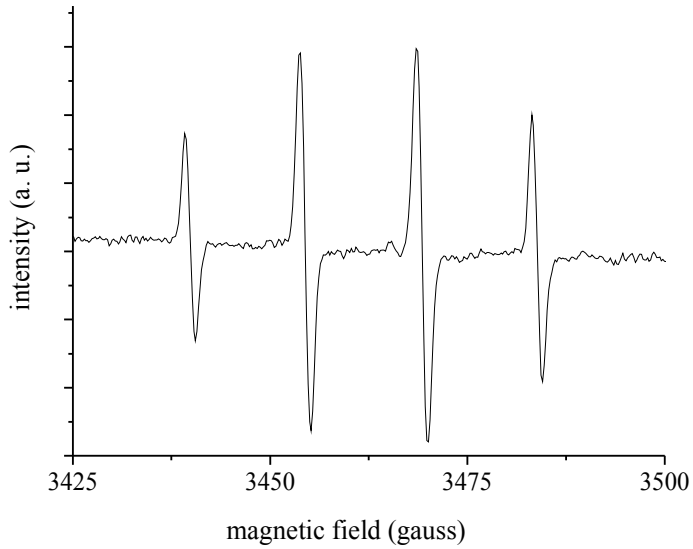

Figure 20. EPR spectrum of $[DMPO\text{-}OH]^{\bullet}$ obtained upon irradiation ($\lambda > 290$ nm) of $Na_4W_{10}O_{32}$ (2.4×10^{-3} M) dissolved in a H_2O/CH_3CN (85/15 v/v) mixture containing, glycerol (1×10^{-2} M) and DMPO (3×10^{-2} M).

The formation of $OH^{\bullet}$ radicals may be ascribed to the reaction between photoexcited polyoxoanion and water according to Scheme 5 (step 1). The possibility to obtain $OH^{\bullet}$ radicals by direct reaction between photoexcited pentakis(isopropylammonium)hydrogenhexatungstate $[NH_3Pr^i]_5[W_6O_{20}(OH)]$ and water was pointed out by Yamase in the early eighties [168]. More recently, Papaconstantinou's group and other researchers proposed that polyoxometalates and TiO_2 exhibit overall similar photocatalytic behaviour in aqueous solution [30, 169-171]. This similarity was attributed to the common formation of $OH^{\bullet}$ radicals. In those works, the formation of $OH^{\bullet}$ radicals was suggested by the detection of hydroxylation products in photocatalytic experiments with aromatic hydrocarbons, and on the basis of the excited state potentials [170].

The photogenerated $OH^{\bullet}$ radicals can initiate glycerol oxidation by abstraction of a hydrogen atom from one of the available C_α atoms, producing a hydroxy alkyl radical (step 3). Then, these radicals may be further oxidized to the corresponding carbonylic compounds (step 4). Reaction between reduced decatungstate and O_2 regenerates the photocatalyst in its initial state (step 5). In our photocatalytic system, direct reaction of photoexcited $W_{10}O_{32}^{4-}$ with the alcoholic substrate seems not to be the main pathway for glycerol oxidation since no radicals coming from the polyalcohol are trapped by DMPO.

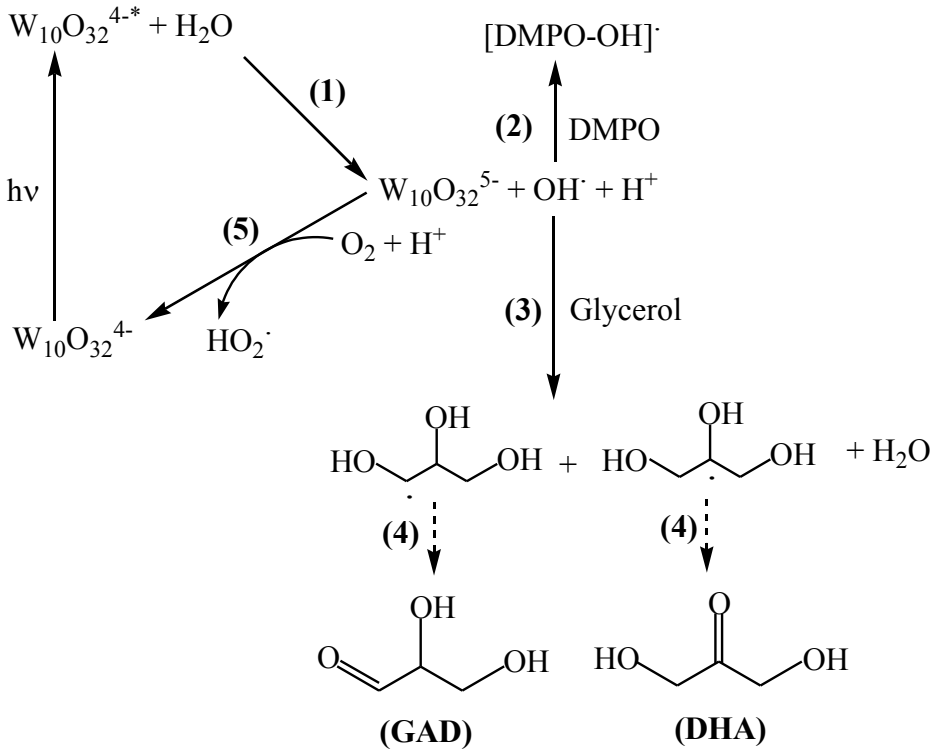

Scheme 5. Proposed reaction mechanism for glycerol oxidation by photoexcited $Na_4W_{10}O_{32}$ in aqueous medium.

Figure 21 shows that addition of glycerol causes a decrease of several times of the signal intensity of [DMPO-OH]•. This indicates that glycerol is a very good competitor for the reaction with OH• radical with respect to the spin trap (Scheme 5 steps 2 and 3). It is also seen that the signal intensity of the paramagnetic [DMPO-OH]• adduct decreases rapidly after the first 120 seconds irradiation. Likely, this adduct can react with other radical species formed during irradiation (see for example step 5) or with the decatungstate itself, as reported in the past by some researchers [172].

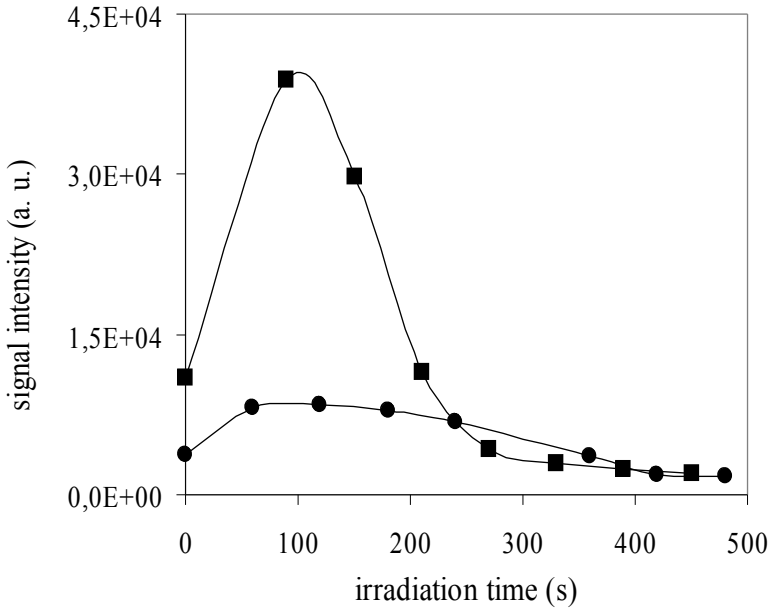

Figure 21. Fixed-field EPR signal intensity of the [DMPO-OH]• adduct in time upon irradiation ($\lambda > 290$ nm) of a H_2O/CH_3CN solution (85/15 v/v) containing $Na_4W_{10}O_{32}$ (2.4 x 10^{-3} M) and DMPO (3 x 10^{-2} M) (squares) and of an analogous solution containing $Na_4W_{10}O_{32}$ (2.4 x 10^{-3} M) and DMPO (3 x 10^{-2} M) and glycerol (1 x 10^{-2} M) (circles).

It has been previously reported that the [DMPO-OH]• species may originate from degradation of the adduct [DMPO-OOH]• between DMPO and O_2^- [173, 174] . This paramagnetic species presents a typical 12-lines EPR spectrum [175]. On the other hand, this source of [DMPO-OH]• is expected to be negligible in our photocatalytic system on the basis of literature data indicating that a maximum level of approximately 3% [DMPO-OH]• should originate from [DMPO-OOH]• [173, 176]. In line with this statement, Figure 21 shows that the [DMPO-OH]• spectrum is the only observed already after few seconds irradiation and that the presence of a scavenger of OH• radicals such as glycerol reduces significantly its intensity.

2. 3. 2 IN HETEROGENEOUS PHASE

Analogous EPR spin-trapping experiments with heterogeneous $Na_4W_{10}O_{32}/SiO_2$ were carried out suspending the photocatalyst in the solution containing DMPO and glycerol, when necessary. Results obtained are qualitatively similar to those in homogeneous phase: the unique signal observed is the quartet relative to the formation of [DMPO-OH]$^{\bullet}$, and in the presence of glycerol a severe decrease of intensity is observed again (Fig. 22).

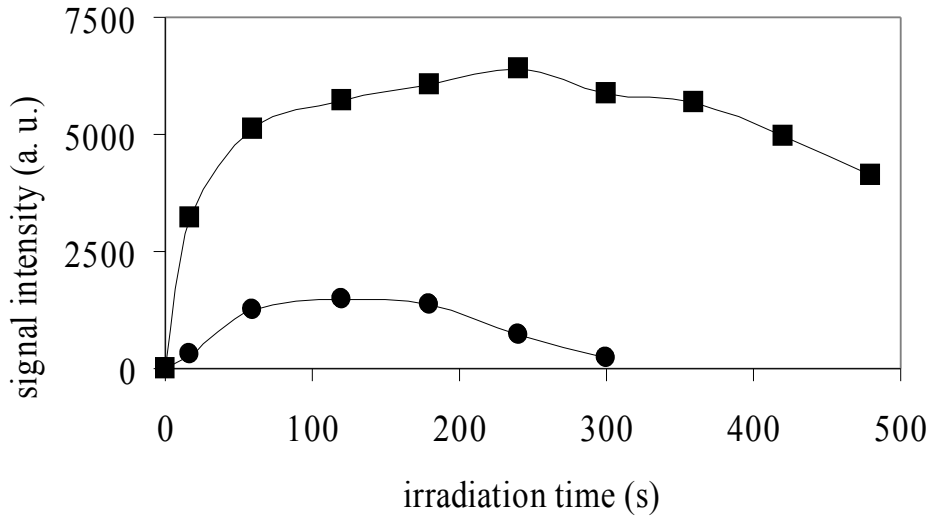

Figure 22. Fixed-field EPR signal intensity of the [DMPO-OH]$^{\bullet}$ adduct in time upon irradiation ($\lambda > 290$ nm) of $Na_4W_{10}O_{32}/SiO_2$ dispersed in a H_2O/CH_3CN solution (85/15 v/v) containing DMPO (3×10^{-2} M) (squares) and in an analogous solution containing also glycerol (1×10^{-2} M) (circles).

This indicates that the mechanism proposed in homogeneous phase is still working when decatungstate is entrapped inside the silica matrix. Intensities of signal obtained upon irradiation of $Na_4W_{10}O_{32}/SiO_2$ are significantly lower than those observed in homogeneous conditions. This

result can be tentatively ascribed to the fact that adsorption phenomena of glycerol on silica are expected to enhance its local concentration in proximity of the decatungstate, so favouring its reaction with the photogenerated $OH^{\bullet}$ (Scheme 5 step 3) in competition with trapping by DMPO (step 2).

Adsorption of alcohols and diols on various siliceous matrices is an efficient phenomenon that has been already pointed out [16, 65, 81] . For this reason, glycerol is expected to adsorb on $Na_4W_{10}O_{32}/SiO_2$ too. A qualitative confirmation of this behaviour is obtained by the experiment described in the following: a huge amount of $Na_4W_{10}O_{32}/SiO_2$ (70 g/L) was suspended in a small volume (0.7 mL) of the aqueous solution containing glycerol (1 x 10^{-2} M) and stirred in the dark for 30 minutes. From HPLC analysis of the solution, performed before and after the contact with the photocatalyst, we observed a decrease of about 35% of the initial amount of glycerol, indicating that it can adsorb and concentrate on the surface.

2. 4 PHOTOCATALYTIC OXIDATION OF GLYCEROL

Typical photocatalytic experiments were carried out irradiating ($\lambda > 290$ nm) $Na_4W_{10}O_{32}$ (4 x 10^{-4} M) or $Na_4W_{10}O_{32}/SiO_2$ (8 g/L) in aqueous solutions containing glycerol (1 x 10^{-2} M) at room temperature and under 760 Torr of O_2. Owing to the presence of three oxidizable hydroxyl groups, a broad range of glycerol derivatives can be formed. Among them, we decided to follow by HPLC the formation of the carbonylic compounds, glyceraldehyde (GAD) and dihydroxyacetone (DHA), and of glyceric acid (GA), the less oxidized among acids, that is obtained from further oxidation of the aldehyde. Moreover, CO_2 has been evaluated as final degradation product.

Irradiation of $Na_4W_{10}O_{32}$ in homogeneous solution leads to the formation of GAD and DHA as primary oxidized products (Table 10). They represent about 75% of all the monitored compounds. According to EPR

spin-trapping evidences, the formation of GAD and DHA should occur through steps 3 and 4 of Scheme 5. The subsequent easy oxidation of GAD may lead to the corresponding carboxylic acid. In fact, GA is about 10% of the detected products.

Table 10. Photocatalytic oxidation of glycerol by $Na_4W_{10}O_{32}$ and $Na_4W_{10}O_{32}/SiO_2$ [a]

Photocatalytic system	Converted glycerol (μmol)	Detected products μmol (selectivity *%*)[b]			
		GAD	DHA	GA	CO_2 [c]
$Na_4W_{10}O_{32}$	19.2	6.3 (*32.8*)	0.54 (*2.8*)	1.8 (*9.4*)	0.45 (*2.3*)
$Na_4W_{10}O_{32}/SiO_2$	9.6	5.7 (*59.4*)	0.54 (*5.6*)	0.51 (*5.3*)	<0.03 (*0.3*)

[a] in a typical experiment $Na_4W_{10}O_{32}$ (4×10^{-4} M) or $Na_4W_{10}O_{32}/SiO_2$ (8 g/L) were put in aqueous solutions (3 mL) containing glycerol (1×10^{-2} M) and irradiated (120 min) at $\lambda >$ 290 nm at 298 ± 1 K and 760 Torr of O_2. Reported values are the mean of three repeated experiments.

[b] selectivity % is expressed as μmol of product divided by μmol of converted glycerol. The remaining to 100% is represented by other oxidized derivatives that have not been identified.

[c] in order to compare directly the values of carbon dioxide with those of GAD, DHA and GA, the μmol of CO_2 have been divided by three.

This photocatalytic system shows quite strong oxidizing ability that it is difficult to control for synthetic purposes. In fact, the total yield to the primary photoproducts GAD, DHA and GA is only the 47% of the converted glycerol, which, likely undergoes over-oxidation to yield a mixture of undetected C_3 and C_2 oxidized products, such as mesoxalic, tartronic, oxalic and glycolic acids. This statement is confirmed by the data of Table 10, which show that the photocatalytic experiment leads also to the formation of significant amounts of carbon dioxide.

These results are in line with EPR spin-trapping findings that demonstrate the formation of $OH^{\bullet}$ radicals, which are very strong and unselective oxidants able to degrade both the initial substrate and the reaction intermediates. This photocatalytic behaviour of $Na_4W_{10}O_{32}$ is also

in agreement to what claimed by Papaconstantinou's group, who attributed the photocatalytic reactivity of polyoxotungstate anions towards phenols and 2-propanol in water to the formation of $OH^{\bullet}$ radicals [170]. Photocatalytic properties of $Na_4W_{10}O_{32}$ in the oxidation of glycerol change significantly after its entrapment inside the silica matrix. Typical experiments were carried out irradiating the photocatalyst (8 g/L) suspended in an aqueous solution containing the alcohol. The amount of 8 g/L was chosen on the basis of measurements with an ultraviolet radiometer, that indicate that photocatalyst absorbs 90% of the impinging radiation at 313 nm, which is the emission line of the employed light source closest to the absorption maximum of decatungstate at 323 nm. Control experiments give evidences that i) irradiation of a dispersion of SiO_2 does not lead to the formation of detectable amounts of oxidation products, allowing us to exclude any kind of photoactivation of the silica matrix; ii) no oxidation of glycerol occurs after the contact between the heterogenized decatungstate and the alcohol in the absence of light. Moreover, UV-vis spectra of solutions recovered after the irradiation of $Na_4W_{10}O_{32}/SiO_2$ show that decatungstate is not released from the support. Further irradiation of these solutions does not accumulate extra oxidation products, thus indicating that the photocatalytic process is truly heterogeneous in nature.

Irradiation of $Na_4W_{10}O_{32}/SiO_2$ leads mainly to the accumulation of GAD and DHA. In fact they represent more than 90% of the monitored products. Further oxidation of GAD to GA occurs only in low degree, since the amount of acid accumulated during the photocatalytic experiment is four times lesser than that formed in the homogeneous sample. Moreover, the sum of GAD, DHA and GA is about the 70% of the converted glycerol and only a negligible amount of carbon dioxide is detected. All these findings indicate that heterogenization has an important effect in decreasing the oxidizing ability of sodium decatungstate.

The EPR spin-trapping investigation described above indicates that heterogenization does not affect the ability of $Na_4W_{10}O_{32}$ to oxidize water to

hydroxyl radicals (Scheme 5 step 1). Therefore, it should be not surprising that differences in selectivity can critically depend on textural features that allow the tuning of photocatalytic properties of $Na_4W_{10}O_{32}$ through the control of surface interactions with substrates and intermediates [157, 170, 171]. In particular, EPR spin-trapping experiments give the indication that the reaction between $OH^{\bullet}$ radical and glycerol occurs efficiently also in the heterogeneous system (Fig. 22). In agreement with this result, it is found that photocatalytic efficiency undergoes a decrease of only 25% after heterogenization. Likely, as mentioned above, adsorption phenomena of glycerol on silica enhance its local concentration in proximity of decatungstate. This substrate accumulation on the surface can favour, on the one hand, the reaction between glycerol and the photogenerated OH• radical and, on the other hand, can prevent the subsequent oxidation of the formed carbonylic compounds.

As far as the stability of the photocatalyst is concerned, irradiated $Na_4W_{10}O_{32}/SiO_2$ has been recovered, washed several times with aliquots of water, dried and then reused in a new photocatalytic experiment. It is found that the photocatalyst is completely recyclable in the second run, but it undergoes a decrease of 50% of efficiency from the third run.

2. 5 CONCLUSIONS

Photoexcitation of $Na_4W_{10}O_{32}$ dissolved in aqueous medium produces a powerful oxidizing reagent that is able to form hydroxyl radicals. It has been evidenced that the photooxidation of glycerol is mediated by OH• radicals; for this reason homogeneous $Na_4W_{10}O_{32}$ presents low selectivity and leads to over-oxidation and complete degradation of the alcoholic substrate. On the contrary, a significant improvement in selectivity towards glyceraldehyde and dihydroxyacetone is obtained after entrapment of $Na_4W_{10}O_{32}$ inside the silica matrix. Its surface favours adsorption of glycerol, enhancing its local concentration. This facilitates its reaction with

OH• radicals photogenerated by decatungstate placed on the surface or inside pores.

3. Fe(III)-porphyrin heterogenized on MCM-41 and on amorphous silica: matrix effects on the oxidation of 1,4 -pentanediol

Molecular modification of solid support surfaces for the development of functional catalytic materials is a research field of high interest in heterogeneous catalysis. Among the inorganic supports, the use of mesoporous MCM-41 type silica has attracted much attention in the last years [177-181]. This material consists of uniform and hexagonal arrays of mesopores [182] and shows a high surface area.

Polyoxoanions [66] and transition-metal complexes with oxidation-resistant aromatic ligands such as phthalocyanines, polypyridines and metalloporphyrins have been heterogenized in molecular sieves [8, 183-189]. Within this framework we decided to prepare and characterize a new photocatalyst, based on the use of a iron *meso*-tetrakis (2,6-dichlorophenyl)porphyrin, bearing an aminopropylsilane chain, that has been covalently linked on the solid surface of MCM-41. An interesting peculiarity of this complex is that the chlorine atoms present in the *meso*-aryl groups provide a steric protection of the porphyrin ring against its radical induced oxidative degradation [178]. This material is also compared with an analogous one where the same iron porphyrin complex is grafted on amorphous silica. The results of this investigation have been the subject of a paper published on catalysis today [16].

3. 1 EXPERIMENTAL SECTION

3. 1. 1 SYNTHESIS OF THE IRON (III) PORPHYRIN COMPLEX

The iron–porphyrin complex bearing a trifluorosilyl function used as precursor to link the surface of the MCM-41 was the Fe(III)–*meso*-tetrakis(2,6-dichlorophenyl)porphyrin (Fe(III)TDCPP).

The silanization of this complex was not possible directly, as already reported for Fe(III)–*meso*-tetrakis(pentafluorophenyl)porphyrin, [190] but it has been necessary to introduce a good leaving group on the phenyl rings. The synthesis of the silanized iron porphyrin has been carried out following a procedure previously reported for anchoring the complex on TiO_2 and is briefly described here [191]. All the intermediates obtained during the preparation are reported in Scheme 6. The porphyrin ring free base H_2TDCPP *(1)* has been prepared following the method suggested by Lindsey et al. [192], using 2,6-dichlorobenzaldehyde and pyrrole as starting reagents. An aromatic electrophylic substitution reaction with $ClSO_3H$ on *(1)* under rigorously controlled conditions (100 ºC, 3 h) gave *(2)*, which has been characterized by ^{1}H NMR [δ 8.62 (s, 8H, *H*-pyrrole), δ 8.60 (4H, *H-m*-phenyl), δ 8.05 (4H, *H-p*-phenyl), δ - 2.51 (s, 2H, NH in $CDCl_3$]. Subsequent hydrolysis yielded *(3)* (IR: stretching frequency of SO_3H groups are observed at 1190 and 1050 cm^{-1}). Then, an aqueous solution of $FeCl_2 \cdot 4H_2O$ was allowed to react with *(3)* under argon at 80 ºC for 18 h to give the iron–porphyrin complex *(4)* (Soret band at 394 nm). After oxygenation of the sample, a solution of KOH (35%) was added until pH 8–9 to precipitate iron in excess as $Fe(OH)_3$. After filtration, the reaction mixture was neutralized with HCl (35%) and the iron–porphyrin complex was purified by column chromatography, concentrated and precipitated from acetone. Chlorination on complex *(4)* was performed using PCl_5 (3.5 g) and $POCl_3$ (10 ml) at 50 ºC for 30 min leading to *(5)*. Finally, this was a suitable complex for the nucleophilic substitution by excess of aminopropyl

triethoxysilane (aptes, 160 mg/50 mg of *(5)*) for 17 h under argon at 70 ºC in the presence of pyridine (30 μL) in THF (4 mL). The monomer *(6)* was obtained, dried in a rotary evaporator and the solid obtained was washed with aliquots of water/acetone/methanol mixture. Then it was recovered and dried in the oven. Solid monomer *(6)* was treated with HF (48 %)/H_2SO_4 (98%) 1:1 (6 mL/100 mg of porphyrin complex *(6)*): the reaction mixture was left in rest for 30 min to produce the porphyrinotrifluorosilane monomer *(7)*. Addition of CH_2Cl_2 allowed the extraction of monomer *(7)* in the organic phase, while the excess of aptes, converted to aminopropyltrifluorosilane, remained in the aqueous acid solution. CH_2Cl_2 solution containing *(7)* was washed several times using aliquots of aqueous solution of HF 20%, then methanol (25 mL) and 2,3-dimethoxypropane (10 mL) were added. After some hours of rest, the solution was concentrated to a final volume of 20 mL: the UV-vis spectrum of the solution (Soret band at λ_{max} = 418 nm) was similar to that of the parent porphyrin *(5)* and of Fe(III)TDCPP itself, indicating that the porphyrin ring was not modified during the preparation.

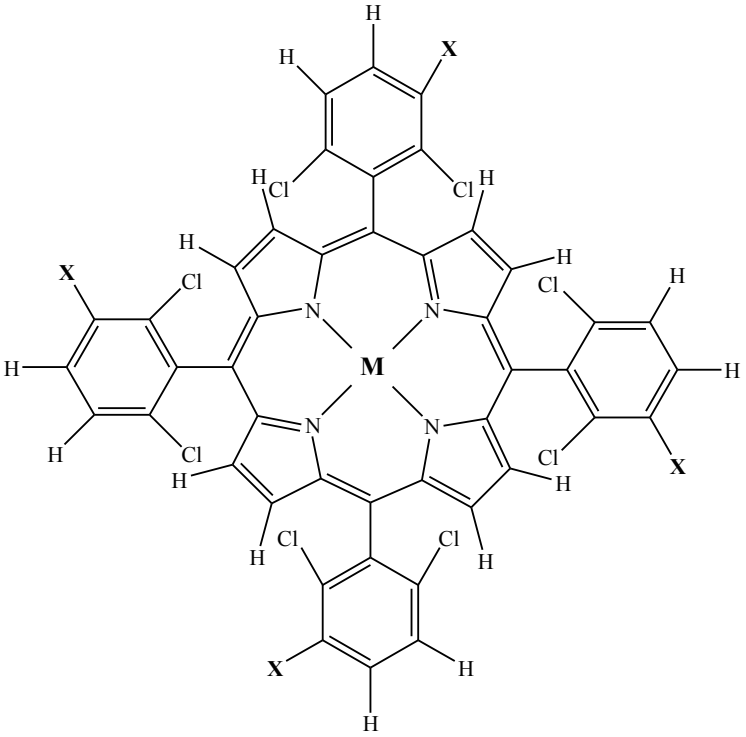

Scheme 6. Synthesis of the modified Fe(III)TDCPP. *(1)* M = H_2, X = H; *(2)* M = H_2, X = SO_2Cl; *(3)* M = H_2, X = SO_3H; *(4)* M = Fe^{3+}, X = SO_3H; *(5)* M = Fe^{3+}, X = SO_2Cl; *(6)* M = Fe^{3+}, X = $SO_2NH(CH_2)_3Si(OEt)_3$; *(7)* M = Fe^{3+}, X = $SO_2NH(CH_2)_3SiF_3$.

3. 1. 2 HETEROGENIZATION OF THE IRON (III) PORPHYRIN ON MCM-41 AND ON SiO_2

Functionalization of MCM-41 with complex *(7)* to prepare Fe(III)P/MCM-41 system has been accomplished as described in the following. MCM-41 (0.1 g) was suspended in the solution containing complex *(7)* (2 x 10^{-4} M, 3 mL). The suspension was stirred in the dark for 20 min, then the coloured MCM-41 was recovered by centrifugation and dried at 80 °C. The amount of complex linked to the support was evaluated recording UV–vis spectra of the solution before and after the contact with MCM-41. An analogous

procedure was followed to prepare Fe(III)P/SiO_2, suspending 0.1 g of amorphous silica in 3mL of the above solution of complex *(7)*. In both cases, the contact between porphyrinotrifluorosilane monomer *(7)* and the silanols of the support leads to the breaking of Si–F bond and to the formation of a Si–O covalent bond: as a result, the iron porphyrin complex is covalently linked on the surface of the silica matrix, as shown in Scheme 7.

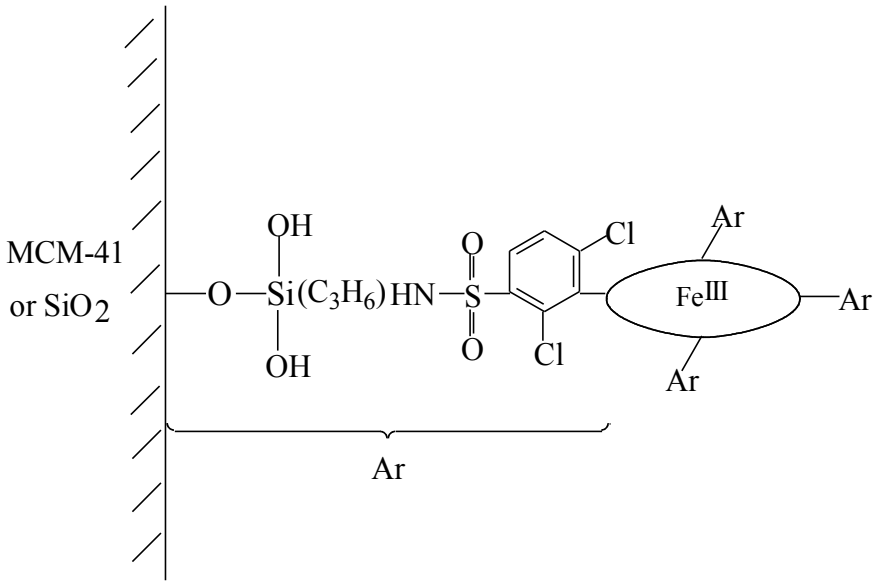

Scheme 7. Schematic representation of Fe(III)P/MCM-41 or of Fe(III)P/SiO_2 structures.

3. 1. 3 TEXTURAL CHARACTERIZATION

Diffuse reflectance UV/vis spectra and N_2 adsorption-desorption experiments were carried out as described above in paragraph 1.1.3.

Adsorption experiments of the mono-alcohols (1-pentanol and 2-pentanol) were carried out suspending Fe(III)P/MCM-41 or Fe(III)P/SiO_2 (33 g/L) in 300 μL of CH_3CN solutions containing increasing concentrations of both alcohols and keeping in the dark for 20 min under magnetic stirring.

The amounts of adsorbed alcohols were obtained by GC analysis evaluating their concentration decrease in the solution. For sensitivity reason, we carried out these experiments reducing the volume of alcoholic solution and increasing the amount of solid sample in respect to the photocatalytic experiments.

3. 1. 4 PHOTOCATALYTIC EXPERIMENTS

Photocatalytic experiments were carried out inside a Pyrex tube of 15 mL capacity at 298 ± 1K joined through an inlet tube to a balloon filled with O_2. Fe(III)P/MCM-41 or Fe(III)P/SiO_2 (4.5 g/L) was dispersed in 3 mL of a CH_3CN solution containing 1,4-pentanediol (3% v/v) and stirred (120 min) to reach equilibrium conditions before irradiation. Photochemical excitation was performed irradiating the sample in the pyrex tube with an external Helios Q400 Italquartz medium-pressure Hg lamp, selecting wavelengths higher than 350 nm with a cut-off filter. The photon flux, measured with a MACAMU UV203X ultraviolet radiometer, was 15 mW/cm^2. At the end of the photocatalytic experiment, the sample was centrifuged, the products that remained adsorbed on the irradiated powders were extracted with CH_2Cl_2 (2 times with aliquots of 3 mL each), and the organic phases were analyzed by GC. Product analyses were carried out by using a HP 6890 gas chromatograph, equipped with a flame ionisation detector and a DB-WAX capillary column. The programme temperature was 423 K (6 min), 4 K/min, 453 K (10 min). Quantitative analyses were performed with calibration curves obtained with standard samples. Each experiment was repeated three times in order to evaluate the error, which remained in the ± 5 % interval around mean values. Homogeneous reactions were carried out dissolving the iron porphyrin (Fe(III) *(1)*, 2×10^{-5} M) obtained through metallation of compound *(1)* of Scheme 6 in mixtures of CH_3CN and 1,4-pentanediol (3%, v/v). Unfortunately, photocatalytic experiments were impossible to carry out

because of the formation of a precipitate involving the iron porphyrin complex.

No oxidation products were obtained when blank experiments were run in the dark or irradiating in the absence of photocatalyst.

Other experiments were carried out in order to test the stability of Fe(III)P/MCM-41 system: after the first run the photocatalyst was recovered, washed with CH_2Cl_2 and CH_3CN, dried at 80 °C for 1 h and then reused in a new experiment. This procedure has been repeated up to five cycles.

3. 2 TEXTURAL CHARACTERIZATION

Textural characterization has been carried out at the University of Torino in collaboration with Dr. Giuliana Magnacca.

In the $Fe^{III}P$/MCM-41 and $Fe^{III}P/SiO_2$ prepared materials, the iron porphyrin complex is covalently linked on the surface of the support, as schematized in Scheme 7. The loading of iron porphyrin on the support corresponds to ~1% w/w. The diffuse reflectance Uv-vis spectra of $Fe^{III}P$/MCM-41 and of $Fe^{III}P/SiO_2$ indicate that the structure of the porphyrin remains unchanged during the immobilization procedure (Figure 23).

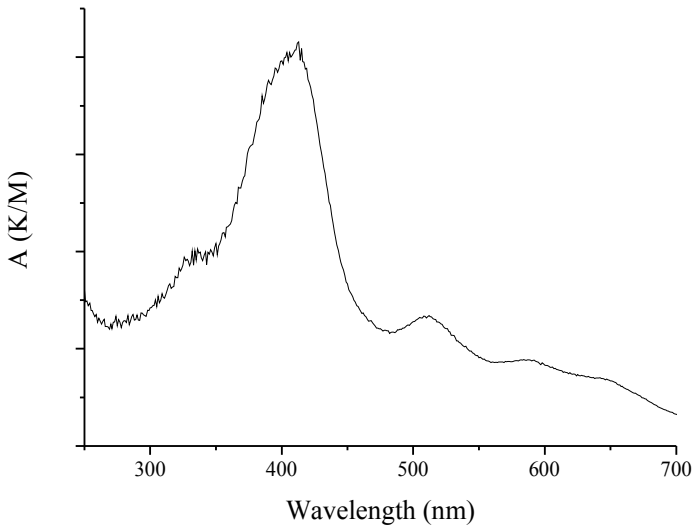

Figure 23. DR-UV-visible spectrum of $Fe^{III}P$/MCM-41.

The effect of porphyrin addition on specific surface area and porosity of $Fe^{III}P/MCM-41$ and of $Fe^{III}P/SiO_2$ has been evaluated by means of BET [150] and BJH [152] model applied to N_2 adsorption/desorption isotherms carried out at 77 K. The results are summarized in Table 11.

Table 11. BET specific surface areas and porosity details of pure and modified supports.

Samples	BET Specific surface area (m^2/g)	BJH Total Porosity (cm^3/g)	BJH Pore size (determined on maximum) (Å)
MCM-41	960	0.73	25
$Fe^{III}P/MCM-41$	826	0.71	23
SiO_2	97	0.44	~100
$Fe^{III}P/SiO_2$	93	0.41	~100

The specific surface area decreases for both samples in the presence of the iron porphyrin, but the change is much more relevant in the MCM-41 case. At the same time, for both supports, the presence of the iron porphyrin decreases the total porosity in a very limited extent.

Deep examination of Figure 24 and 25, which report the shape of the isotherms and the curves relative to pore size distribution respectively allows to evaluate better the modification of the MCM-41 sample induced by the Fe^{III}-porphyrin presence. It appears clearly that the MCM-41 sample presents a significant modification due to the presence of porphyrin. More specifically, the isotherm shape typical of a MCM-41 material (Figure 24, solid-line curve) results modified (Figure 24, circle-symbol curve): the first capillary condensation, typically narrow and present at $p/p^0 = 0.35$ for unmodified MCM sample, moves downwards and it is accompanied by another not so evident capillary condensation (indicated in the figure by an arrow) which covers up to $p/p^0 = 0.65$, indicating a modification in the very regular mesoporous structure of MCM sample. Moreover, the porphyrin-

containing material shows a small hysteresis loop associated to this capillary condensation (the hysteresis loop is evidenced in the figure by an arrow and closes at p/p° ≈ 0.42, in agreement with what expected for the tensile strength of N_2 used as adsorptive gas). This indicates a modification in the pore shape with respect to what observed for unmodified MCM-41. In fact, the presence of a hysteresis loop is compatible with ink-bottle-like pores, i.e., pores characterized by cavities with a small access. A last capillary condensation (and corresponding hysteresis loop) is present at very high values of relative pressure (p/p° > 0.90), indicating the possible presence of large mesoporosity, probably induced by interparticle spaces due to particle aggregation, but this feature seems to be not affected by the presence of the porphyrin, so it will be not considered anymore.

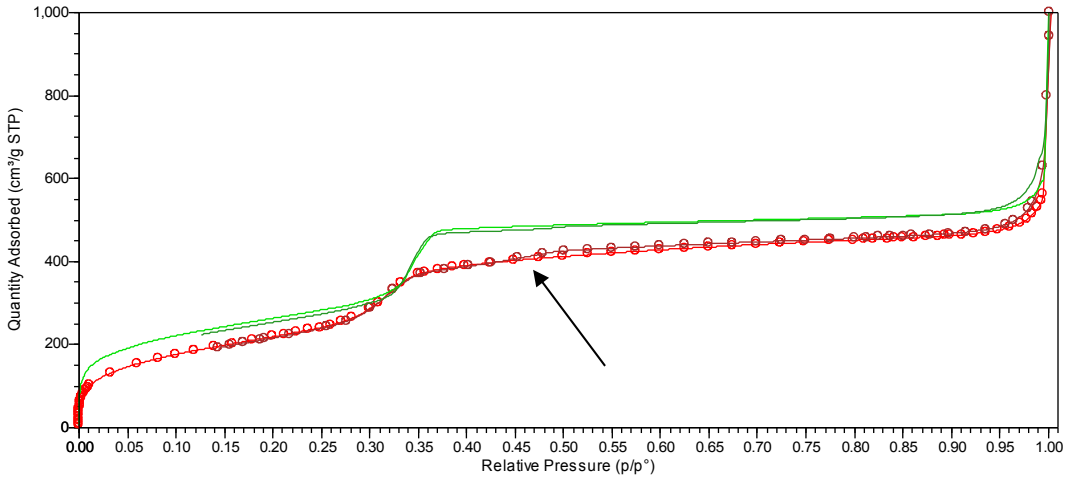

Figure 24. Adsorption/desorption isotherms of N_2 adsorbed at 77 K obtained for MCM-41 material: comparison between unfunctionalized sample (no symbols) and the functionalized one (circle symbols). The arrow indicates the presence of capillary condensation and corresponding hysteresis loop.

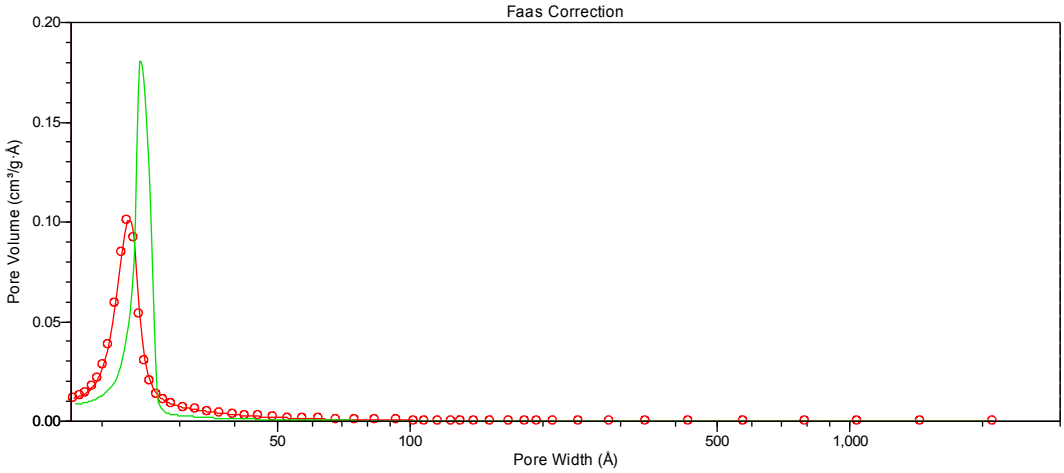

Figure 25. BJH pore size distribution obtained from N_2 adsorption at 77 K for MCM-41 sample: comparison between unfunctionalized sample (full line, no symbols) and the functionalized one (full line, circle symbols).

No analogous modification is evidenced by isotherms relative to SiO_2 samples with or without porphyrin (Fig. 26). The curves are those typical of an almost not porous system (an hysteresis loop is visible in the range of relative pressure 0.75-1 but it is probably caused by particle aggregation, as mentioned above for MCM samples) and no visible changes are induced by porphyrin presence.

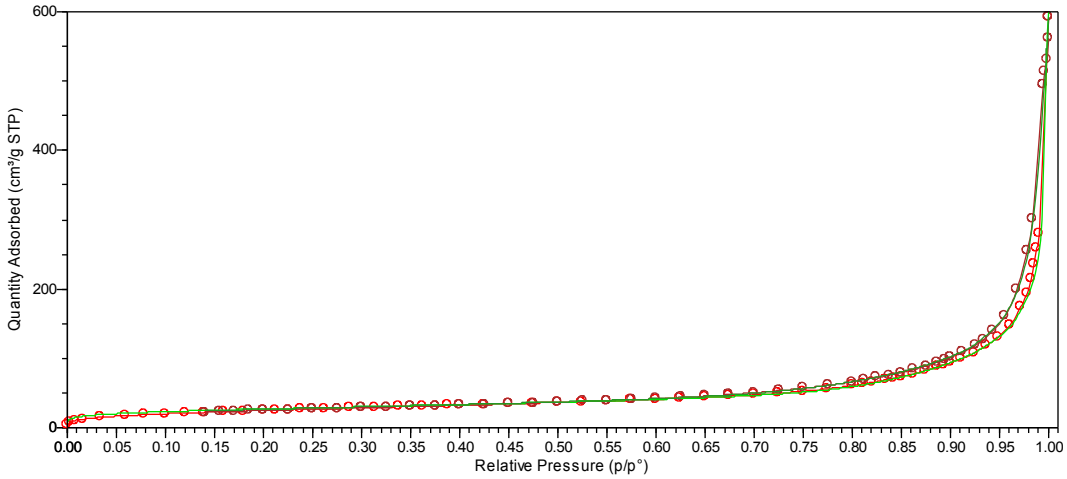

Figure 26. Adsorption/desorption isotherms of N_2 adsorbed at 77K obtained for SiO_2 material: comparison between unfunctionalized sample (no symbols) and the functionalized one (circle symbols).

In order to confirm the consideration made above, the BJH model has been applied to adsorption branch and the following can be attained (compare Table 11 and Figure 25). Total mesoporosity decreases slightly in the case of $Fe^{III}P$/MCM-41 compared to unmodified MCM material, but the pore size changes in average value and distribution, the pores formed in the presence of porphyrin being smaller and presenting a larger distribution. Again, no analogous modifications were evidenced in the case of SiO_2 systems (Fig. 27).

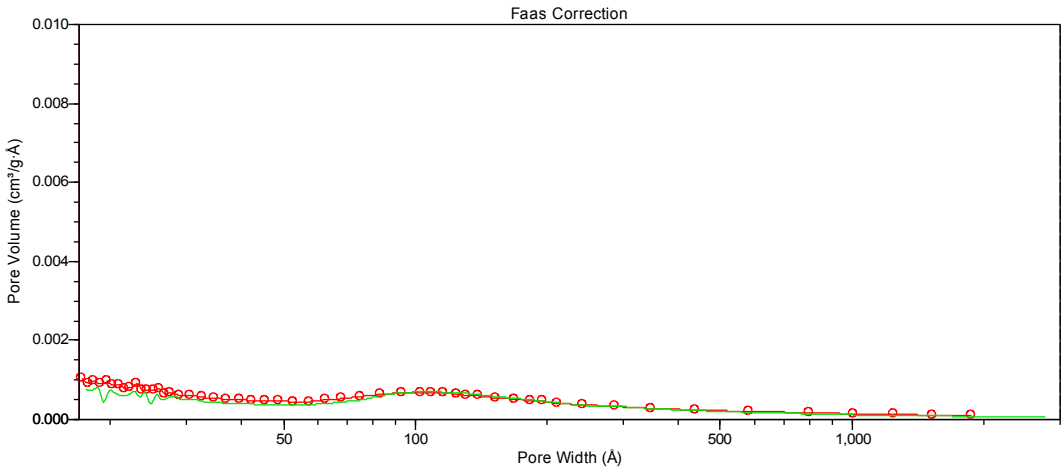

Figure 27. BJH pore size distribution obtained from N_2 adsorption at 77 K for SiO_2 sample: comparison between unfunctionalized sample (full line, no symbols) and the functionalized one (full line, circle symbols).

In conclusion, the morphological features of MCM-41 have been clearly changed by porphyrin presence. The modification of the porous texture may be explained considering that porphyrin molecules, when localized near a pore, likely cause a partial block of the cavity access. This renders slightly smaller and less accessible the mesopores of MCM material, giving reason of the specific surface area decrease and of the porous arrangement modification (different capillary condensation, presence of the hysteresis loop indicated by the arrow in Figure 24). No analogous features can be deduced by N_2-gas-volumetric studies for SiO_2 material, but in this case a much less ordered starting structure can induce a camouflage effect.

3. 3 PHOTOCATALYTIC OXIDATION OF 1,4-PENTANEDIOL

It is well-established that iron porphyrin complexes are able to induce the photocatalytic oxidation of primary and secondary alcohols in homogeneous solution according to the mechanism described by Equations 1-3 [8, 193, 194].

More specifically, irradiation in LMCT bands (λ = 300-400 nm) of the Fe(III) porphyrin ($Fe^{III}P$) in the presence of a primary or a secondary alcohol (R_1R_2CHOH, where R_1 = alkyl chain and R_2 = alkyl chain or H) induces the homolytic cleavage of the bond between Fe(III) and the axially coordinated alkoxide ion. This process causes oxidation and detachment of an alkoxide radical which may undergo further oxidation by $Fe^{III}P$ yielding the corresponding carbonylic derivative (Eq. 2). The starting $Fe^{III}P$ can be regenerated as a consequence of the very fast reaction of the ferrous complex with molecular oxygen (Eq. 3).

The photocatalytic activity of Fe(III)P/MCM-41 and of Fe(III)P/SiO_2 has been assessed in the oxidation of a multifunctional molecule such as 1,4-pentanediol in the presence of molecular oxygen. It is to be underlined that the selective oxidation of one of the alcoholic functionalities present in diols is an important transformation in fine chemistry. Particular attention is devoted to the effects of the two different matrices on the photocatalytic activity. Acetonitrile suspensions of these photocatalysts containing 1,4-pentanediol were irradiated (λ > 350 nm) at room temperature and under 760 Torr of O_2. Photoexcitation caused the conversion of the diol to the products reported in Scheme 8: 4-hydroxypentanal **(a)** and 5-hydroxy-2-pentanone **(b)** derive from the selective oxidation of primary or secondary hydroxy functional group of the diol. From chromatographic analysis, other two peaks were attributed to the cyclic emiacetalic diastereoisomers **(c)** derived from the closure of product **(a)**.

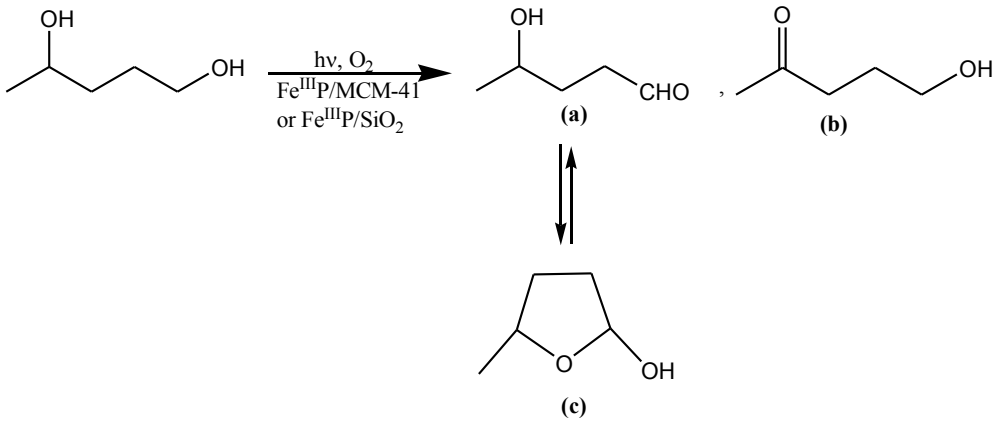

Scheme 8. Oxidized products obtained upon irradiation of $Fe^{III}P/MCM-41$ or $Fe^{III}P/SiO_2$ suspended in CH_3CN solutions containing 1,4-pentanediol in the presence of O_2.

After 240 min irradiation, **(a)**, **(b)** and **(c)** represented about the 95% of the overall gas chromatographic area of the detected products. No oxidation products were obtained when blank experiments were run in the absence of light or irradiating the dispersing medium without $Fe^{III}P/MCM-41$. From UV-vis spectra, no release of Fe^{III} porphyrin was detected during the photocatalytic experiment, thus confirming that we were in the presence of real heterogeneous catalytic processes. A loss of photocatalyst activity of about 30% in terms of detected products after irradiation was observed after five repeated cycles.

On the basis of the described results, we can state that the ability of photoexcited iron porphyrins to induce alcohol oxidation according to Equations (1) – (3) is retained also in the heterogeneous systems $Fe^{III}P/MCM-41$ and $Fe^{III}P/SiO_2$. In fact, the nature of the photoproducts is consistent with the oxidation of one alcoholic functionality of the diol. It is noteworthy that the partially oxidized products **(a)**, **(b)** and **(c)** can be accumulated with no formation of ketoacids.

The photocatalytic properties of $Fe^{III}P/MCM-41$ and of $Fe^{III}P/SiO_2$ in the oxidation of 1,4-pentanediol are summarized in Table 12 as μmoles of

aldehyde and its isomers (***n*(a+c)**) and ketone (***n*b**) obtained after 120 and 240 min irradiation. The concentration ratio between aldehyde and ketone (last column of Table 12) enables us to evaluate the regioselectivity of the photocatalytic process. It is seen that $Fe^{III}P$/MCM-41 is able to photooxidize 1,4-pentanediol in 1-position with good selectivity, since the aldehyde to ketone concentration ratio is 2.4 after 240 min photoexcitation.

Table 12. Photocatalytic properties[a] of $Fe^{III}P$/MCM-41 and $Fe^{III}P/SiO_2$ in the oxidation of 1,4-pentanediol.

Photocatalyst	***n*(a+c)** [b]	***n*b**[b]	***n*(a+c)/*n*b**
$Fe^{III}P$/MCM-41 120 min	2.6	1.5	1.7
$Fe^{III}P$/MCM-41 240 min	5.1	2.1	2.4
$Fe^{III}P/SiO_2$ 120 min	0.3	0.7	0.4
$Fe^{III}P/SiO_2$ 240 min	0.3	1.6	0.2

[a] In a typical experiment the employed photocatalyst (4.5 g L^{-1}) was suspended in a CH_3CN solution (3 mL) containing 1,4-pentanediol (3% v/v) and irradiated ($\lambda > 350$ nm) at 298 $\pm$ 1 K and 760 Torr of O_2. Reported values are the mean of three repeated experiments (error = $\pm$ 5%).

[b] Amount of carbonylic compounds as μmoles obtained in 3 mL of solution.

The photocatalytic activity of the iron porphyrin is significantly lower when it is bound on the surface of amorphous silica rather than on the mesoporous material. In fact, Table 12 indicates that the overall oxidation yield of 1,4-pentanediol to carbonylic compounds with $Fe^{III}P$/MCM-41 is about four times higher than that obtained with $Fe^{III}P/SiO_2$. It is plausible that the mesoporous photocatalyst, with its very wide surface area, is able to disperse better the added amount of iron porphyrin, thus providing a greater number of photocatalytic sites and preventing the formation of photochemically inactive aggregates.

Table 12 shows that $Fe^{III}P/MCM-41$ and $Fe^{III}P/SiO_2$ differ also in terms of regioselectivity; in fact, the ketone **(b)** is the main product when the iron porphyrin is linked on the surface of amorphous silica. This difference may be due, at least in part, to surface phenomena that can control how diol molecule approaches to the photoactive iron porphyrin. Previous investigations on the photocatalytic oxidation of diols by titanium dioxide [195] or heterogenized polyoxotungstates [81] have demonstrated the important role played by uptake phenomena on the surface. For this reason, we carried out some experiments in order to evaluate the interaction strength of the two hydroxy functional groups of the diol with the solid surfaces of $Fe^{III}P/MCM-41$ and $Fe^{III}P/SiO_2$. These materials were suspended in CH_3CN mixtures containing both the monofunctional alcohols 1-pentanol and 2-pentanol, which simulate the two different hydroxy groups present in 1,4-pentanediol. We evaluated the uptake of these alcohols after 20 minutes of stirring in the dark. For sensitivity reason, we carried out these experiments reducing the volume of the alcoholic solutions employed and increasing the amount of solid samples with respect to the photocatalytic experiments. Figure 27 shows that 2-pentanol interacts with $Fe^{III}P/SiO_2$ in a greater extent than 1-pentanol (circles). This is an indication that also the secondary -OH functional group of 1,4-pentanediol undergoes a preferential interaction with the surface of $Fe^{III}P/SiO_2$, so explaining why the ketone **(b)** is the main product upon irradiation of $Fe^{III}P/SiO_2$.

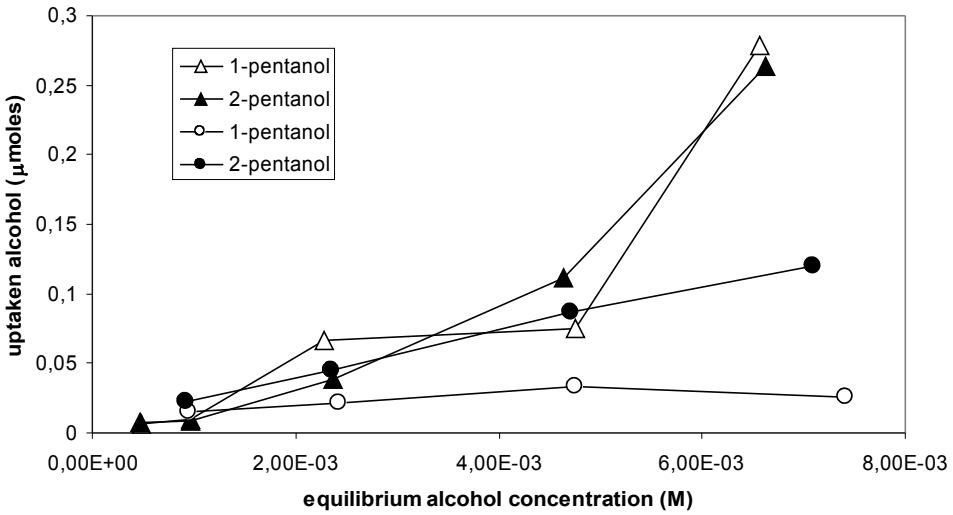

Figure 27. Uptake of 1-pentanol (empty symbols) and 2-pentanol (full symbols) on $Fe^{III}P/SiO_2$ (circles) and on $Fe^{III}P$/MCM-41 (triangles). $Fe^{III}P/SiO_2$ or $Fe^{III}P$/MCM-41 (33 g/l) were suspended in 0.3 ml of CH_3CN containing increasing amounts of the two alcohols.

Figure 27 shows that the interaction strengths of 2-pentanol and 1-pentanol on $Fe^{III}P$/MCM-41 are comparable (triangles), suggesting that in this case, besides uptake phenomena on the surface, other textural effects must be responsible of the observed ability of this material to convert preferentially 1,4-pentanediol to the corresponding hydroxyl-aldehyde **(a)**. The physico-chemical characterization described above is compatible with a modification of the pore shape with respect to what observed for unmodified MCM-41 and with the formation of ink-bottle-like pores. The modification of the porous texture has been explained above considering that Fe^{III}-porphyrin molecules are mainly localized near the ordered mesopore entrance, creating some kind of channel narrowing. As a consequence, a sort of steric control may favour the preferential coordination and the subsequent oxidation of the primary hydroxy functional group of 1,4-pentanediol to give the aldehydic derivative.

Other experimental evidences showed that Fe^{III}(**1**) complex can not be employed as it is for the photocatalytic oxidation of 1,4-pentanediol in homogeneous solution. In fact, dissolution of Fe^{III}(**1**) in mixtures of CH_3CN and diol led to the formation of a precipitate with a concomitant decay in absorbance in all the Uv-visible spectrum. We believe that the bifunctional character of diol favours the formation of insoluble 1,4-pentanediol-bridged Fe^{III}(**1**) oligomers (in fact, no spectral changes and no precipitate were observed when Fe^{III}(**1**) was dissolved in pure CH_3CN) and this provokes a loss of the active molecules. This problem does not occur when the photo-active component is covalently bonded to the support of the heterogeneous catalyst.

3. 3 CONCLUSIONS

The heterogenization of a silanized Fe(III)porphyrin by covalent bond on MCM-41 leads to a robust photocatalyst able to induce the O_2-assisted oxidation of 1,4-pentanediol with good regioselectivity. By comparison with amorphous silica, it has been pointed out that mesoporous support can control this regioselectivity by: i) uptake phenomena, which govern how the diol molecule approaches to the photoactive iron porphyrin and ii) some kind of steric control that favours the preferential coordination and subsequent oxidation of the primary OH group of the diol. Finally, considering that photocatalytic oxidation of polyalcohols can not be carried out by iron porphyrins in homogeneous conditions, this new heterogeneous system opens a new way to perform this interesting chemical transformation, preventing the formation of inactive oligomers and affecting regioselectivity by tuning the characteristics of the support.

BIBLIOGRAPHY

) M. A. Fox, Synthetic applications of photocatalytic oxidation and reduction reactions of organic reactants on irradiated semiconductors surfaces. In: Balzani V (ed) Electron transfer in chemistry, Vol. I Principles and theories, Wiley-VCH: Weinheim, (2001), p 271.
2) Y. Li, L. Wang, Stud. Surf. Sci. Catal., (1997), 103, 391.
3) B. Ohtani, Trends Photochem. Photobiol., (1994), 3, 531.
4) A. Fujishima, T. N. Rao, D. A. Tryk, J. Photochem. Photobiol. C: Photochem. Rev., (2000), 1, 1.
5) Y. Shiraishi, T. Hirai, J. Photochem. Photobiol. C: Photochem. Rev., (2008), 9, 157.
6) G. Palmisano, V. Augugliaro, M. Pagliaro, L. Palmisano, Chem. Commun., (2007), 3425.
7) M. Fagnoni, D. Dondi, D. Ravelli, A. Albini, Chem. Rev., (2007), 107, 2725.
8) A. Maldotti, A. Molinari, R. Amadelli, Chem. Rev., (2002), 102, 3811.
9) M. D. Tzirakis, I. N. Lykakis, M. Orfanopoulos, Chem. Soc. Rev., (2009), 38, 2609.
10) H. Kisch, Adv. Photochem., (2001), 62, 93.
1) A. G. Griesbeck, J. Mattay, Synthetic Organic Photochemistry, Dekker: New York., (2005).
2) C. Gambarotti, C. Punta, F. Recupero, T. Caronna, L. Palmisano, Curr. Org. Chem., (2010), 14, 1153.
3) A. Maldotti, A. Molinari, Topics in Current Chemistry, (2011), 303, 185.
4) F. Zaera, Phys Chem Lett., (2010), 1, 621.
5) A. Molinari, A. Bratovcic, G. Magnacca, A. Maldotti, Dalton Trans., 39 (2010), 7826.
6) A. Molinari, A. Maldotti, A. Bratovcic, G. Magnacca, Cat. Today, 161 (2011), 64.
7) A. Molinari, A. Maldotti, A. Bratovcic, G. Magnacca, Catal. Today, in press doi: doi.org/10.1016/j.cattod.2011.11.033.
8) M. T. Pope, Hetero and Isopoly Oxometallates in Inorganic Chemistry Concepts 8, C. K. Jorgensen et al. eds., Springer Verlag, West Berlin, (1983).
19) E. Papaconstantinou, Chem. Soc. Rev., (1989), 18, 1.
20) V. W. Day, W. G. Klemperer, Science, (1985), 228, 533.
21) C. M. Prosser-McCartha, M. Kadkhodayan, M. M. Williamson, D. A. Bouchard, C. L. Hill, J. Chem. Soc. Chem. Comm., (1986), 1747.
22) D. L. Kepert, "Comprehensive inorganic chemistry", A. F. Trotman-Dickerson et al. Editors, Pergamon Press, Oxford, (1973), 4, 607.
23) G. A. Tsigdinos, "Heteropoly Compounds of Molybdenum and Tungsten" Topics in Current Chemistry, (1978), 76, 1.
24) Volume 98 (issue 1) of Chem. Rev. (1998) has been entirely devoted to polyoxometalates, C. L. Hill guest editor.
25) M. Misono, Cat. Rev. (1987), 29, 269.

26) C. L. Hill, C. M. Prosser-McCartha, in: Photosensitization and Photocatalysis Using Inorganic and Organometallic Compounds, Kluwer Academic, Dordrecht, (1993).
27) R. Neumann, M. Dahan, Nature, (1997), 388, 353.
28) C. L. Hill, C. M. Prosser-McCartha, Coord. Chem. Rev. (1995), 143, 407.
29) C. Tanielian, Coord. Chem. Rev., (1998), 178, 1165.
30) A. Hiskia, A. Mylonas, E. Papaconstantinou, Chem. Soc. Rev., (2001), 30, 62.
31) "Polyoxometalates in catalysis" special issue of J. Mol. Catal., (1996) 114 (issue 1-3), C. L. Hill editor.
32) J. Berzelius, Pogg. Ann. (1826), 6, 369.
33) L. Svanberg and H. Struve, J. Prakt. Chem., (1848), 44, 257.
34) A. Werner, Ber. Dtsch. Chem. Ges., (1907), 40, 40.
35) A. Miolati and R. Pizzigelli, J. Prakt. Chem., (1908), 77, 417.
36) A. Rosenheim, Handbuch der Anorganischen Chemie; Abegg, R., Auerbach, F., Eds; Hirtzel Verlag: Leipzich, (1921); Vol. Part 1, ii, p. 997-1064.
37) L. C. Pauling, J. Am. Chem. Soc. (1929), 51, 2868.
38) J. F. Keggin, Nature, (1933), 131, 908.
39) H. T. Jr. Evans, J. Am. Chem. Soc., (1948), 70, 1291.
40) B. Dawson, Acta Crystallogr., (1953), 6, 113.
41) P. Souchay, A. Tezè, G. Harvè, C.R. Acad. Sci. C. (1972), 275, 1013.
42) R. D. Shannon, C. L. Prewitt, Acta Cryst., (1969), B25, 925.
43) N. N. Lipscomb, Inorg. Chem., (1965), 4, 132.
44) M. T. Pope, Inorg. Chem., (1972), 11, 1973.
45) O. Glemser, W. Hoeltje, Z. Naturforsch., (1965), 20b, 492.
46) J. Fuchs, H. Hartl, W. Schiller, U. Gerlach, Acta Cryst., (1976), 332, 740.
47) J. Fuchs, H. Hartl, W. Schiller, Angew. Chem. Int. Ed. Eng., (1973), 12, 420.
48) K. Y. Lee, T. Arei, S. Nakata, S. Asaoka, T. Okuhera, M. Misono, J. Am. Chem. Soc., (1992), 114, 2836.
49) T. Yamase, N. Takabayashi, M. Keji, J. Chem. Soc. Dalton Trans., (1984), 793.
50) M. T. Pope, G. M. Varga, Inorg. Chem., (1966), 5, 1249.
51) E. Papaconstantinou, M. T. Pope, Inorg. Chem., (1967), 6, 1152.
52) M. T. Pope, E. Papaconstantinou, Inorg. Chem., (1967), 6, 1147.
53) J. P. Launay, J. Inorg. Nucl. Chem., (1976), 38, 807.
54) R. Acerete, S. P. Harmalker, C. F. Hammer, M. T. Pope, L. C. W. Baker, J. Chem. Soc. Chem. Comm., (1979), 777.
55) G. M. Varga Jr., E. Papaconstantinou, M. T. Pope, Inorg. Chem. (1970), 9, 662.
56) E. Papaconstantinou, M. T. Pope, Inorg. Chem., (1970), 9, 667.
57) N. Mizuno, M. Misono, Chem Rev., (1998), 98, 199.

58) A. M. Khenkin, R. Ben-Daniel, A. Rosenberger, I. Vigdergauz, R. Neumann in Polyoxometalate Chemistry From Topology via Self-Assembly to Applications, M. T. Pope and A. Muller Editors, Kluwer Academic Publishers: Dordrecht, Boston, London, (2001), p 347.
59) A. Maldotti, A. Molinari in Progress in Heterogeneous Catalysis, D. L. Marmaduke Ed., Nova Science Publishers, New York (2008) p. 1.
60) D. C. Duncan, T. L. Netzel, C. L. Hill, Inorg. Chem., (1995), 34, 4640.
61) C. Tanielian, K. Duffy, A. Jones, J. Phys. Chem. B, (1997), 101, 4276.
62) D. C. Duncan, M. A. Fox, J. Phys. Chem. A, (1998), 102, 4559.
63) A. Maldotti, R. Amadelli , G. Varani, S. Tollari, F. Porta, Inorg. Chem., (1994), 33, 2968.
64) A. Molinari, R. Amadelli, L. Andreotti, A. Maldotti, J. Chem. Soc. Dalton Trans., (1999), 1203.
65) A. Molinari, R. Amadelli, A. Mazzacani, G. Sartori, A. Maldotti, Langmuir (2002), 18, 5400.
66) A. Maldotti, A. Molinari, G. Varani, M. Lenarda, L. Storaro, F. Bigi, R. Maggi, A. Mazzacani, G. Sartori, J. Catal. (2002), 209, 210.
67) A. Molinari, R. Amadelli, V. Carassiti, A. Maldotti, Eur. J. Inorg. Chem. (2000), 1, 91.
68) A. Maldotti, R. Amadelli, I. Vitali, L. Borgatti, A. Molinari, J. Mol. Catal. A: Chem., (2003), 204-205, 703.
69) M. D. Tzirakis, I. N. Lykakis, G. D. Panagiotou, K. Bourikas, A. Lycourghiotis, C. Kordulis, M. Orfanopoulos, J Catal., (2007) 252, 178.
70) H. Y. Shen, H. L. Mao, L.Y. Ying, Q. H. Xia, J. Mol. Catal. A: Chem., (2007), 276, 73.
71) R. R. Ozer, J. L. Ferry, J. Phys. Chem. B., (2002), 106, 4336.
72) Y. Guo, C. Hu, X. Wang, Y. Wang, E. Wang, Y. Zou, H. Ding, S. Feng, Chem. Mater., (2001), 13, 4058.
73) Y. Guo, C. Hu, S. Jiang, C. Guo, Y. Yang, E. Wang, Appl. Catal. B: Environ., (2002), 36, 9.
74) S. Farhadi, M. Afshari, J. Chem. Res., (2006), 3, 188.
75) S. Farhadi, M. Afshari, M. Malesi, Z. Babazadeh, Tetrahedron Lett., (2005), 46, 8483.
76) S. Farhadi, Z. Momeni, J. Mol. Catal. A: Chem., (2007), 277, 47.
77) S. Farhadi, M. Zaidi, J. Catal., (2009), 354, 119.
78) S. Farhadi, S. Sepahvand, J. Mol. Catal. A: Chem., (2010), 318, 75.
79) D. A. Friesen, D. B. Gibson, C. H. Langford, Chem. Commun., (1998), 543.
80) D. A. Friesen, L. Morello, J. V. Headley, C. H. Langford, J. Photochem. Photobiol. A: Chem., (2000), 133, 213.
81) A. Maldotti, A. Molinari, F. Bigi, J. Catal., (2008), 253, 312.
82) L. Ni, J. Ni, Y. Lv, P. Yang, Y. Cao, Chem. Commun., (2009), 2171.
83) E. Fornal, C. Giannotti, J. Photochem. Photobiol. A: Chem., (2007), 188, 279.
84) A. Molinari, G. Varani, E. Polo, S. Vaccari, A. Maldotti, J. Mol. Catal. A: Chem., (2007), 262, 156.

85) M. Bonchio, M. Carraro, G. Scorrano, E. Fontananova, E. Drioli, Adv. Synth. Catal., (2003), 345, 1119.
86) M. Bonchio, M. Carraro, M. Gardan, G. Scorrano, E. Drioli, E. Fontananova, Top. Catal., (2006), 40, 133.
87) M. Carraro, M. Gardan, G. Scorrano, E. Drioli, E. Fontananova, M. Bonchio, Chem. Commun., (2006), 4533.
88) L. C. Lopez, M. G. Buonomenna, E. Fontananova, G. Iacoviello, E. Drioli, R. d'Agostino, P. Favia, Adv. Funct. Mater., (2006), 16, 1417.
89) E. Fontananova, L. Donato, E. Drioli, L C. Lopez, P. Favia, R. d'Agostino, Chem. Mater., (2006), 18, 1561.
90) K. S. Suslick, "Shape-selective oxidation in metalloporphyrins" in The porphyrin handbook, vol. 4, chapter 28, K. M. Kadish, K. M. Smith, R. Guilard editors, Academic Press, San Diego, San Francisco, New York, Boston, London, Sydney, Tokyo, 2000.
91) S. Nakagaki, K. A. D. F Castro, G. S. Machado, M. Halma, S. M. Drechsel, F. Wypych, J. Braz. Chem. Soc. (2006), 17, 1672.
92) J. D. Harvey, C. J. Zeigler, J. Inorg. Biochem., (2006), 100, 869.
93) F. Bedioui, Coord. Chem. Rev., (1995), 144, 39.
94) J. Haber, L. Matachowski, K. Pamin, J. Poltowicz, J. Mol. Catal. A: Chem., (2003), 198, 215.
95) B. Meunier, Chem. Rev. (1992), 92, 1411.
96) J. T. Groves, Y. Z. Han, in:, Cytocrome P-450: Structure, Mechanism and Biochemistry, Ortiz de Montellano Ed., 2nd ed., Plenum Publishing, New York, (1995).
97) D. Mansuy, Coord. Chem. Rev., (1993), 125, 129.
98) C. K. Chang, F. Ebina, J. Chem. Soc., Chem. Commun., (1981), 778.
99) T. G. Traylor, S. Tsuchiya, Y. S. Byun, C. Kim, J. Am. Chem. Soc., (1993), 115, 2775.
100) T. G. Traylor, S. Tshuchiya, Inorg Chem., (1987), 26, 1338.
01) K. Kalyanasundaram, Photochemistry of Polypyridine and Porphyrin complexes, Academic Press, London, San Diego, (1992), 384.
02) A. Maldotti, C. Bartocci, R. Amadelli, V. Carassiti, J. Chem. Soc. Dalton Trans., (1989), 1197.
03) D. N. Hendrickson, M. G. Kinnaird, K. S. Suslick, J. Am. Chem. Soc., (1987), 109, 1243.
04) M. W. Peterson, D. S. Rivers, R. M. Richman, J. Am. Chem. Soc., (1985), 107, 2907.
05) T. Berthold, D. Rehorek, H. Hennig, Zeitschrift fur Chemie, (1986), 26, 183.
06) D. N. Hendrickson, M. G. Kinnaird, K. S. Suslick, J. Am. Chem. Soc., (1987), 109, 1243.
07) L. Weber , R. Hommel, J. Behling, G. Haufe, H. Hennig, J. Am. Chem. Soc., (1994), 116, 2400.
08) K. S. Suslick, R. A. Watson, Inorg Chem., (1991), 30, 912.
09) A. Maldotti, C. Bartocci, G. Varani, A. Molinari, P. Battioni, D. Mansuy, Inorg. Chem. (1996), 35, 1126.

10) P. Battioni, J. F. Bartoli, D. Mansuy, Y. S. Byun, T. G. Traylor, J. Chem. Soc. Chem. Comm., (1992), 1051.
11) P. Battioni, J. P. Lallier, L. Bartoly, D. Mansuy, J. Chem. Soc. Chem. Comm., (1989), 1149.
12) A. Maldotti, L. Andreotti, A. Molinari, V. Carassiti, J. Biol. Inorg. Chem., (1999), 4, 154.
13) A. Maldotti, A. Molinari, L. Andreotti, M. Fogagnolo, R. Amadelli, Chem. Commun., (1998), 507.
114) T. G. Traylor, Y. S. Byun, P. S. Traylor, P. Battioni, D. Mansuy, J. Am. Chem. Soc., (1991), 113, 7821.
15) K. S. Suslick, P. Bhyrappa, J. H. Chou, M. E. Kosal, S. Nakagaki, D. W. Smithenry, S. R. Wilson, Acc. Chem. Res. (2005), 38, 283.
16) F. L. Benedito, S. Nakagaki, A. A. Saczk, P. G. Peralta-Zamora, M. C. M. Costa, Appl. Catal., A: General (2003), 250, 1.
17) Y. Iamamoto, Y. M. Idemori, S. Nakagaki, J. Mol. Catal. A: Chem. (1985), 99, 187.
18) S. Nakagaki, C. R. Xavier, A. J. Wosniak, A. S. Mangrich, F. Wypych, M. P. Cantão, I. Denicoló, L. T. Kubota, Colloids Surf., A, (2000), 168, 261.
19) N. Herron, Coord. Chem. Rev. (1998), 19, 25.
20) L. Barloy, J. P. Lallier, P. Battioni, D. Mansuy, Y. Pitfard, M. Tournoux, J. B. Valim, W. Jones, New J. Chem. (1992), 16, 71.
21) A. M. Machado, F. Wypych, S. M. Drechsel, S. Nakagaki, J. Colloid Interface Sci. (2002), 254, 158.
22) A. L. Faria, T. O. C. Mac Leod, V. P. Barros, M. D. Assis, J. Braz. Chem. Soc. (2009), 20, 895.
23) S. Nakagaki, M. Halma, A. Bail, G. G. C. Arízaga, F. Wypych, J. Colloid. Interface Sci., (2005), 281, 417.
24) F. Wypych, A. Bail, M. Halma, S. Nakagaki, J. Catal., (2005), 234, 431.
25) S. Nakagaki, F. Wypych, J. Colloid Interface Sci., (2007), 315, 145.
26) E. A. Vidoto, M. S. M. Moreira, F. S. Vinhado, K. J. Ciuffi, O. R. Nascimento, Y. Iamamoto, J. Non-Cryst. Solids (2002), 304, 151.
27) H. C. Sacco, K. J Ciuffi, J. C. Biazzotto, M. R. Zucchi, C. A. M. Leite, O. R. Nascimento, O. A. Serra, Y. Iamamoto, J. Non-Cryst. Solids (2000), 273,150.
28) D. C. Oliveira, H. C. Sacco, O. R. Nascimento, Y. Iamamoto, K. J. Ciuffi, J. Non-Cryst. Solids (2001), 284, 27.
29) A. T. Papacídero, L. A. Rocha, B. L. Caetano, E. Molina, H. C. Sacco, E. J. Nassar, Y. Martinelli, C. Mello, S. Nakagaki, K. J. Ciuffi, Colloids Surf., A (2006), 275, 27.
30) H. Podbielska, A. Ulatowska-Jarza, G. Müller, I. Holowacz, J. Bauer, U. Bindig, Biom. Eng., (2007), 24, 425.
31) H. Tanaka, T. Yamada, S. Sugiyama, H. Shiratori, R. Hino, J. Colloid Interface Sci., (2005), 286, 812.
32) I. Dror, D. Baram, B. Berkowitz, Environ. Sci. Technol., (2005), 39, 1283.

33) H. Wang, Y. Song, Z. Wang, C. J. Medforth, J. E. Miller, L. Evans, P. Li, J. A. Shelnutt, Chem. Mat., (2008), 20, 7434.
34) D. Dolphin, T.G. Traylor, L.Y. Xie, Acc. Chem. Res., 30, (1997), 251.
35) K. A. D. F. Castro, M. Halma, G. S. Machado, G. P. Ricci, G. M. Ucoski, K. J. Ciuffi, S. Nakagaki, J. Braz. Chem. Soc., (2010), 21, 1329
36) W. Stöber, A. Fink, J. Colloid Interface Sci., (1968), 62, 26.
37) E. Polo, R. Amadelli, V. Carassiti, A. Maldotti, Inorg. Chim. Acta (1992), 192, 1.
38) K. Kalyanasundaram, Ed. in Photochemistry in Microheterogeneus Systems, Academic Press: London, 1987.
39) A. Maldotti, L. Andreotti, A. Molinari, G. Varani, G. Cerichelli, M. Chiarini, Green Chem. (2001), 3, 42.
140) C. Tanielian, I. N. Lykakis, R. Seghrouchni, F. Cougnon and M. Orfanopoulos, J. Mol. Catal. A: Chem., (2007), 262, 170.
41) I. N. Lykakis, C. Tanielian, R. Seghrouchni and M. Orfanopoulos, J. Mol. Cat. A: Chem., (2007), 262, 176.
42) I. N. Lykakis and M. Orfanopoulos, Tetrahedron Lett., (2005), 46, 7835.
43) I. Texier, J. A. Delaire and C. Giannotti, Phys. Chem. Chem. Phys., (2000), 2, 1205.
44) Y. Guo, C. Hu, J. Mol. Cat. A: Chem., (2007), 262, 136.
145) Y. Guo, D. Li, C. Hu, E. Wang, Y. Wang, Y. Zhou, S. Feng, Appl. Catal. B, (2001), 30, 337.
146) Y. Izumi, K. Hisano, T. Hida, Appl. Catal. A: General, (1999), 181, 277.
147) M. Filowitz, R. K. C. Ho, W. G. Klemperer, W. Shun, Inorg. Chem., (1979), 18, 93.
148) A. Chemseddine, C. Sanchez, J. Livage, J. P. Launay, M. Fournier, Inorg. Chem., (1984), 23, 2609.
149) Y. Guo, Y. Wang, C. Hu, Y. Wang and E. Wang, Chem. Mater., (2000), 12, 3501.
150) S. Brunauer, P. H. Emmet, E. Teller, J. Am. Chem. Soc., (1938), 60 309.
151) I. Langmuir, J. Am. Chem. Soc., (1918), 40, 1361.
152) E. P. Barret, L. S. Joyner, P. P. Halenda, J. Am. Chem. Soc., (1951), 73, 373.
153) R. Horvath, K. J. Kowazoe, J. Chem. Eng. Jpn., (1983), 16, 470.
154) D. L. Ou, P. M. Chevlier, I. A. Mackinnon, K. Eguchi, R. Boisvert, K. Su, J. Sol-Gel Sci. Technol., (2003), 26, 407.
155) J. P. Olivier, Carbon, (1998), 36, 1469.
156) M. A. Fox, H. Ogawa, P. Pichat, J. Org. Chem., (1989), 54, 3847.
157) A. Molinari, M. Montoncello, H. Rezala, A. Maldotti, Photochem. Photobiol. Sci., (2009), 8, 613.
158) R. A. Sheldon, J. A. Kochi, in “Metal-catalyzed Oxidations of organic Compounds”, Academic Press, New York, (1981).
159) T. Mallat, A. Baiker, Chem. Rev., (2004), 104, 3037.

160) V. Maurino, A. Bedini, M. Minella, F. Rubertelli, E. Pelizzetti, C. Minero, J. Adv. Oxid. Technol., (2008), 11, 184.
161) V. Augugliaro, H. A. Hamed El Nazer, V. Loddo, A. Mele, G. Palmisano, L. Palmisano, S. Yurdakal, Catal. Today (2010), 151, 21.
162) F. Bigi, A. Corradini, C. Quarantelli, G. Sartori, J. Catal., (2007), 250, 222.
163) E. G. Janzen, Acc. Chem. Res., (1971), 4, 31.
164) A. Maldotti, R. Amadelli, V. Carassiti, A. Molinari, Inorg. Chim. Acta, (1997), 256, 309.
165) M. L. Ganadu, L. Andreotti, I. Vitali, A. Maldotti, A. Molinari, G. M. Mura, Photochem. Photobiol. Sci., (2002), 1, 951.
66) D. Dondi, M. Fagnoni, A. Molinari, A. Maldotti, A. Albini, Chem. Eur. J., (2004), 10, 142.
167) D. Dondi, D. Ravelli, M. Fagnoni, M. Mella, A. Molinari, A. Maldotti, A. Albini, Chem. Eur. J., (2009), 15, 7949.
168) T. Yamase, Inorg. Chim. Acta, (1983), 76, L25.
169) P. Kormali, A. Troupis, T. Triantis, A. Hiskia, E. Papaconstantinou, Catal. Today, 124, (2007), 149.
170) A. Mylonas, A. Hiskia, E. Androulaki, D. Dimotikali, E. Papaconstantinou, Phys. Chem. Chem. Phys., 1, (1999) 437.
171) S. Kim, H. Park, W. Choi, J. Phys. Chem. B, 108, (2004), 6402.
172) J. Zakrzewski, C. Giannotti, J. Photochem. Photobiol. A: Chem., (1991), 57, 453.
173) E. Finkelstein, G. M. Rose, E. J. Rauckman, Mol. Pharmacol., (1982), 21, 262.
174) A. Lipovsky, Z. Tzitrinovich, H. Friedmann, G. Applerot, A. Gedanken, R. Lubart, J. Phys. Chem. C, (2009), 113, 15997.
175) G. R. Buettner, L. W. Oberley, S. W. H. C. Leuthauser, Photochem. Photobiol., (1978), 28, 693.
176) G. R. Buettner, Free Rad. Res. Comms, (1993), 19, S79.
177) L. Washmon- Kriel, V. L. Jimenez, K. J. Balkus jr., J. Mol. Catal. B Enzym., (2000), 10, 453.
178) R. Y. V. Subba, D. E. De Vos, P. A. Jacobs, Angew. Chem. Int. Ed. Engl., (1997), 36, 2661.
179) S. Jun, R. Ryoo, J. Catal., (2000), 195, 237.
180) A. Martiez, G. Prieto, Top. Catal., (2009), 52, 75.
181) A. Fuerte, A. Corma, M. Iglesias, E. Morales, F. Sanches, J. Mol. Catal. A: Chem., (2006), 246, 109.
182) C. T. Kresge, M. E. Leonowicz, W. J. Roth, J. C. Vartulli, J. S. Beck, Nature, (1992), 359, 710.
183) R. F. Parton, I. F. J. Vankelecom, M. J. A. Casselman, C. P. Bezonkhanova, J. B. Uytterhoeven, P. A. Jacobs, Nature, (1994), 370, 541.
184) S. B. Ogunwumi, T. Bein, J. Chem. Soc. Chem. Commun., (1997), 901.
185) M. J. Sabater, A. Corma, A. Domenech, V. Fornes, H. Garcia, J. Chem. Soc. Chem. Commun., (1997), 1285.

186) B. Z. Zhan, X. Y. Li, Chem. Commun., (1998), 349.
187) J. – L. Zhang, Y. - L. Liu, C. –M. Che, Chem. Commun., (2002), 2906.
188) M. Pal, V. Ganesan, Langmuir, 25, (2009), 13264.
189) A. Hamza, D. Srinivas, Catal. Lett., 128, (2009), 434.
190) P. Battioni, E. Cardin, M. Louloudi, B. Schollhorn, G.A. Spyroulias, D. Mansuy, T.G. Traylor, Chem. Commun., (1996), 2037.
191) A. Molinari, R. Amadelli, L. Antolini, A. Maldotti, P. Battioni, D. Mansuy, J. Mol. Catal. A: Chem., (2000), 158, 521.
192) J. S. Lindsey, H. C. Hsu, I. C. Schreiman, Tetrahedron Lett., 27, (1986), 4969.
193) C. Bartocci, A. Maldotti, G. Varani, P. Battioni, V. Carassiti, D. Mansuy, Inorg. Chem., (1991), 30, 1255.
194) A. Maldotti, A. Molinari, I. Vitali, E. Ganzaroli, P. Battioni, D. Mathieu, D. Mansuy, Eur. J. Inorg. Chem., (2004), 3127.
195) A. Molinari, M. Bruni, A. Maldotti, J. Adv. Oxid. Technol., (2008), 11, 143.